NOVEL TWO-PHOTON ABSORBING DYES: THEIR POSSIBLE USE IN PHOTOACTIVE APPLICATIONS

by

Özlem Şengül

B.S., Integrated B.S.&M.S. Program in Teaching Chemistry, Boğaziçi University, 2016

Submitted to the Institute for Graduate Studies in
Science and Engineering in partial fulfillment of
the requirements for the degree of
Master of Science

Graduate Program in Chemistry
Boğaziçi University
2019

ACKNOWLEDGEMENTS

First and foremost, I wish to express my sincere gratitude to my thesis supervisor Assoc. Prof. Saron Catak for her valuable scientific guidance and support. I am also grateful to her giving me the chance to work with Prof. Antonio Monari. I am appreciative of him for his extensive scientific guidance and advices during my stays in University of Lorraine, France; along with his invaluable support during my defense seminar. I wish to extend my appreciation to Assoc. Prof. Oktay Demircan for elaborately reviewing the latest manuscript and supporting remarks. Special gratitude extended to Prof. Viktorya Aviyente for her advices in my master studies.

This study has been supported by the bilateral project (TUBITAK-PIA Project No. 115Z863) between France and Turkey. I acknowledge TUBITAK ULAKBIM High Performance Computing Center for computational resources.

My hearty thanks go to all current and former members of Computational Chemistry and Biochemistry group (CCBG) for their friendship and support. I thank profusely to all my friends at Bogazici University for their endless friendship and assistance.

I owe my deepest gratitude to my family for their eternal love, perpetual encouragement, enthusiasm and everlasting support. This journey would not have been possible without them, I would like to dedicate my thesis to my beloved parents.

ABSTRACT

NOVEL TWO-PHOTON ABSORBING DYES: THEIR POSSIBLE USE IN PHOTOACTIVE APPLICATIONS

In this study, the linear and non-linear optical properties of two recently synthesized polythiophene based dyes, DTP1 and DTP2, were investigated.

In the first part, a thorough conformational search was performed, the absorption spectra have been obtained at time-dependent density functional theory (TD-DFT) level considering vibrational and dynamical effects via a Wigner exploration of the potential energy surface. Furthermore, the excited state topology and electronic density reorganization have been characterized using natural transition orbitals and the charge transfer character quantified through recently developed descriptors, also allowing for the rationalization of the poor interfacial electron injection properties exhibited by the dyes when grafted on TiO_2 surfaces. Finally, two-photon absorption (TPA) spectra have been calculated, extremely high cross sections have been obtained in the infrared region paving the way to the possible exploitation of the dyes for the development of photoactive smart materials or photodynamic therapy.

In the second part, the possible pathways leading to the intersystem crossing and triplet manifold population were examined. In particular, using high level state-of-the-art molecular modeling methodologies, the remarkable two-photon absorption (TPA) cross-section was underlined. Intersystem crossing pathways were elucidated by considering the energy difference between the relevant triplet and singlet states on the potential energy surfaces as the key critical points. The spin-orbit coupling is also assessed, and the results globally point to a possible, albeit probably slow, intersystem crossing that could allow the use of the two dyes as singlet oxygen photosensitizers, for instance in photodynamic therapy, owing to their high TPA cross-sections.

ÖZET

YENİ GELİŞTİRİLMİS İKİ FOTON ABSORBE EDEN BOYA MOLEKÜLLERİ: FOTOAKTİF MATERYALLERDE KULLANIMLARI

Bu çalışmada, yakın zamanda sentezlenen polythiophene bazlı iki organik boya molekülünün, DTP1 ve DTP2, lineer ve lineer olmayan optik özellikleri incelendi.

İlk kısımda, boya moleküllerinin konformasyonal araştırması yapıldı ve absorpsiyon spektraları zamana bağlı yoğunluk fonksiyoneli (TD-DFT) kullanılarak incelendi. Dinamik ve titreşim etkilerinin absorpsiyon ve emisyon üstüne etkileri, Wigner dağılımı kullanılarak konformasyonel alan örnekleri yardımıyla gerçekleştirildi. Ayrıca, uyarılmış hal topolojisi ve elektronik yoğunluktaki değişimin, doğal geçiş orbitalleri ve yeni geliştirilmiş tanımlayıcılar ile ölçülen yük aktarım özellikleri de dikkate alınarak karakterizasyonu yapıldı. TiO_2 yüzeyine yerleştirilen boya moleküllerinin elektron enjeksiyon özellikleri dikkate alındı. İki foton absorbsiyon özellikleri hesaplandı ve dikkat çekici kızıl ötesi iki foton absorbsiyon değerleri nedeniyle, optikçe aktif, akıllı materyal olarak enerji depolama amacıyla ve fotodinamik terapide kullanabileceklerini gözlemlendi.

İkinci kısımda, sistemler arası geçiş özelliği ve triplet popülasyonu incelendi. Özellikle, yüksek seviyede molekül modelleme metodolojileri kullanılarak, yüksek değerlere sahip iki foton absorpsiyon özelliklerine değinildi. Sistemler arası geçiş özelliği, sürece dahil olan uyarılmış hal durumları arasındaki enerji farkları dikkate alınarak incelendi. Spin orbit eşlenmesi değerleri de dahil edilerek, sistemler arası geçisin, yavaş da olsa, gerçekleşebileceği ve bahsi geçen moleküllerin yüksek değerdeki iki photon absorbsiyon özellikleri sayesinde fotodinamik terapide, tekli oksijen üretimi için kullanılabilecekleri sonucuna varıldı.

TABLE OF CONTENTS

LIST OF FIGURES

LIST OF TABLES

LIST OF SYMBOLS

$E^{\ddagger}$	Electronic activation energy
E_c^{VWN}	Vosko-Wilk-Nusair correlation functional
E_x^{exact}	Exact exchange energy
$E_c[\rho]$	Correlation energy
$E_x[\rho]$	Exchange energy
$E_{\sigma\sigma^*}$	Non-covalent contributions to the energy
$G^{\ddagger}$	Gibbs free energy of activation
$J[\rho]$	Coulomb energy
P_0	Ground state matrix
P_x	Excited state matrix
$T[\rho]$	Kinetic energy of interacting electrons
$T_s[\rho]$	Kinetic energy of non-interacting electrons
U_x^{σ}	Exchange energy density
$V_{ee}[\rho(r)]$	Interelectronic interactions
$V_{ext}(r)$	External potential
V_{KS}	Kohn-Sham potential
ΔE_x^{B88}	Becke's gradient correction
ΔH_{rxn}	Heat of reaction as electronic energy
$v(r)$	External potential
$\rho(r)$	Electron density
ψ_i	Kohn-Sham orbitals
ϕ_s	Quantitative topological descriptor
Γ	Detachment density matrix
Λ	Attachment density matrix
λ_{ij}	Reorganization energy
Ψ	Many electron wavefunction

LIST OF ACRONYMS/ABBREVIATIONS

ADF	Amsterdam Density Functional
B3LYP	Becke-3-parameter Lee-Yang-Parr functional
B88	Becke 88 Exchange Functional
CAM-B3LYP	Coulomb Attenuated Method
COSMO	Conductor-like Screening Model
DFT	Density Functional Theory
GGA	Generalized Gradient Approximation
$\widehat{H}$	Hamiltonian Operator
h_i	One-electron Hamiltonian
HOMO	Highest Occupied Molecular Orbital
HF	Hartree-Fock
IEF-PCM	Integral Equation formalism Polarizable Continuum Model
ISC	Intersystem Crossing
J_{ij}	Charge Transfer Integral
K	Exchange Integral
KS	Kohn-Sham
k_{ij}	Electron Transfer Rate
LDA	Local Density Approximation
LUMO	Lowest Unoccupied Molecular Orbital
M06-2X	Empirical Exchange-Correlation Functional
NTO	Natural Transition Orbital
oNTO	Occupied Natural Transition Orbitals
PCM	Polarizable Continuum Model
PDT	Photodynamic Therapy
SOC	Spin Orbit Coupling
TD-DFT	Time Dependent Density Functional Theory
vNTO	Virtual Natural Transition Orbitals
ωB97x-D	Long-Range Corrected Hybrid Functional with Dispersion Correction

1. INTRODUCTION

The increasing attention towards clean energy sources creates an impressive surge in the development and production of optically active materials [1] and dyes. The prominent interest in clean energy production [2, 3] and designing more efficient systems lead the scientific efforts for developing systems with applications in varied areas like molecular mechanics [4,5], medical and biological devices for using in imaging [6,7] or therapy [8]. The process of designing potent devices and systems [9] requires assessing and rationalizing the complicated mechanisms that imply nonadiabatic transitions [10, 11] among different excited states, operating the photochemical and photophysical features at the electronic level.

The spectacular development in the control of the light-dependent function gave rise to optically active materials to improve and commercialize, and these materials are also attracting more attention with the possibility to use in a wide range of applications. Solar energy conversion is one of the areas that chromophores actively use as light harvesting unit that starts with the foundation of the photovoltaic effect in 1839 by E. Becquerel and further developed with the new applications like dye sensitized solar cells (DSSC) [12] in 1991 by Grätzel and O'Regan [13].

Dye-sensitized solar cell (DSSC) mechanism is proceeding with the absorption of the light in which the dye particles act as photoactive material. The material consists of a semiconductor with a wide band gap, dye molecules and electrolyte (iodide/triiodide). Upon photo-excitation, an electron is boosted into the conduction band of semiconductor that is produced with a hole injection in a redox electrolyte. The electric current can be generated after the diffusion of the charges to anode and cathode. The difference of the Fermi level and conductors corresponds to the open circuit voltage.

In this context, absorbing in the low energy region of the spectrum enables activation of red or infrared light sources, is one of the most desired properties of optically active materials. Indeed, a deeper penetration of the activating source will be achieved

with such a characteristic feature which is highly beneficial and allows using in a wide range of applications. As the conjugation pattern of the chromophore is increased, it would be easier to achieve a global red-shift of the absorption spectrum. As emerging in recent years, one may resolve the nonlinear optical challenges with two photon absorption (TPA) that is theoretically conceptualized by Göppert-Meyer in the early 1930s [14]. Upon the excitation, two photons absorb simultaneously in TPA. Hence, one may expect a monochromatic light source; however, due to the division of the vertical excitation energy in two, unlike one-photon absorption, and as a result, light intensities will be doubled.

Different empirical or theoretical rules have been developed in the last years to rationalize the relationship between chromophores structure and TPA intensity (cross-section). For instance, centrosymmetric molecules such as donor-π- acceptor-π-donor (D-π-A-π-D) [18] generally give high cross-section for the $S_0 \rightarrow S_2$ transition. Polythiophenes structures and π-bridged donor- acceptor molecules (D-π-A) have also been recognized as efficient TPA absorber as confirmed both experimentally [15] and computationally [16]. TPA-based drugs for PDT are particularly attractive to obtain a significant red-shifted absorption profile. Indeed, Merocyanine 540 (Figure 1.1) is a commercially used drug, with π-bridged donor-acceptor structure, and have been used for the treatment of lymphoma.

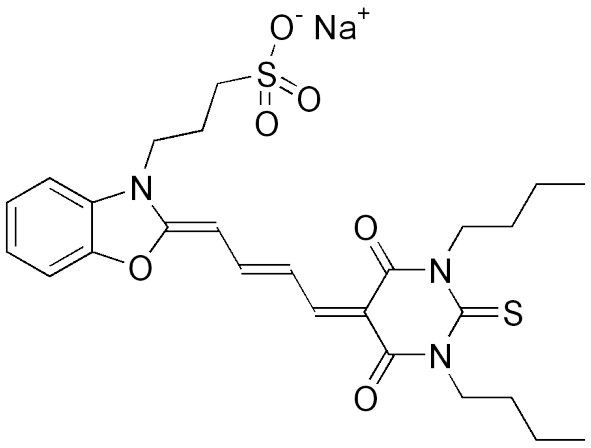

Figure 1.1: Chemical formula of Merocyanine 540

Consequently, TPA efficiency decreasing much faster than the corresponding OPA, and, hence, will form only in the focal area of the laser and resulting as a better spatial resolution and also, managing of the optically active material. In particular, having a red-shifted absorption and the extremely high spatial resolution make two-photon absorption an ideal candidate for medical applications such as therapeutic implications, or for imaging; recently the new improvements in drug design allowing to perform treatment and diagnosis simultaneously .

In the past few decades, the exploitation of light for therapeutic objectives has attracted renowned interest, pushed by the possibility of an efficient and selective treatment limiting the unwanted side effects of more conventional approaches. In this domain, the photosensitization of biological macromolecular structures, such as nucleic acids [17, 14], membranes [18, 10], and proteins [19], is performed to induce the death of undesired cellular lines, such as cancer cells or bacteria. Light-assisted therapy exploits the photophysical or photochemical processes triggered by the initial photoexcitation of a specific drug interacting with a specific cellular compartment. In particular, it usually requires the population of the drug's triplet manifold, followed by either direct photosensitization via electron or energy transfer to the biological structures, or the energy transfer to molecular oxygen to produce the highly reactive singlet oxygen ($^1O_2$) that will subsequently induce oxidative lesions leading to cellular death [20]. Even though the former represents the most common processes in light-assisted therapy, other mechanisms involving different photochemical channels, such as photo-induced hydrogen abstraction [30] is possible and have been reported.

The activation of singlet oxygen ($^1O_2$) gave rise to the well-known phenomenon photodynamic therapy (PDT) that has gained recognition in the therapeutic modality in number of diseases, among antibacterial, antiviral [21] and anticancer applications, even it still remains underutilized clinically. Selectivity in light-induced therapy, and photoactive components are should not have dark-toxicity; hence a general systemic effect should be avoided by the selective application of the light stimulus. Other pertinent desired features of an efficient PS agent; absorption in the therapeutic window ($600-900$ nm) to allow an appropriate light penetration depth and, hence, the treat-

ment of tumors deeper in the body interstitial. In addition, photosensitizer should also be characterized by an efficient intersystem crossing (ISC), without the presence of competitive deactivation channels, hence, leading to the population of the triplet state manifold necessary to achieve oxygen activation. Indeed, the interaction with the biological systems and the bioavailability profile should also be considered. These precautions notably provide a significant reduction in the drug side effects by its specific spatial activation achieved through irradiation.

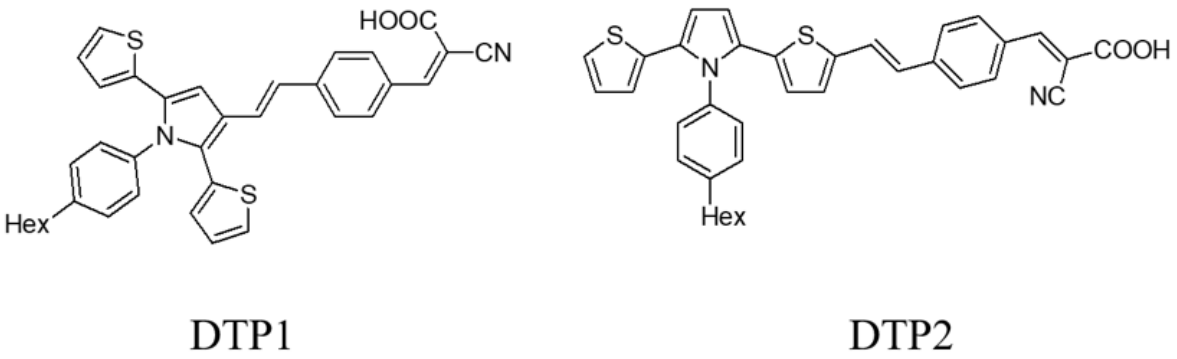

DTP1 DTP2

Figure 1.2: Chemical formula of DTP1 and DTP2

As potential materials, two organic dyes DTP1 and DTP2 that were synthesized by Sharmoukh *et al.* and shown in Figure 1.2, will be assessed towards the possibility of using in photoactive applications; dye sensitized solar cells (DSSC) and photodynamic therapy (PDT).

2. METHODOLOGY

2.1. Density Functional Theory

Density Functional Theory (DFT) [23] introduced by Hohenberg and Kohn in 1964 [24,25] which mainly states the ground state energy of a system as a functional of the electronic density. The theory is implemented with Kohn-Sham equations that also reminiscence non-linear form of the Schrodinger's equation. The first theorem applies that the external potential $V_{ext(r)}$ on the molecule, is related to nuclei and determined by the electron density $\rho(r)$. The variational principle is introduced by the second theorem.

The electron density ρ(r) is depicted as;

$$\rho(\mathbf{x}) = N \int ... \int |\Psi(x_1, x_2, ..., x_n)|^2 dx_1 dx_2 ... dx_n \tag{2.1}$$

where x is the representation of spin and spatial coordinates of the electron.

Noting that,

$$E[\rho] = \int v(r)\rho(r)dr + T[\rho] + V_{ee}[\rho] \tag{2.2}$$

electronic energy can be described as a functional of electron density with the sum of the kinetic energy of the interacting electrons ($T[\rho]$) and the interelectronic interaction energy $V_{ee}[\rho]$. Rewriting the electron energy by including,

$$E[\rho] = \int v(r)\rho(r)dr + T_s[\rho] + J[\rho] + E_{xc}[\rho] \tag{2.3}$$

the coulomb energy ($J[\rho]$) which defines the unfavorable electron-electron repulsion energy, the kinetic energy of the non-interacting electrons ($T_s[\rho]$) and the exchange-correlation energy functional ($E_{xc}[\rho]$) that is the addition of an exchange functional

$E_x[\rho]$ and a correlation functional $E_c[\rho]$. Considering density functional theory in means of Kohn-Sham approach, the Schrodinger's equation is expressed with a set of independent reference orbitals , Ψ_i

$$[-\frac{1}{2}\nabla^2 + V_{KS}]\,\Psi_i = \varepsilon_i\,\Psi_i \tag{2.4}$$

and V_{KS} term is described as;

$$V_{KS} = V(R) + \frac{\partial J[\rho]}{\partial \rho(r)} + \frac{\partial E_{xc}[\rho]}{\partial \rho(r)} \tag{2.5}$$

$$V_{KS} = v(r) + \frac{\rho(r')}{|r - r'|}dr' + v_{xc}(r) \tag{2.6}$$

in which $v_{xc}(r)$ represents the exchange-correlation potential. Ψ_i are the independent orbitals (Kohn-Sham orbitals), and the exact density is equal to;

$$\rho(r) = \sum_i^N |\,\Psi_i|^2 \tag{2.7}$$

in the case of the exchange-correlation functional is known exactly. On the contrary, approximate forms need to be developed like local density approximation (LDA), because of not knowing the exact form. Local density approximation provides the energy of a uniform electron gas system where the energy functional is,

$$E[\rho] = T_s[\rho] + \int \rho(r)v(r)dr + J[\rho] + E_{xc}[\rho] + E_b \tag{2.8}$$

E_b corresponds to the electrostatic energy of a positive background. In the presence of a uniform distribution of particles, the energy expression could be reduced to:

$$E[\rho] = T_s[\rho] + E_{xc}[\rho] \tag{2.9}$$

$$E[\rho] = T_s[\rho] + E_x[\rho] + E_c[\rho] \tag{2.10}$$

Starting the kinetic energy functional as,

$$T_s[\rho] = C_F \int \rho(r)^{5/3}\, dr \tag{2.11}$$

where C_F is a constant equal to 2.8712. The exchange functional is given by,

$$E_x[\rho] = -C_x \int \rho(r)^{4/3}\, dr \tag{2.12}$$

and C_x is equal to 0.7386.

Exchange energy is undervalued by the LDA approach and the correct asymptotic behavior could not be calculated exactly with it. Therefore, the exact asymptotic behavior of the exchange energy density of any finite many-electron system can be obtained with:

$$\lim_{x\to\infty} U_x^\sigma = -\frac{1}{r} \tag{2.13}$$

U_x^σ is correlated to $E_x[\rho]$ with the equation:

$$E_x[\rho] = \frac{1}{2} \sum_\sigma \int \rho_\sigma\, U_x^\sigma\, dr \tag{2.14}$$

Becke also suggested a gradient-corrected functional, (B88) [25];

$$E_x = E_x^{LDA} - \beta \sum_\sigma \int \rho_\sigma^{4/3} \frac{x_\sigma^2}{1 + 6\beta x_\sigma sinh^{-1} x_\sigma}\, dr \tag{2.15}$$

in which the component

$$x_\sigma = \frac{|\nabla \rho_\sigma|}{\rho_\sigma^{4/3}} \tag{2.16}$$

and the empirical constant β is equal to 0.0042.

The non-interacting Kohn-Sham reference system ($\lambda = 0$) is connected to the fully-interacting real system ($\lambda = 1$) by the adiabatic connection formula;

$$E_{xc} = \int_0^1 U_{xc}^{\lambda} d\lambda \tag{2.17}$$

λ corresponds to the inter-electronic coupling-strength parameter and U_{xc}^{λ} represents the potential energy of exchange-correlation at the intermediate coupling strength. The approximation of the adiabatic connection formula is:

$$E_{xc} = \frac{1}{2} E_x^{exact} + \frac{1}{2} U_{xc}^{LDA} \tag{2.18}$$

$U_{xc}^{0} = E_x^{exact}$ and $U_{xc}^{1} = U_{xc}^{LDA}$ [26].

The closed shell Lee-Yang-Parr (LYP) functional [27] is;

$$E_c = -a \int \frac{1}{1 + d\rho^{-1/3}} \left\{ \rho + b\rho^{-2/3} \left[C_F \rho^{5/3} - 2t_w + (\frac{1}{9} t_w + \frac{1}{18} \nabla^2 \rho) \right] e^{-cp^{-1/3}} \right\} dr \tag{2.19}$$

where,

$$t_w = \frac{1}{8} \frac{|\nabla \rho(r)|^2}{\rho(r)} - \frac{1}{8} \nabla^2 \rho \tag{2.20}$$

The hybrid functionals [28] are obtained with the mixing of LDA, B88, E_x^{exact} and the gradient-corrected functionals ;

$$E_{xc} = E_{xc}^{LDA} + a_0 (E_x^{exact} - E_x^{LDA}) + a_x \Delta E_x^{B88} + a_c \Delta E_c^{non-local} \tag{2.21}$$

$$\Delta E_c^{non-local} = E_c^{LYP} - E_c^{VWN} \tag{2.22}$$

in which ΔE_x^{B88} represents the Becke's gradient correction to the exchange functional and in Equation 2.20, the B3LYP functional, the gradient-correction ($\Delta E_c^{non-local}$) to the correlation functional is obtained by subtracting the Vosko-Wilk-Nusair correlation functional (E_c^{VWN}). The empirical coefficients are $a_0 = 0.20$, $a_x = 0.72$ and $a_c = 0.81$ [29].

2.2. Time Dependent Density Functional Theory

Time Dependent Functional Theory (TD-DFT) is the quantum mechanical approach for the excited state of the molecules. The Hamiltonian equation is;

$$\widehat{H} = \widehat{T}(\underline{r}) + \widehat{W}(\underline{r}) + \widehat{V}_{ext}(\underline{r}, t) \tag{2.23}$$

the sum of the kinetic energy of the electrons ($\widehat{T}$), the Coulomb interactions between the electrons ($\widehat{W}$), and time-dependent potential on the electrons ($\widehat{V}_{ext}$). The effect of the potential is crucial to assess the electronic states of the molecule since it depends on the external potential.

The Hohenberg-Kohn Theorem is implied a variational principle in the presence of the action;

$$A = \int_{t_0}^{t_1} \left\langle \Psi(t) | i\frac{\partial}{\partial_t} - \widehat{H} | \Psi(t) \right\rangle dt \tag{2.24}$$

Ψ is dependent on time-dependent constant,t;

$$\Psi(r_1, ..., r_N, t) = \Psi[\rho](t) e^{-i\alpha(t)} \tag{2.25}$$

and the constant is added by the phase factor and therefore,

$$A[\rho] = \int_{t_0}^{t_1} \left\langle \tilde{\psi}[\rho](t) | i\frac{\partial}{\partial_t} - \widehat{H}(t) | \tilde{\Psi}[\rho](t) \right\rangle dt + \alpha(t_1) - \alpha(t_0) = A[\rho] + const. \tag{2.26}$$

$A[\rho]$ can be expressed as:

$$A[\rho] = B[\rho] - \int dr \int_{t_0}^{t_1} (r,t)\rho(r,t)dtv \tag{2.27}$$

In Equation 2.25, $B[\rho]$ is not dependent on the external potential. An independent system with the property is;

$$\rho(r,t) = \sum_i f_i |\, \Psi_i(r,t)|^2 \tag{2.28}$$

shown in Equation 2.26 and by rewriting $B[\rho]$,

$$E_c = -a \int \frac{1}{1 + d\rho^{-1/3}} \left\{ \rho + b\rho^{-2/3} \left[C_F \rho^{5/3} - 2t_w + (\frac{1}{9} t_w + \frac{1}{18} \nabla^2 \rho) \right] e^{-cp^{-1/3}} \right\} dr \tag{2.29}$$

In the equation of $B[\rho]$, the correlational and exchange functional is stated as $A_{xc}[\rho]$ and by implementing the variational principle to Equation 2.25 with limitation:

$$\rho(r,t) = \sum_i f_i |\, \Psi_i(r,t)|^2 = \sum_i^N |\, \Psi_i(r,t)|^2 \tag{2.30}$$

Kohn-Sham equation with time dependency is obtained in Equation 2.29:

$$\left[-\frac{1}{2} \nabla^2 + V_{eff}(r,t) \right] \Psi_i(r,t) = i \frac{\partial}{\partial_t} \Psi_i(r,t) \tag{2.31}$$

$$v_{eff}(r,t) = v_H(r,t) + v_{xc}(r,t) + v_{exc}(r,t) \tag{2.32}$$

Time dependent xc-potential in Equation 2.30 can be driven as:

$$v_{xc}(r,t) = \frac{\delta A_{xc}[\rho]}{\delta \rho(r,t)} \tag{2.33}$$

Because of not knowing the exchange-correlation functional exactly, approximations should be presented. Besides that, the equations in time dependent density approach are exact. The Adiabatic Approximation (AA) is;

$$v_{xc}[\rho](r,t) = \frac{\delta A_{xc}[\rho]}{\delta \rho(r,t)} \approx \frac{\delta E_{xc}[\rho]}{\delta \rho(r)}|_{\rho=\rho(r,t)} \tag{2.34}$$

in the case of changing of the electron densities, the exchange and correlation potential change instantaneously.

2.3. Computational Choices

2.3.1. Basis Sets

The wavefunctions are described by basis sets and they are necessary for solving the Schrodinger's approach. 3-21G, 6-21G, 6-31+G and 6-311G* are the most preferred split-valence basis sets that developed by Pople *et al.* The first number in the basis set represents the primitives in the core function and the second part in the basis sets denotes to the number of primitives that are used in the valence functions. The valence double-ζ basis and valence triple-ζ basis are showed by two and three numbers in the basis sets, respectively. Adding the polarization function by deviating the basis set will also help to assess the system better. In the case of an electron that is far away from the core, diffuse functions can be added to the basis set to increase flexibility by "+" sign for the heavy atoms and "++" sign for hydrogen atoms. The non-hydrogen atoms are depicted with "*" and in the presence of "**", that means the polarization functions are also included for the light atoms, hydrogen and helium.

2.3.2. Continuum Solvation Models

Continuum solvation models are the most effective approach for the characterization of solvent effects into the quantum mechanical approach [30]. The number of degrees of freedom in the system is decreased by defining the models in the continuous framework and that is one of the advantages of the system [31, 32].

In these models, the solute is placed in a cavity that is surrounded by a dielectric environment and solvent is identified as a polarizable medium that is defined by the static dielectric constant ϵ. Total free energy of the solvation is given by;

$$\Delta G_{solvation} = \Delta G_{cavity} + \Delta G_{dispersion} + \Delta G_{electrostatic} + \Delta G_{repulsion} \tag{2.35}$$

in which ΔG_{cavity} is the cost of energy of locating the solute in the medium. In the solute and solvent interactions, $\Delta G_{dispersion}$ is dispersion effect, $\Delta G_{electrostatic}$ is the electrostatic component and finally, $\Delta G_{repulsion}$ represents the exchange interactions.

The Poisson equation underlines the main problem of the continuum solvent models which is related to the electrostatics;

$$-\overrightarrow{\nabla}[\epsilon(\overrightarrow{r})\nabla\overrightarrow{V}(\overrightarrow{r})] = 4\pi\rho_M(\overrightarrow{r}) \tag{2.36}$$

by simplifying,

$$-\nabla^2 V(\overrightarrow{r}) = 4\pi\rho_M(\overrightarrow{r}) \quad \text{within C} \tag{2.37}$$

$$-\epsilon\nabla^2 V(\overrightarrow{r}) = 0 \quad \text{outside C} \tag{2.38}$$

In Equation 2.37 and 2.38, the portion of space occupied by the cavity is presented with C, the dielectric function with ϵ, the sum of electrostatic potential with V.

$$V(\overrightarrow{r}) = V_M(\overrightarrow{r}) + V_R(\overrightarrow{r}) \tag{2.39}$$

V_M generated by the charge distribution ρ_M and the reaction potential V_R generated by the polarization of the dielectric medium. The Polarizable Continuum Model (PCM) is the most preferred continuum solvent approach and considers the electrostatic, dispersion-repulsion and cavitation energy while calculating the free energy of

the molecule in a solution. In atomic position, a cavity is defined by means of the interlocking Van der Waals spheres.

The polarization charges placed on the cavity surface defines the reaction field. Dielectric PCM (D-PCM), Conductor like PCM (C-PCM) and the integral equation formalism (IEF-PCM) form the three approach to PCM studies. IEF-PCM methodology is preferred in this study.

2.3.3. Wigner Distribution Function

The Wigner distribution [33] is the probability distribution function, introduced by Eugene Wigner in 1932. Linking the wave function defined by Schrödinger to a probability distribution maintains the aim of the theory and the shortfall of the functional is giving negative probabilities in some parts of the phase space, however, the charge and current densities are sufficiently provided by the method.

The functional is expressed as:

$$P(x,p) = \frac{1}{\pi\hbar}\int_{-\infty}^{\infty} \varphi^*(x+y)\,\Psi(x-y)\,e^{2ipy/\hbar}dy \tag{2.40}$$

in which x is the position and ρ is the momentum of any conjugate variable and Ψ is the wavefunction. The equation is symmetrical in x and p,

$$P(x,p) = \frac{1}{\pi\hbar}\int_{-\infty}^{\infty} \Psi^*(p+q)\,\Psi(p-q)\,e^{2ipy/\hbar}dy \tag{2.41}$$

and φ is the representation of the Fourier transform of Ψ.

In 3D,

$$P(\overrightarrow{r},\overrightarrow{p}) = \frac{1}{(2\pi)^3}\int \Psi^*\left(\overrightarrow{r}+\frac{\hbar\overrightarrow{s}}{2}\right)\Psi(\overrightarrow{r}-\frac{\hbar\overrightarrow{s}}{2}\Big)e^{i\overrightarrow{p}\,\overrightarrow{s}}\,d^3s \tag{2.42}$$

In the mixed states, Wigner distribution with density matrix is:

$$P(x,p) = \frac{1}{\pi\hbar}\int_{-\infty}^{\infty} \langle x+y|\widehat{p}|x-y\rangle e^{-2ipy/\hbar}dy \tag{2.43}$$

2.3.4. Functional Choices

The drawback of Density functional theory is the unknown exchange-correlation term (E_{xc}) and to overcome this and approximate the term properly, different methodologies are developed such as Local Density Approximation. LDA is one of the well-known methods to determine the E_{xc}, coming with the shortfall of the assumption of the electron density being the same in each state as a uniform electron gas. Generalized gradient approximation (GGA) method [34] is filling the gap by considering the non-homogeneous feature of the electron density, as shown in Equation 2.42.

$$E_{xc}^{GGA}[n] = \int drn(r)\varepsilon_{xc}(n(r), |\Delta n(r)| \tag{2.44}$$

Hybrid density functionals are the alternate methods and they are the combination of GGA with a percentage of exact functionals. B3LYP [35] is the most known hybrid density functional and based on GGA and LDA functionals:

$$E_{xc}^{B3LYP} = (1-a)E_x^{LSDA} + aE_x^{HF} + b\Delta E_x^B + (1-c)E_c^{LSDA} + cE_c^{LYP} \tag{2.45}$$

in which a, b and c components are stated in the order of 0.20, 0.72 and 0.81.

In some cases, like the polarizability of long chains and TD-DFT calculations such as excitations, B3LYP is not adequate and that point CAM-B3LYP [36] is exhibited by Tawada *et al.* It is the combination of the hybrid side of B3LYP and long-range correction. In its short range, HF is equal to 0.19 and B88 is 0.81 and in its long range, 0.65 and 0.35, respectively.

M06-2X [37] is another functional and belong to Minnesota Functional family and introduced by Prof. Donald Truhlar and his research team. The functional can be presented as ;

$$E_{xc}^{hyb} = \frac{X}{100} E_x^{HF} + (1 - \frac{X}{100}) E_x^{DFT} + E_c^{DFT} \tag{2.46}$$

where X is the percentage of Hartree-Fock exchange and equals to 54.

3. AIM OF THE STUDY

The study is mainly about assessing of optical properties of two chromophores for their applications in dye sensitized solar cells (DSSC) and photodynamic therapy (PDT).

In the first part, considering the good optical properties of the DTP dyes, an extensive state-of-the-art modelling investigation of their linear and nonlinear optical spectroscopy were performed. This includes the sampling of their conformational space taking into account the dynamic and vibrational effects on the optical properties. Dynamic effects can be crucial especially in the case of large-scale low-frequency vibration, such as out-of-plane bending of conjugated rings. Moreover, such effects can be efficiently included by semiclassical molecular dynamics or Hessian based (Wigner) sampling of the ground state potential energy surface. The topological analysis of the excited states density reorganization, also performed via the use of charge transfer descriptors, allows for rationalizing the rather poor interfacial charge separation. In addition to the one-photon absorption (OPA), two-photon absorption (TPA) spectra is also reported, which show remarkably high cross sections in the infrared region.

In the second part, the detailed photophysical analysis of the chromophores and the intersystem crossing efficiency was evaluated. DTP1 and DTP2 show an efficient TPA cross-section in the infrared portion of the spectrum and could lead to efficient singlet oxygen activation.

4. PROBING OPTICAL PROPERTIES OF THIOPHENE DERIVATIVES FOR TWO-PHOTON ABSORPTION

4.1. Background

The growing demand in energy supply has reached a point that may not compensate the needs exactly and cause resource depletion in terms of carbon based energy sources such as oil, coal and natural gas. One of the most significant shortcomings of current demand on fossil fuels is the lack of knowledge on the serious negative effects, and the lack of adequate methods to accurately identify them: this is an essential point to consider for the environmental sustainability. Furthermore, the rising global consciousness has heightened the interest in clean energy sources and accelerate the advancement of sustainable and renewable sources. An immense number of alternative energy initiatives are emerging such as wind, geothermal, hydraulic and solar energy. It is important to point out that photovoltaic technology is getting attention by being environmentally friendly and offers a reliable, direct conversion of sunlight into electrical energy.

Solar energy has the highest theoretical energy potential, comparing to other alternative energy sources, which is around 89000 terawatts (TW) [38] and 13 TW energy is needed to sustain the lifestyle of 6.5 billion people and the researches are presented mankind will need an extra 10 TW energy to maintain the current lifestyle [39]. For the reasons cited above, solar energy is having the highest interest among other alternative sources of energy. Hence, the process of new materials in terms of harvesting sunlight in better efficiency and compensate for the growing demand and cost of production is the main target in the PV market.

The development of photovoltaic devices started with the silicon solar cell that was introduced by Bell Laboratories in 1954 [40]. Silicon is still dominating the PV market; the most probable reason is, silicon is a cost-effective material and highly

abundant in nature; also it can be processed well and most importantly, it conducts very well by absorbing the light in the right optical range [41]. Three different manufacture processes that are up to 15-20 % efficiency was developed for silicon-based solar cells; monocrystalline, polycrystalline and amorphous. It is interesting to note that crystalline solar cells have surpassed the market, in spite of having a high cost.

The conversion efficiency is important as well as the low production costs and that leads to an improvement in production towards new classes of materials. Long-term stability, non-toxicity, efficient photovoltaic conversion capacity, being suitable for large area applications are some of the expectations for the ideal material for solar cells. The improvement in the efficiency consists of a large portion of priority in the manufacturing and production and it is significant that as a competitive. Nevertheless, reducing the cost is an industrial goal for the market, and that is a challenging issue as the energy conversion efficiency as affecting the entire value-chain cost of the market from material manufacture to installation of the system. The loss in the efficiency of solar cells is arising from three reasons; losing photon because of the surface reflection, silicon bulk transmission and back contact absorption [42]. In spite of the wide range of requirements, the market came up with different technologies. In general, inorganic materials are preferred in the commercialized solar cells, however considering the advancement in the area, organic solar cells, dye-sensitized solar cells and perovskite solar cells are also getting the attention.

An interesting new technology was Dye Sensitized Solar Cells (DSSC) that differs from the conventional solar technology by being cost-effective and user-friendly applications. The mechanism (Figure 4.1) is similar to the p-n junction photovoltaic effect; however, it contains titanium dioxide as a porous layer covered with dye particles in the form of the monomolecular layer. The process starts with the excitation of the dye molecules by absorbing light and the excited electrons transport to the conduction band of the titanium dioxide layer. The electrical current is sustained with the contact between the dye molecules and an electrolyte. The main drawback of the DSSC technology being temperature dependent: at high temperatures, there is the possibility of leakage and freezing in low temperatures. They are still in early research of devel-

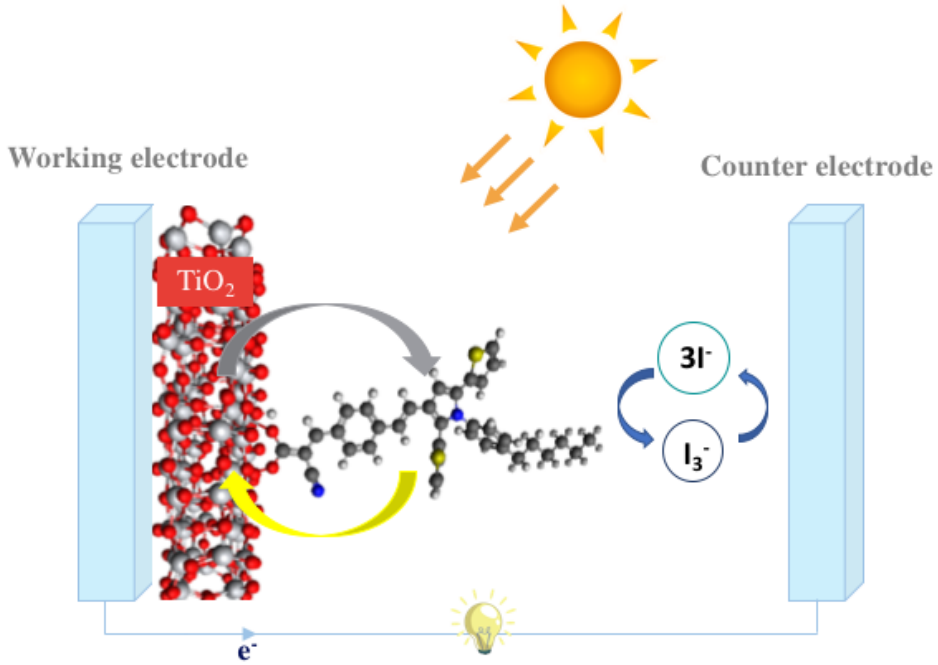

Figure 4.1: Mechanism of Dye-Sensitized Solar Cells

opment and that kind of unique problems waiting to be solved, besides the negative qualities, they also meet up with the expectations towards higher efficiency with 16 % at laboratory conditions.

4.2. Methodology

4.2.1. Computational Procedure

A conformational search was performed on both chromophores, aiming to get the most stable geometries, with hybrid B3LYP and meta-hybrid GGA M06-2X functionals. Additionally, long-range corrected hybrid functionals CAM-B3LYP and ωB97X-D were selected for the characterization of excited state nature of the dyes with the help of the compensation feature of Hartree-Fock (HF) on limitations of DFT in critical points of charge transfer states. 6-31G(d) and 6-31+G(d,p) were employed for the modeling process of the ground and excited states, respectively. In order to be consistent with experimental findings, the solvent was selected as dichloromethane (DCM)

and polarizable continuum method (IEF-PCM) is preferred for the solvent effects.

Charge transfer characterization is the basis of determining the photovoltaic efficiency in solar cells. Hence, for modeling charge transfer nature of electronic states quantitatively, the ϕ_s index is implemented. As mentioned above, ϕ_s index is the numerical depiction of electron density re-organization and Natural Transition Orbitals (NTOs) also included for representation spatial distribution of charge on the surface of the target dyes by using Nancy_ Ex code.

In the aim of having a precise representation of the optical properties, dynamic and vibrational environments are adopted by sampling 20, 40 and 60 initial geometries via Wigner distribution function as implemented in Newton-X code. The vertical transitions examined with ωB97X-D/6-31+G(d,p) level of theory, also convoluted to a fixed width at half length of 0.2 eV. All quantum chemistry calculations were carried out with Gaussian 09 code [43].

Two-photon absorption (TPA) values were examined at TD-DFT level (CAM-B3LYP/6-31G(d)) with linear response method as implemented in DALTON2016 code and Göppert-Mayer (GM) units (10^{-50} cm^4/photon) used for the representation of cross-section values.

4.2.2. ϕ_s Index

ϕ_s [44] index is proposed by SRSMC research group from University of Lorraine to get quantitative information about the charge transfer nature of excited states with the elucidation of several quantum mechanical descriptors. Assessment of the topology of the excited states with ϕ_s index is an efficient way to rationalize charge separation. In the first step of analyzing of density matrices, the difference between X^{th} excited P_x and ground state P_0 density matrix is calculated

$$\Delta = P_x - P_0 \Rightarrow \sum_{k=1}^{K} (\Delta S)_{kk} = 0 \tag{4.1}$$

The investigation of electronic transition is performed in a N-electron system with K-sized basis set and S term correspond to basis set overlap matrix. ΔS is found as zero as expected since there is not an electron gaining or losing in the system. The density matrix, Δ, is diagonalized into δ to obtain the orbitals of attachment and detachment [44];

$$\exists U | \delta = U^{\dagger} \Delta U; (\delta)_{ij} = 0 \quad \forall \quad i \neq J \tag{4.2}$$

The diagonalized matrix splits into two ways based on sign, σ_- and σ_+

$$(\sigma_{\pm})_{kj} = \frac{1}{2}\left(\sqrt{(\delta)_{kk}} \pm (\delta)_{kk} \right) x \delta_{kj} | \delta = \sum_{\omega=+,-} \omega \sigma_w \tag{4.3}$$

σ_+ includes the positive values and zeros; conversely, σ_- includes the negative δ values and sets non-negative ones to zero. By back transformation process of the two diagonal matrices,

$$\left.\begin{aligned} \delta &= U \delta U^{\dagger} \\ \Gamma &= U \sigma_{-} U^{\dagger} \\ \Lambda &= U \sigma_{+} U^{\dagger} \end{aligned}\right\} \quad \Delta = \Lambda - \Gamma \tag{4.4}$$

the detachment Γ, depletion of electron density with the chromophore's absorbing light and the attachment Λ, the electron density increment in the electronic state, density matrices are obtained. As underlined in Equation 4.1, when the molecule is excited, no electron lost from the system and that also can be seen as;

$$\sum_{\mu=1}^{K} (\Gamma S)_{\mu\mu} = \sum_{\mu=1}^{K} (\Lambda S)_{\mu\mu} \tag{4.5}$$

In the 3D space, detachment/attachment matrices are shown with three spatial coordinates ξ_1, ξ_2, ξ_3

$$\varrho_{\tau}(\xi_1 \xi_2 \xi_3) = \sum_{\mu=1}^{K} \sum_{\upsilon=1}^{K} (\tau)_{\mu\upsilon} \varphi_{\mu}(\xi_1 \xi_2 \xi_3) \varphi_{\upsilon}^{*}(\xi_1 \xi_2 \xi_3) \tag{4.6}$$

$$\tau \equiv \Gamma, \Lambda \tag{4.7}$$

and the charge ϑ_τ can be depicted as:

$$\vartheta = \int_R d\xi_2 \int_R d\xi_2 \int_R d\xi_3 \varrho_\tau((\xi_1 \xi_2 \xi_3) \equiv \int_{R^3} d^3 \xi_{\varrho\tau}(\xi) \tag{4.8}$$

$$\tau \equiv \Gamma, \Lambda \tag{4.9}$$

Finally, ϕ_s index can be defined in the 3-D real space:

$$\phi_s = \vartheta^{-1} \int_{R^3} d^3 \xi \sqrt{\varrho_\Gamma(\xi) \varrho_\Lambda(\xi)} \tag{4.10}$$

$$\vartheta \equiv \frac{1}{2} \left[\int_{R^3} d^3 \xi \sum_{\tau=\Gamma,\Lambda} \varrho_\tau(\xi) \right] \quad \phi_s \in [0; 1] \tag{4.11}$$

The charge transfer nature of the excited states can be identified by quantitatively evaluating the ϕ_s index values that characterize the detachment (ϱ_Γ)/ attachment (ϱ_Λ) densities overlap. ϕ_s descriptor values range 0 to 1, low values (close to zero) indicates small overlap between the electronic states and conversely, the values close to 1 imply high overlap. One may consider that a tridimensional integration grid surrounding the chromophore will integrate the detachment/attachment densities over the delimited volume Ω as depicted in Figure 4.2.

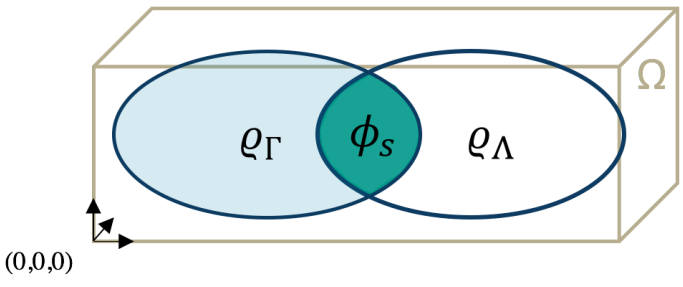

Figure 4.2: Graphical representation of the quantitative topological descriptor ϕ_s.

4.3. Results and Discussion

4.3.1. Conformational Analysis

The DTP-π-A dyes have a π-conjugated system which enhances the absorption in the low energy region of the spectrum and make them proper candidates for optical devices. Triphenylamine associate the donor part and based on the attachment of the styryl π-spacer to the pyrrole (DTP1) and to the thiophene (DTP2) on the DTP moiety, the dyes are classified in two as DTP1 and DTP2 and their photovoltaic performance is characterized.

In the light of information cited above, the conformational analysis is applied to both chromophores to evaluate them better in terms of electronic properties. The lowest energy conformers, within the free energy range of 10 kJ/mol, were selected for further analysis as can be seen from Table 4.1. In the case of DTP1, the main energy difference stems from the relative positions of cyano and carboxylate functional groups that facing the opposite sides in the 1^{st} and 2^{nd} conformers and in the same direction the last three ones. The increasing trend in the relative energies possibly stems from the electronic repulsion between these functionalities. The almost isoenergetic conformers DTP1-1 and DTP1-2, structurally differ only in the relative positions of the thiophene rings that results as a 0.3 kJ/mol difference.

Unlike DTP1 conformers, the cyano and carboxylate group only have trans orientation in the 5^{th} conformer among DTP2 conformers. On the other hand, the alignment of the hexyl group and the positions of thiophene rings maintain the real energy difference among the molecules. 2^{nd} and 3^{rd} conformers have 3.8 kJ/mol energy difference based on the orientation of hexane and the same trend can be seen between 4^{th} and 5^{th} conformers. It is clear that the hexyl chain has a significant effect on the energy of DTP2 comparing to DTP1. One may suggest that the hexyl chain causes a competition among dispersion-driven attraction and entropic factors with the former affirming compact structures; considering the free energy values depicted in Table 4.1 and a better solvent stabilization is enhanced by the disordered structures that are presented by

Table 4.1: S_0 optimized structures of the lowest energy conformers of DTP1 and DTP2.

DTP1-1	**DTP1-2**	**DTP1-3**	**DTP1-4**	**DTP1-5**
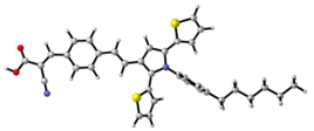	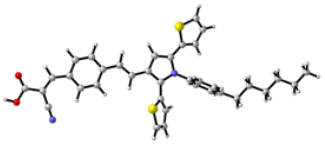	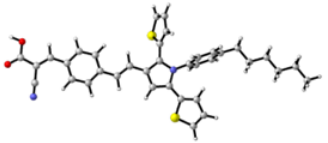	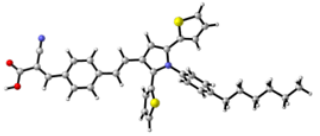	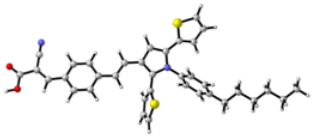
0.0	0.3	4.1	10.5	11.2
DTP2-1	**DTP2-2**	**DTP2-3**	**DTP2-4**	**DTP2-5**
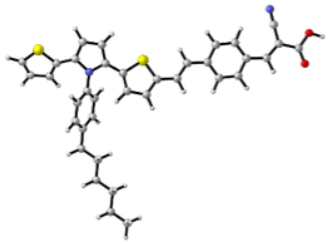	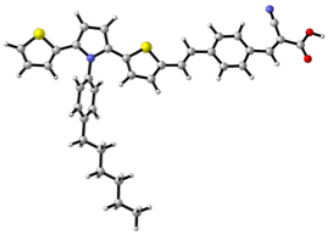	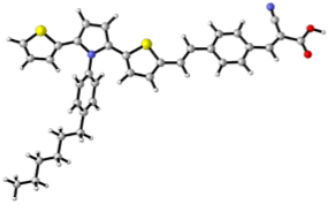	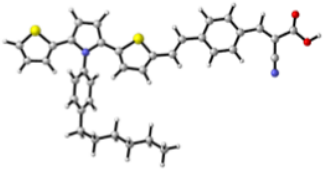	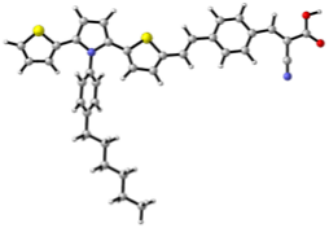
0.0	1.4	5.2	7.6	8.3

the entropic disorder.

4.3.2. Static Level of Theory: Assessment by Considering Functional Performance

Absorption spectra was evaluated for all conformers of DTP1 and DTP2 by using different functionals: CAM-B3LYP and ωB97X-D. In Table 4.2, the vertical excited energies were analyzed in comparison with experimental data, in nm and eV.

The λ_{max} values were red-shifted for CAM-B3LYP comparing to ω97X-D, for both dyes. The reason behind the difference in the trend is the inclusion of empirical atom–atom dispersion correction in ω97X-D functional. The other reason may stem from the small charge separation, that will be analyzed in the next section, which causes CAM-B3LYP to give big deviations in the process of reproducing excitation energies. Considering the vertical transition energies, ω97X-D functional is more consistent with experimental data and favorable for assessing absorption properties of the organic dye molecules.

The excitation energies were reproduced for each conformer in static terms in comparison with experimental findings. As depicted in Table 4.2, an extension of absorption to the red region of the spectrum can be seen for all conformers of DTP2 which is the result of the extended conjugation in the dye molecule.

The experimental findings are almost reproduced for both dyes with the static approach. Looking at the structural differences between the dyes, one may recognize DTP2 conformers have absorption maxima values generally in the lower energy region of the spectra as aforementioned that is possibly due to the extended conjugation.

4.3.3. Excited State Profile

In the characterization of excited state nature of the molecules, as the charge transfer density re-organization capability is the main target for the usage capacity in

Table 4.2: Statistical evaluation of different functionals for absorption spectra of DTP1 and DTP2

λ_{ab} **for DTP1**				λ_{ab} **for DTP2**			
Dye	**ωB97X-D**	**CAM-B3LYP**	**Expt.**	**Dye**	**ωB97X-D**	**CAM-B3LYP**	**Expt.**
DTP1-1	414 (2.99)	431 (2.87)	415 (2.98)	**DTP2-1**	458 (2.70)	479 (2.58)	457 (2.71)
	306 (4.05)	311 (3.98)	334 (3.71)		291 (4.26)	316 (3.92)	364 (3.40)
DTP1-2	414 (2.99)	431 (2.87)	-	**DTP2-2**	458 (2.70)	480(2.58)	-
	306 (4.05)	311 (3.98)	-		292 (4.24)	317(3.91)	-
DTP1-3	415 (2.98)	431 (2.87)	-	**DTP2-3**	458 (2.70)	479 (2.58)	-
	305 (4.07)	310 (3.99)	-		290 (4.27)	318 (3.89)	-
DTP1-4	405 (3.06)	418 (2.96)	-	**DTP2-4**	457 (2.71)	478 (2.59)	-
	287 (4.32)	290 (4.27)	-		291 (4.26)	316 (3.92)	-
DTP1-5	405 (3.06)	419 (2.95)	-	**DTP2-5**	455 (2.72)	477 (2.60)	-
	287 (4.32)	290 (4.27)	-		290 (4.27)	315 (3.93)	-

solar cells, the selected conformations were scanned as the starting point to see the most probable alternatives of the organic dyes.

Table 4.3: Natural transition orbitals of the selected conformers of DTP1 and DTP2

Dye	**oNTO**	**vNTO**
DTP1-1 $S_0 \rightarrow S_1$ $\phi_s = 0.83$	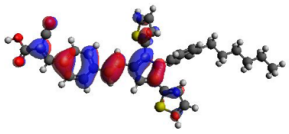	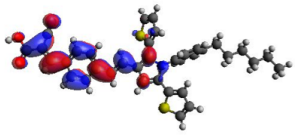
DTP1-1 $S_0 \rightarrow S_2$ $\phi_s = 0.88$	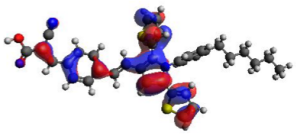	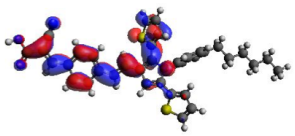
DTP2-1 $S_0 \rightarrow S_1$ $\phi_s = 0.90$	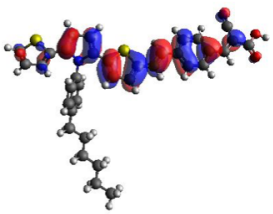	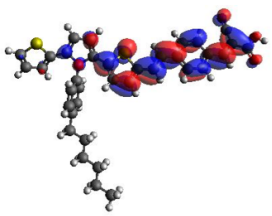
DTP2-1 $S_0 \rightarrow S_2$ $\phi_s = 0.93$	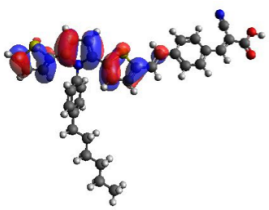	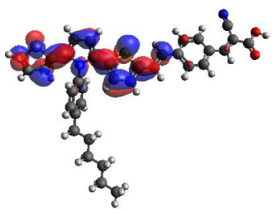

Two approaches take into account to determine the characteristics: ϕ_s index and natural transition orbitals (NTOs). ϕ_s index is the source of the quantitative approach and it is the overlap matrix between the electron density removed from the ground state and the rearranged density in the excited state and as the value of the ϕ_s index gets closer to 1, the chance of the charge transfer is increasing in order with that. ϕ_s

values are shown in Table 4.3 and as can be seen from the table, most of the conformers indicate a local charge transfer. It is clear that the quantitative methodology pointed out the dyes are not compatible for use in solar cells because of the inefficient charge transfer capacities. In correlation with ϕ_s findings, NTOs for $S_0 \rightarrow S_1$ and $S_0 \rightarrow S_2$ are analyzed and the visual representation of the charge transfer is consistent with the quantitative approach and indicate a local charge transfer characteristic.

4.3.4. Optical Conditions in the Presence of Dynamic and Vibrational Effects

Both chromophores have an extended π-conjugation and so, one may expect the conformational space scanning will have an impact on the results compared to static ones and may give an improvement with experimental data. Thus, 20, 40 and 60 initial geometries were generated via Wigner distribution to have a better insight about the absorption properties of the organic dyes (Figure 4.3 and Figure 4.4). The findings are presented in Table 4.4 and as a result of the vibrational environment the λ_{max} values for all molecules in the red or near visible region of the spectrum and red-shifted in the presence of dynamic effects. Also, when the conformation space is extended to 40 initials in the potential energy surface, the results shift to the lower energy region of the spectrum in comparison to 20 initials, especially for DTP1. However, the same effect cannot be seen for 60 initials, so one may conclude that the number of the initial geometries do not have a correlational effect on the vertical excitation energy.

In the case of DTP2, almost all of the values were red-shifted and in particular, for the 4^{th} conformer, λ_{ab-60} value is remarkably high comparing to static TD-DFT results. In general terms, the presence of dynamic and vibrational effects exhibit a relatively less impact on the Wigner distribution results than expected.

Finally, Boltzmann-weighted absorption spectra is obtained with 60 vertical transitions (via Wigner) for each conformer to have the best resolved band shape similar to the experimental one. The obtained absorption spectrum can be seen in Figure 4.5.

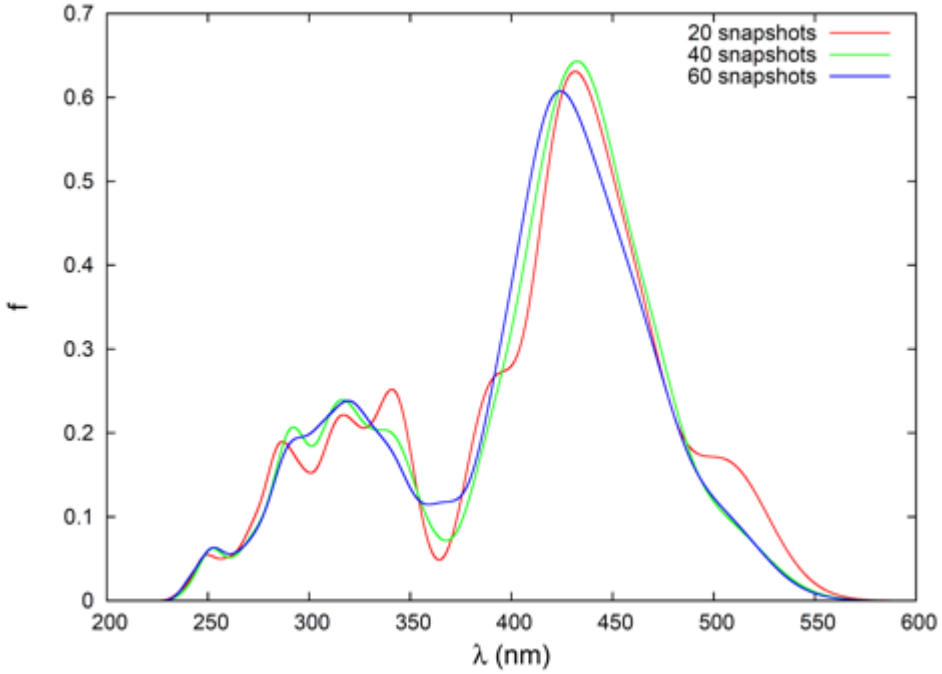

Figure 4.3: Wigner distribution result for the absorption spectra of DTP1.

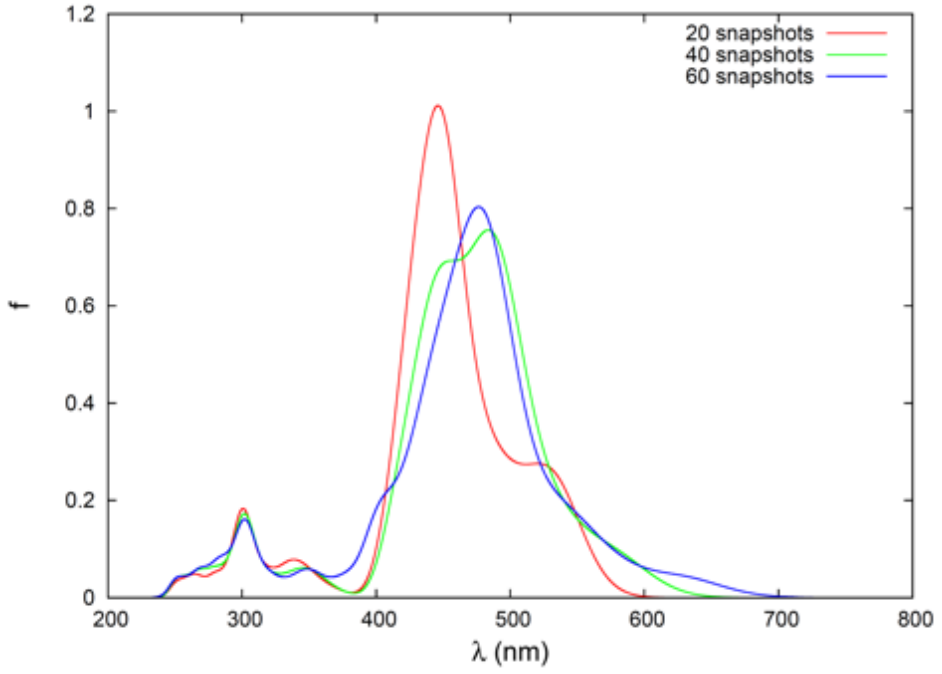

Figure 4.4: Wigner distribution result for the absorption spectra of DTP2.

Table 4.4: Wigner Distribution results for λ_{ab} of the conformers of DTP1 and DTP2

Dye	λ_{ab-20}	λ_{ab-40}	λ_{ab-60}	λ^{c}_{ab}
DTP1-1	431 (2.87)	432 (2.87)	423 (2.93)	414 (2.99)
DTP1-2	406 (3.05)	448 (2.76)	408 (3.03)	414 (2.99)
DTP1-3	443 (2.79)	445 (2.78)	425 (2.91)	415 (2.98)
DTP1-4	385 (3.22)	420 (2.95)	421 (2.94)	405 (3.06)
DTP1-5	392 (3.16)	423 (2.93)	427 (2.90)	405 (3.06)
DTP2-1	446 (2.77)	483 (2.56)	476 (2.60)	458 (2.70)
DTP2-2	452 (2.74)	456 (2.71)	466 (2.66)	458 (2.70)
DTP2-3	449 (2.76)	459 (2.70)	463 (2.67)	458 (2.70)
DTP2-4	467 (2.65)	470 (2.63)	501 (2.47)	457 (2.71)
DTP2-5	466 (2.66)	462 (2.68)	462 (2.68)	455 (2.72)

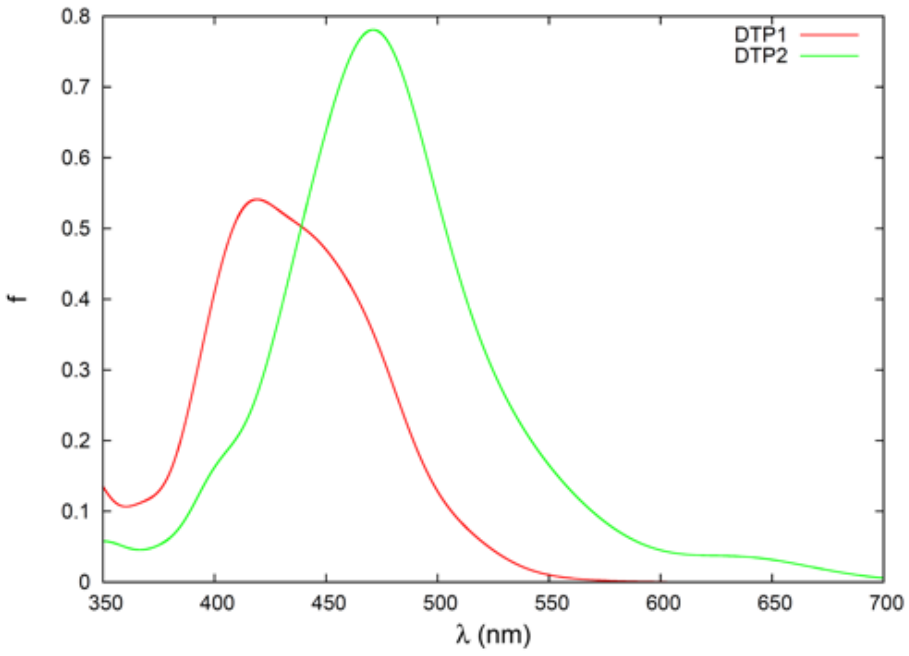

Figure 4.5: Boltzmann-weighted absorption spectra of the chromophores.

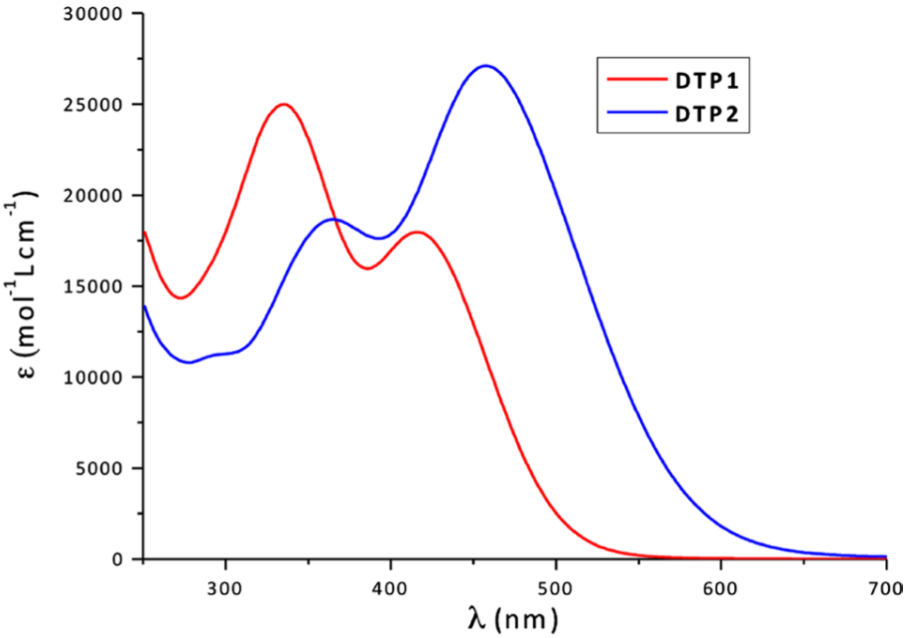

Figure 4.6: Experimental absorption spectra of DTP1 and DTP1.

The proper application of vibration effects can be observed from the λ maxima values that have small deviations from the experimental ones, only 0.04 and 0.07 eV for DTP1 and DTP2, respectively. Indeed, the general band shape is reproduced in similar to the experimental one (Figure 4.6) that is the proof of the vibrational effects is a good treatment for both dyes.

4.3.5. Two-photon Absorption

Two-photon absorption is the absorption of two photons simultaneously in which the absorption maxima shift towards the lower energy region of the spectrum as the result of having higher energy. In addition, TPA spectrum generally appears in the near-IR, which gives the advantage of the wider scope of application than conventional one- photon absorption.

TPA absorption results in the vibrational environment for the chromophores tabulated in 4.6 and considering the dynamic resolution of the TPA band, the maxima values are found as quite satisfying in the optimal phototherapeutic window, for both dyes. In the spectrum, $S_0 \rightarrow S_1$ absorption is around 850 nm and resulted as a broad

symmetric band. DTP1 cross section value is 450 Göppert-Mayer (GM) while DTP2 presents the cross section up to 740 GM. This shift is due to the extended conjugation in DTP2 that made it a remarkable candidate for medical applications. The $S_0 \rightarrow S_2$ transition is also characterized by high TPA with maximum absorption at 566 nm for DTP1 and 624 nm for DTP2. Cross sections are extremely high exceeding 1000 GM for DTP1 and reaching the impressive value of 7000 GM for DTP2.

Table 4.5: Two-photon absorption via Wigner distribution, DTP1 and DTP2.

DTP1		DTP2	
$\lambda_{Max}(nm)$	$\Phi(GM)$	$\lambda_{Max}(nm)$	$\Phi(GM)$
820	442	870	742
566	1243.6	624	6977.7

4.3.6. Conclusion

In the first part of the study, the linear and non-linear optical properties of the two organic dyes were reported with a state of-the- art theoretical modeling approach. One photon absorption spectra was sampled based on Wigner distribution for modulating vibrational and conformational flexibility. The charge transfer capabilities were examined by quantitatively via ϕ_s descriptor and natural transition orbitals were taking into account for better understanding. It is shown that the dyes generally presented local charge transfer characteristic and considering that founding, the potential usage of the chromophores in solar devices was considerably low.

On the contrary, both chromophores showed a remarkable two-photon absorption cross section values in the red and infrared region of the spectra both for $S_0 \rightarrow S_1$ and $S_0 \rightarrow S_2$ transitions that make them extremely promising candidates for medical applications and for this reason, the study will be continued with the exploration of the photophysical features of the dyes in terms of singlet oxygen generation.

5. PHOTOPHYSICAL AND PHOTOCHEMICAL PROPERTIES: ASSESSING THEIR POSSIBLE USE FOR SINGLET OXYGEN GENERATION

5.1. Background

Photodynamic therapy (PDT) is a well-known phenomenon; the use of light activated drugs, photosensitizers, in the treatment of several diseases, including tumors. The idea was emerged from the experiment of Oscar Raab, at that time a Ph.D. student of von Tappeiner, in the study of the toxic effects of acridine on paramecia [46]. The extensive observation of the effect of light on living cells resulted in the introduction of the term "Photodynamic action" [47, 48]. The requirement of singlet oxygen for the action of the photodynamic therapy was introduced by the German group after several trials. In 1904, the first treatment of the PDT drug, eosin, was presented with the application to a patient with rodent ulcer in the lower lip. The recovery of the tumor cells was occurred in a relatively short time, three months, and gave an impressive surge to the investigation in the area with the design of new photoactive molecules.

Hematoporphyrin was introduced by Scherer in an impure form with the inspiration of the structure of the hemoglobin molecule and extensively analyzed for the therapeutic purposes [49]. The removal process of the iron from dried cow blood and later the treatment with sulfuric acid gave life to the leading drug of the PDT history [49]. The development of the Hematoporphyrin derivate, HPD (Schwartz, Winkelman and Lipson) [50,51] and the following period with the systematic studies on human and animals by Dougherty, induced a peak in Photodynamic Therapy [52] and the trend followed by the first drug approval in the world by Canada government in 1993 which was a milestone for PDT history.

Photodynamic Therapy is a multidisciplinary approach and as presented in Figure 5.2, starts with the excitation of the molecule by absorbing a photon, from the ground

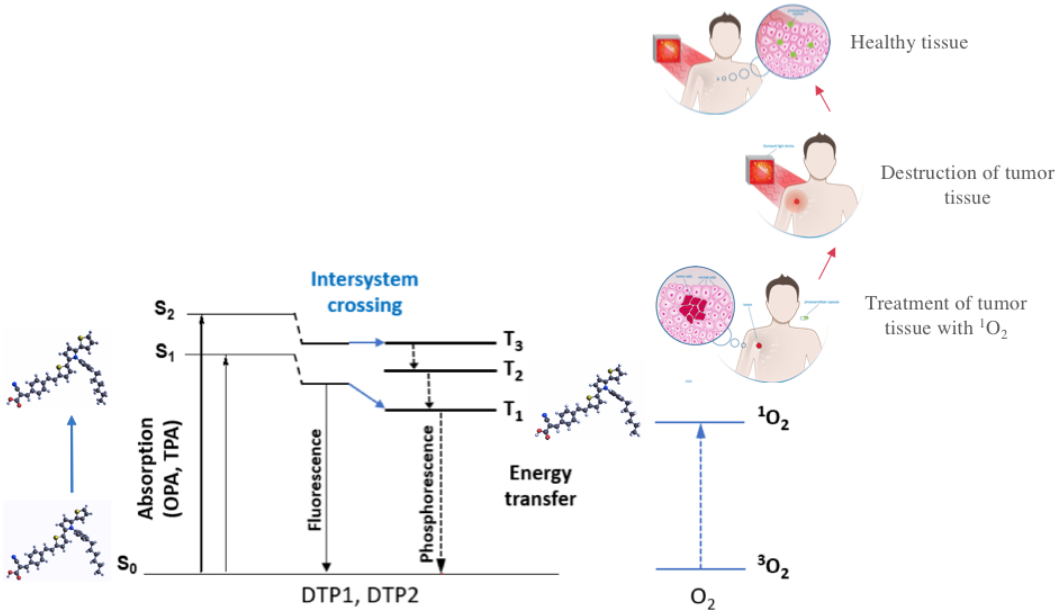

Figure 5.1: Energy scheme presenting the overall photoreactivity for DTP1 and DTP2.

state (S_0) to singlet states. At that energy level, the molecule needs to get rid of the excess energy, so undergoes different transitions to different electronic states. The molecule may initiate an intersystem crossing to the triplet states that are relevant to the biological reactions or alternatively, may relax back to the ground state. The triplet state population may undergo two types of reactions simultaneously: the direct interaction with the targeted substrate by transferring an electron and forming radicals to react with oxygen and that resulted with oxygenated products (Type I) or as the main interaction for most PDT photosensitizers in current use, transferring the energy to oxygen (Type II) and having a highly reactive oxidizing species (ROS). The type of the photosensitizer, substrate and oxygen concentrations mainly affect the ratio between these two types of reactions. The destructive path to tumors consist of three mechanisms: ROS can directly attack the tumor cells, the shutdown of microvessels and the activation of an immune response. These three mechanisms may influence each other and for the long-term controlling of tumor cells, the combination of the mechanisms is required.

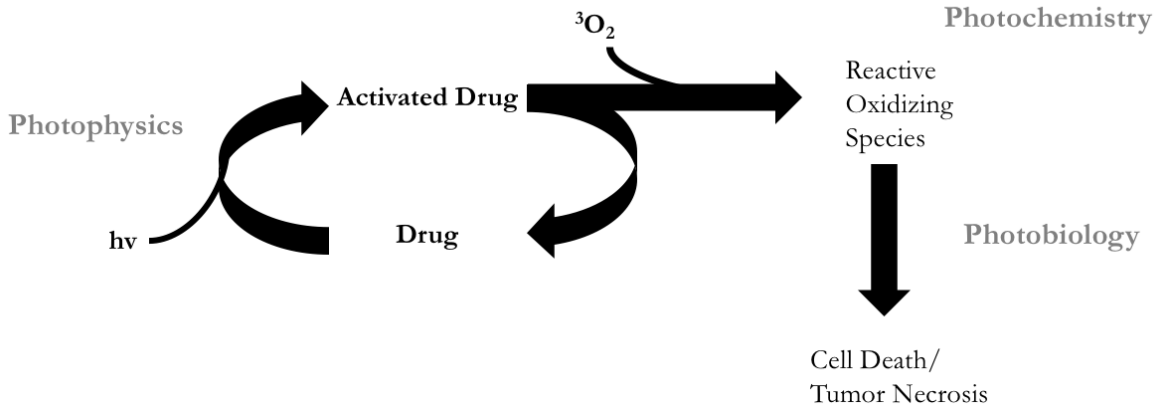

Figure 5.2: Principles of Photodynamic Therapy

Two main components of the PDT are photosensitizer and light in proper wavelength as mentioned above. Rapid clearance, chemical purity, selectivity for tumor cells, chemical and physical stability are some of the desired features of an ideal sensitizer. In the case of light, the preferred range is in 600-900 nm since hemoglobin has an effective absorption rate under 600 nm and may capture the incoming photons and at higher wavelengths, the energy will be insufficient for initiating the generation of singlet oxygen. In that therapeutic window, designing the molecules with more efficient photochemical properties forms the main interest of the research as these molecules may provide the capacity to penetrate deeper into the activating source. The efforts through achieving that goal continue with developing new systems or molecules.

Two-photon absorption (TPA) is an alternative emerging area in medical applications and getting attention by efficient absorption values in the redshifted area of the spectrum. TPA differs from one photon absorption (OPA) by doubling the wavelength and unlike OPA, it is the non-linear process of absorption of two photons simultaneously. The light intensities are close to the desired optimal threshold of cell damage and the positive aspects of 2PA-PDT are demonstrated by Collins *et al.* in the blood vessel closure in mice and by Zou *et al.* in xenograft tumors.

5.2. Methodology

5.2.1. Computational Procedure

Conformational analysis has been implied to model the photophysical properties appropriately of the two polythiophene-based dyes and the conformations assess through reproducing singlet oxygen by contemplating the relative positions of the singlet and triplet excited states. S_0, S_1 and T_1 minima geometries of the molecules have been optimized at the hybrid B3LYP exchange correlational functional with the 6-31G* basis set. Density functional theory (DFT) was selected for the optimization of the ground state geometries and The Tamm-Dancoff approximation (TDA) was employed for the excited state calculations with CAM-B3LYP/6-31+G(d,p) level of theory. All quantum chemistry calculations were carried out with the Gaussian 09 software package and Polarizable Continuum Model (PCM) were used to parametrize solvent effects for water.

In order to model the potential energy surface with the critical points, dynamic and vibrational effects were included, 20 snapshots have been sampled from Wigner distribution for absorption, fluorescence and phosphorescence spectra via Newton-X program. The vertical transitions have been convoluted with Gaussian functions of 0.2 eV full width at half maximum. The absorption spectra that corresponds to vertical transitions from the S_0 to S_1 state has been modeled by convolution of the vertical transitions from ground (S_0) state and the fluorescence spectra which is the de-excitation of singlet excited state to ground state computed by employing vertical transitions from first excited (S_1) state and the solvent is equilibrated to the excited state of interest. Phosphorescence, originates between the states of different spin multiplicity, analyzed in coherence with fluorescence spectrum. The charge transfer characteristic of the electronic transitions, by means of natural transition orbitals (NTOs), has been obtained by using Nancy_ EX software package.

Two-photon absorption (TPA) cross sections are computed at TD-DFT level (CAM-B3LYP/6-31G*) using linear response methodology as implemented by Rizzo

and co-workers by using DALTON2016 code and the cross-section values are represented in Göppert-Mayer (GM) units (10^{-50} cm^4 photon^{-1}).

Finally, to properly quantify the intersystem crossing mechanism, the interpolation coordinate is generalized between the first singlet (S_1 minima) and triplet state (T_1 minima) optimized geometries that are calculated B3LYP/6-31G* level of theory. The spin orbit coupling values have been obtained with Amsterdam Density Functional at CAM-B3LYP/DZP level.

5.2.2. Tamm-Dancoff Approximation

Tamm-Dancoff approximation is an alternative approach to TD-DFT since it has some inadequacy in extrapolating the excitation energies of the charge-transfer states and obtaining the long-range 1/R dependence on donor-acceptor distance accurately, examining the double excitations and it also some troubles in triplet instability problems [55].

Hence, ad-hoc approximations gain attention by giving more accurate results for solving the aforementioned problems. In this way, Tamm-Dancoff Approximation (TDA) is considering only positive energy electron-hole pairs and in particular, one electron pair's propagation is assumed in any time interval by reason of the interplay among electron-hole pairs at negative, and positive energies are not included [57].

The polarization functions could be presented with ab-inito Bethe-Salpeter (BS) equation and external parameters are disregarded. Moreover, TDA provides a reliable result for an unstable stable system in the calculations of singlet and triplet excitation energies and the other advantage [58] is, it has comparatively short operation period in contrast to TD-DFT. As a comprehensive approach on analyzing the excitation energies that can be presented as the solution of the generalized eigenvalue equation:

$$\begin{pmatrix} \tilde{M} & \tilde{N} \\ \tilde{N} & \tilde{M} \end{pmatrix} \begin{pmatrix} X_p \\ Y_p \end{pmatrix} = \omega_p \begin{pmatrix} 1 & 0 \\ 0 & -1 \end{pmatrix} \begin{pmatrix} X_p \\ Y_p \end{pmatrix} \tag{5.1}$$

In Equation 5.1, the amplitude vectors are Xp and Y_p [59]. In the case of the single excited configuration interaction, $\tilde{N}$ matrix is eliminated and the simplified equation is:

$$\widetilde{M}X_p = \omega_p X_p \tag{5.2}$$

ω_p, the excitation energy is defined as:

$$\omega_p = \sum_{ai}(\epsilon_a - \epsilon_i)X_{ai}^2 + \sum_{abij}\left[\langle ib||aj\rangle + B_{a_i,b_j}\right]X_{ai}X_{bj} \tag{5.3}$$

In the presence of a solvent, the total energy of excited state p;

$$G_p^{TDA} = G_{gs}^{HF} + \omega_p \tag{5.4}$$

in which G_{gs}^{HF} is the energy of the ground state and ω_p is the Tamm-Dancoff approximation excitation energy.

5.2.3. Spin Orbit Interactions

Spin orbit interactions or spin orbit coupling can be defined as the interaction of magnetic movements of spin and orbital. Energy level splitting occurs as a result of the interaction and the first-order perturbation may use for describing the shifts in orbital energies. Electrons have angular ($\overrightarrow{l}$) and spin angular momentum ($\overrightarrow{s}$)

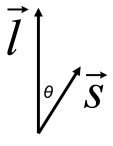

Figure 5.3: Orbital and spin angular momentum vectors

As depicted in Figure 5.3, the total momentum ($\overrightarrow{j}$) is the vector addition of the momentums:

$$\overrightarrow{j} = \overrightarrow{l} + \overrightarrow{s} \tag{5.5}$$

These magnets have the most stability in the antiparallel position and conversely, least stable while they are parallel to each other. The energy of the interaction of spin and orbital momentum is,

$$\overrightarrow{j_{max}} = \overrightarrow{l} + \overrightarrow{s} = \overrightarrow{l} + \frac{1}{2} \tag{5.6}$$

$$\overrightarrow{j_{min}} = |\overrightarrow{l} - \overrightarrow{s}| = |\overrightarrow{l} - \frac{1}{2}| \tag{5.7}$$

In the Hamiltonian operator, spin orbit coupling is introduced with an extra term:

$$\widehat{H}_{S-O} = f(r)\widehat{L}\widehat{S} \tag{5.8}$$

in which $f(r)$ term is;

$$f(r) = \frac{1}{2M^2c^2r}\frac{dV(r)}{dr} \tag{5.9}$$

and by evaluating Equation 5.3 with

$$\overrightarrow{J}^2 = (\overrightarrow{L}^2 + \overrightarrow{S}^2) \tag{5.10}$$

the term we get

$$\widehat{H}_{S-O} = \frac{1}{2}f(r)\widehat{J}^2 - \widehat{L}^2 - \widehat{S}^2 \tag{5.11}$$

Stating this

$$\widehat{J}^2 - \widehat{L}^2 - \widehat{S}^2|n, j, m_j, l, s\rangle = j(j+1) - l(l+1) - s(s+1)\hbar^2\langle f(r)\rangle \tag{5.12}$$

$$\langle n, j, m_j, l, s|\widehat{H}_{S-O}|n, j, m_j, l, s\rangle = \frac{1}{2}j(j+1) - l(l+1) - s(s+1)|\hbar^2\langle f(r)\rangle \tag{5.13}$$

$f(r)$ is not related to spin or angular momentum and expressed as,

$$\langle f(r)\rangle = \frac{Z^3}{8\pi\epsilon_0 M^2 c^2}\int_0^\infty \frac{1}{r^3}|R_{nl}(r)|^2 r^2\, dr \tag{5.14}$$

the term Z corresponds to the effective atomic number.

5.3. Results and Discussion

5.3.1. Conformational Analysis of S_1 Minima

For assessing the photophysical characteristics of the molecules, the complete set of conformers (free energy range of 10 kJ/mol) are optimized at the lowest electronic state (S_1) state (Table 5.1). The main difference between the conformers is based on the orientation of the carboxyl and cyano groups which is the probable reason for the electric repulsion. Hence, the relative positions of the energy landscapes are modeled and for quantitative analysis; spin-orbit coupling (SOC) values are compared. The minor differences in SOC values are examined in combination with the vertical excitation energies, and the outcome can be ascribed to the slight difference in their relative free energies which have virtually no effect on the cross sections. Considering the results, the lowest energy conformers are decided to use for further analysis.

Table 5.1: S_1 optimized structures of the lowest energy conformers of DTP1 and DTP2

DTP1-1	**DTP1-2**	**DTP1-3**	**DTP1-4**	**DTP1-5**
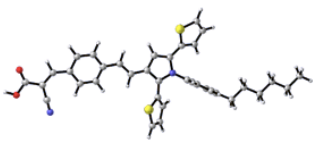	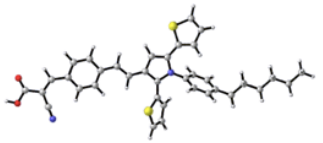	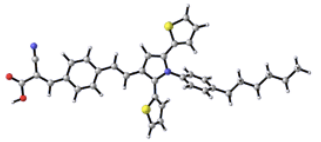	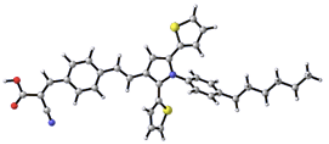	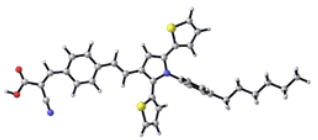
0.0	0.03	3.87	1.75	1.82
DTP2-1	**DTP2-2**	**DTP2-3**	**DTP2-4**	**DTP2-5**
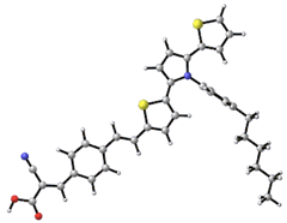	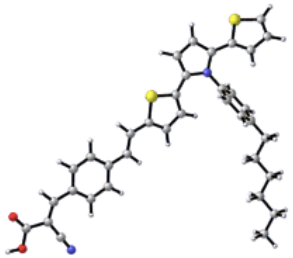	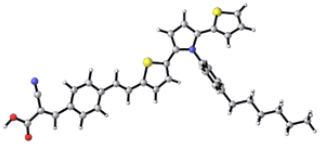	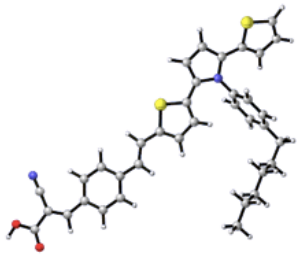	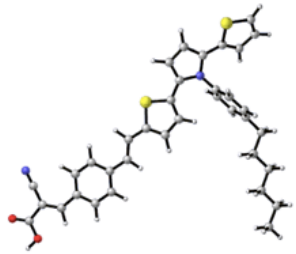
0.0	0.07	5.37	2.36	3.57

5.3.2. One and Two-Photon Absorption

Two-photon absorption has advantages over one photon excitation and has several application areas like therapeutic purposes, laser scanning, and microscopy. Considering the good TPA absorption properties of DTP dyes, one photon absorption (OPA) and two-photon absorption (TPA) spectrums have been investigated and reported in Figure 5.4. and Figure 5.5. Emission of two photons of identical frequencies resulting populating much longer wavelengths than conventional one photon absorption (OPA) at a higher intensity. Concerning the general band shapes, the resemblance is significant and almost superimposable images of each other due to the non-symmetric feature of the dyes. On the other hand, the absorption maxima for the Q-bands in the lower energy region and have less intensity than Soret bands.

The results obtained with the long-range corrected hybrid functional CAM-B3LYP in water and the absorption maxima of the dyes compatible with the experimental data, with a minor difference of only 0,01 eV for DTP2. (Experimental absorption maxima in DCM is 2,98 eV (415nm) and 2,71 eV (457nm), respectively for DTP1 and DTP2). The effect of solvent is evident that molecules appear to be slightly affected by the polar environment and the inclusion of different solvents have a moderate impact on λ_{max} values for both dyes.

The TPA absorption cross-sections also, as expected, lie in the red or near infrared region of the spectrum for both DTP1 and DTP2. TPA cross-sections are remarkably high around 1000 GM for DTP1 and 8000 GM for DTP2 due to the larger conjugation of poly-thiophene rings. The π-conjugated bridge linked with a thiophene moiety in DTP2 enhances the effect and in particular, DTP2 has the highest observed TPA intensity among the neutral compounds in the literature.

Hence, the particular analysis of natural transition orbitals (NTOs) may give an understanding of the OPA and TPA spectra. Based on the vertical excitation, acceptor (A) and donor (D) parts can change: $S_0 \rightarrow S_1$ NTOs depict A-π-D, noncentrosymmetric dipolar chromophores, and the charge transfer is obtained from thiophene moiety to

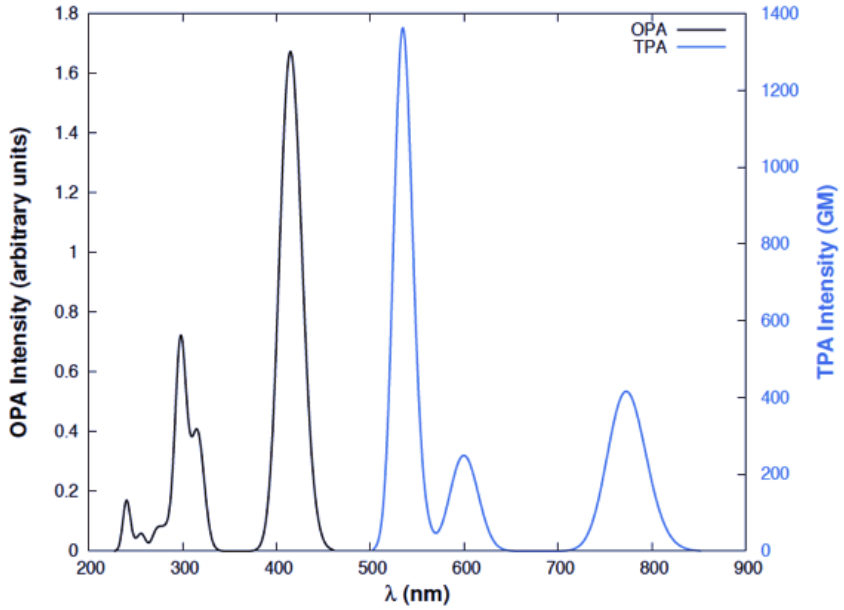

Figure 5.4: One-photon (OPA) and two-photon (TPA) absorption spectra of DTP1.

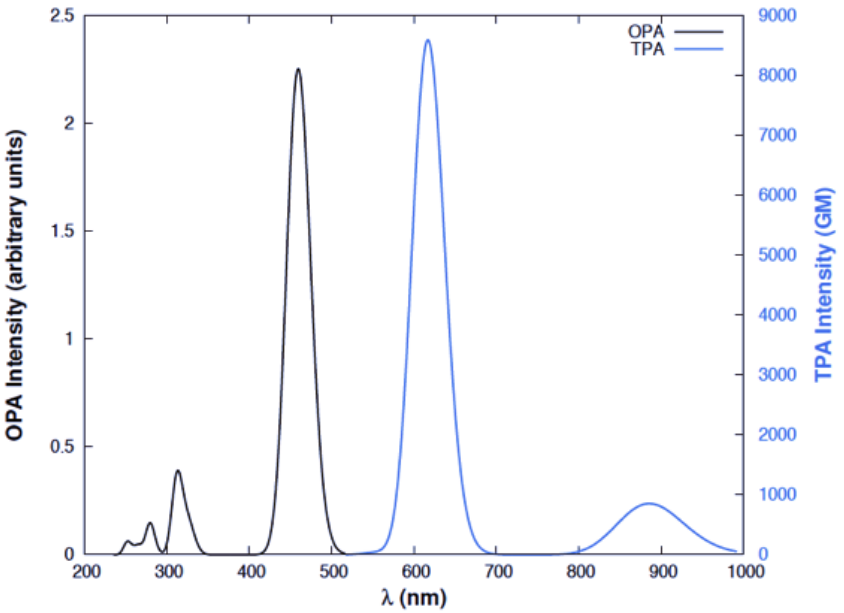

Figure 5.5: One-photon (OPA) and two-photon (TPA) absorption spectra of DTP2.

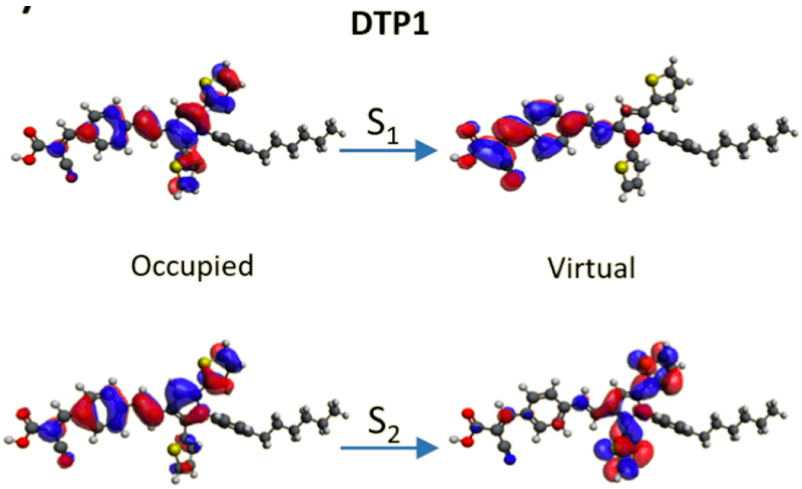

Figure 5.6: Natural transition orbitals presenting $S_0 \rightarrow S_1$ and $S_0 \rightarrow S_2$ transition for DTP1

cyano group across the backbone. As mentioned above, to maximize TPA absorption characteristic, two requirements are needed: the molecule should be centrosymmetric which will favor the second requirement; an intermediate state between the ground and final excited state. These conditions are also fulfilled for $S_0 \rightarrow S_2$ NTOs: the dyes act as almost centrosymmetric A-π-D-π-A system. In DTP1: both of centered thiophene ring behave as acceptors and bridge as a donor; on the other hand, in DTP2: two thiophene rings and the cyano group behave as acceptors, including the central phenyl moiety as the donor. DTP2 chromophore has a higher TPA cross-sections values comparing to DTP1, thanks to extended conjugation and the more centrosymmetric feature.

The inversion in the peak intensities between TPA and OPA can also be explained in the light of these findings: the $S_0 \rightarrow S_2$ ($S_0 \rightarrow S_1$) transition is much brighter than the $S_0 \rightarrow S_1$ ($S_0 \rightarrow S_2$), for TPA (OPA), nearly preserving the intensity ratio.

Coherently, there are two possible relaxation pathways for the excited molecules; one is fluorescence from S_1 state (following interval conversion, $S_2 \rightarrow S_1$) and the other one is phosphorescence from T_1 state, in the presence of intersystem crossing. The probability of intersystem crossing was evaluated by considering SOC values and the energy window between the relevant states: 4 eV was found for 20 initial geometries, generated via Wigner distribution functional around the Franck-Condon region. Two

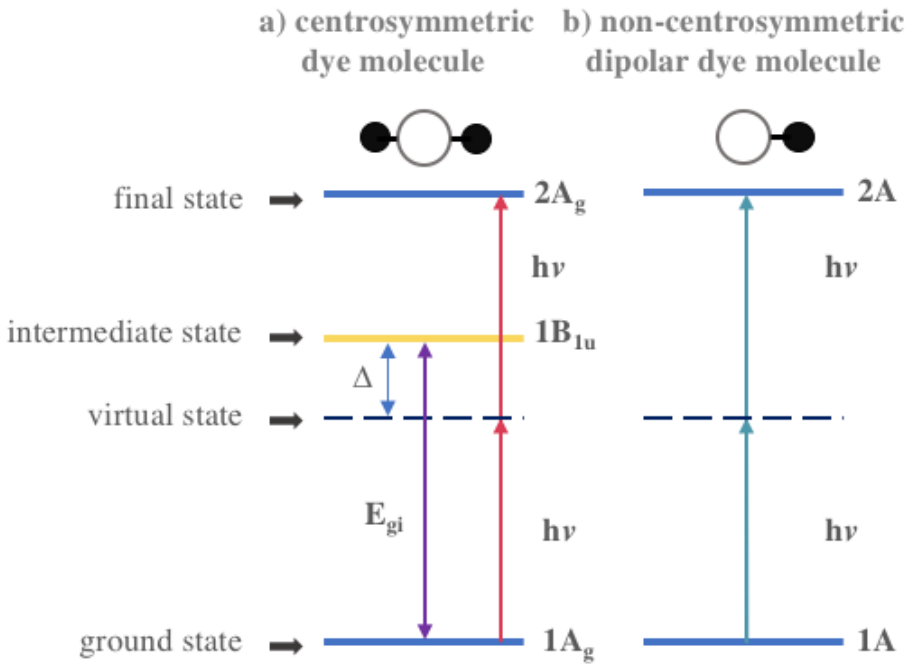

Figure 5.7: Energy level diagrams for the chromophores.

requirements need to be fulfilled for an efficient ISC: the energy difference between the involved singlet and triplet states and the SOC: the higher values represent the small energy gap between singlet-triplets and the higher probability for ISC to the triplet manifold.

Considering the energy window (Figure 5.14a,d) for both chromophores, the S_1 state is lying close to T_2 and S_2 places in between T_4 and T_5. The second requirement, SOC values are calculated for the quantitative approach for the possible cases; $S_1 \rightarrow T_2$ (Figure 5.14b,e) and $S_2 \rightarrow T_{4,5}$ (Figure 5.14c,f) and the values were smaller than 5 cm^{-1}. Therefore, one may conclude that relaxation from S_1 state is definitely more desired path than ISC, at least in the neighborhood of the Franck−Condon area.

Two possible relaxation pathways in principle should be taking into account as possible and the emission spectra for both dyes are shown in Figure 5.9 and Figure 5.10 in which they are behaving in similar. Noting that the process of geometry relaxation from both singlet and triplet electronic states does not include any vital change in the conformations of the dyes. As expected, the spin-forbidden feature of the phosphorescence resulted as a broader band shape than fluorescence with less intensity.

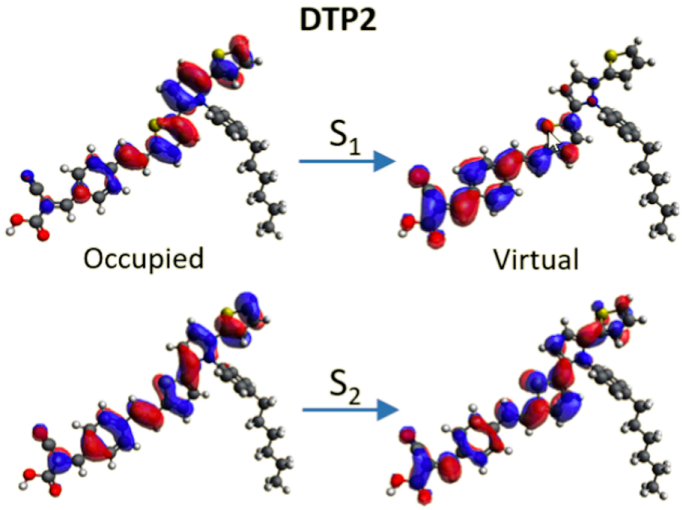

Figure 5.8: Natural transition orbitals presenting $S_0 \rightarrow S_1$ and $S_0 \rightarrow S_2$ transition for DTP2

Both spectra obtained by sampling around the relative minima (S_1 and T_1) in terms of vertical transition via Wigner distribution which is also an indirect representation of potential energy surface and as depicted in Figure 5.10: phosphorescence has a wider and smoother region comparing to fluorescence, ranging from 900nm to 3000nm. However, S_1 minimum region has a narrow and steeper character and centered around 500nm for both dyes. Coherently with the band shapes, the stroke shift is smaller for DTP2 compare to DTP1 which is around 100 nm.

Considering SOC values around S_1 minima, one may think that ISC possibility is almost non-present. On the other hand, the relevant states for ISC efficiency are close energetically, at that point, fluorescence still has a higher chance; however, based on the observations, it will be in competition with triplet population from excited singlets as being energetically feasible, but probably in a slow pace.

5.3.3. Effects of Conformations on Absorption and Emission Spectra

Looking at the conformational space for both dyes, several conformations were stated both for S_0 and S_1 minima, even the isoenergetic ones, thanks to structural flexibility. The absorption and emission spectra were obtained by convoluting the vertical excited energies of five selected geometries with a multiconformational static approach

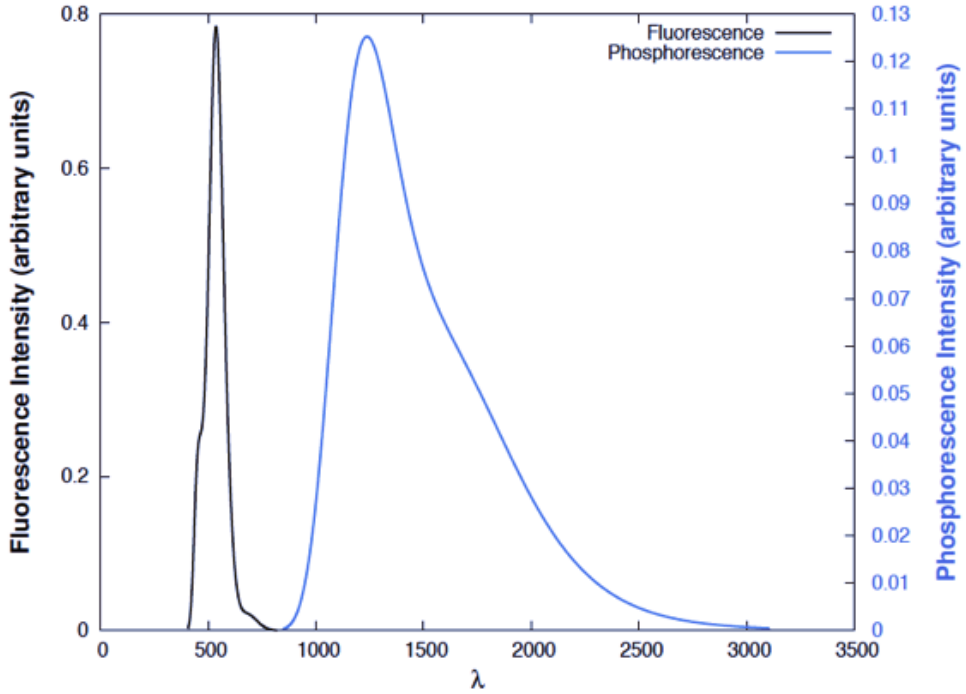

Figure 5.9: Fluorescence (black) and phosphorescence (blue) spectra of DTP1.

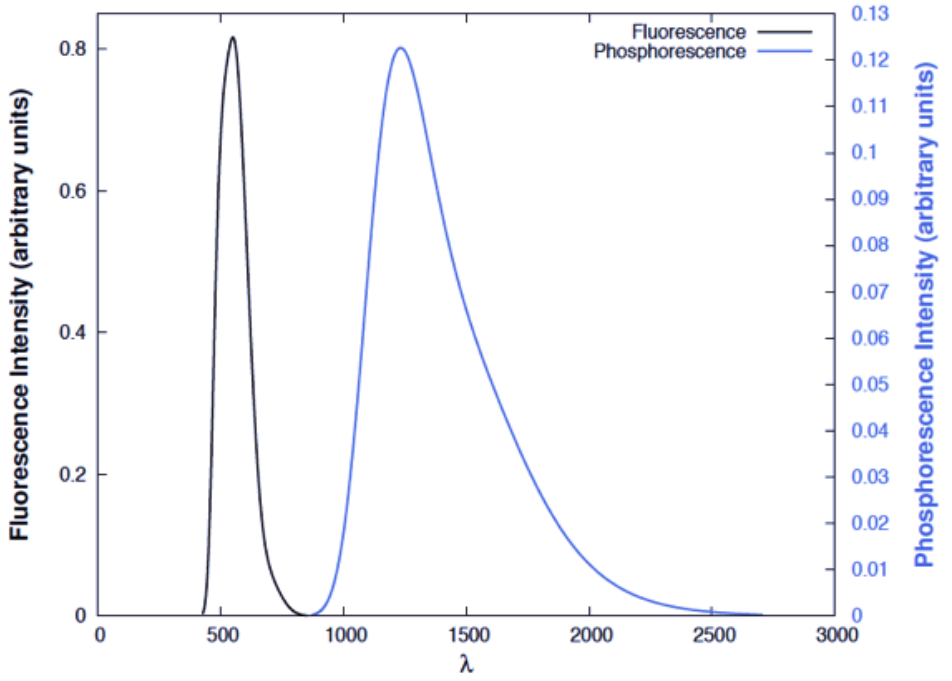

Figure 5.10: Fluorescence (black) and phosphorescence (blue) spectra of DTP2.

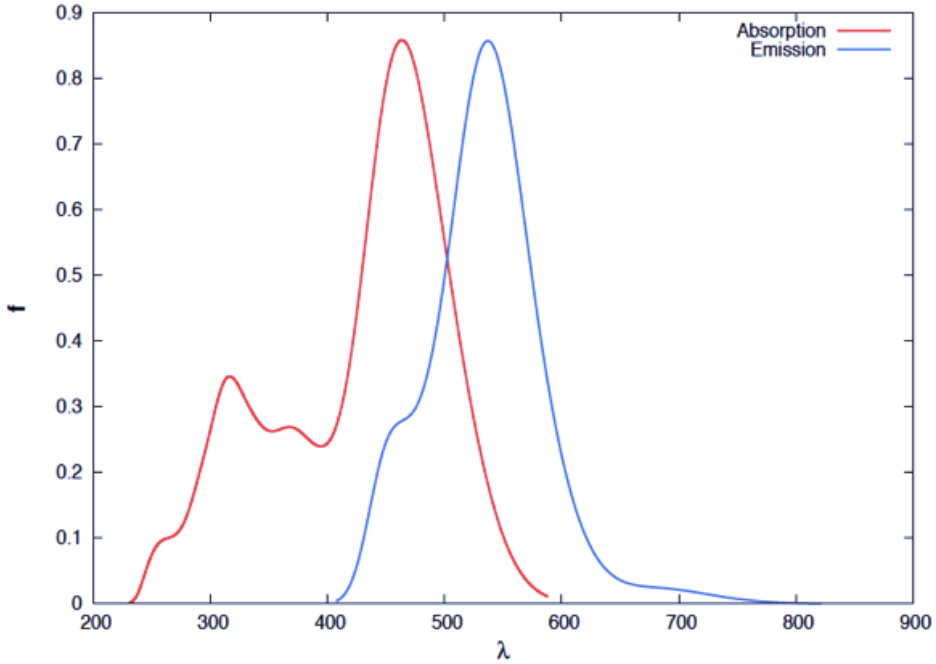

Figure 5.11: Absorption (red) and fluorescence (blue) spectra of DTP1.

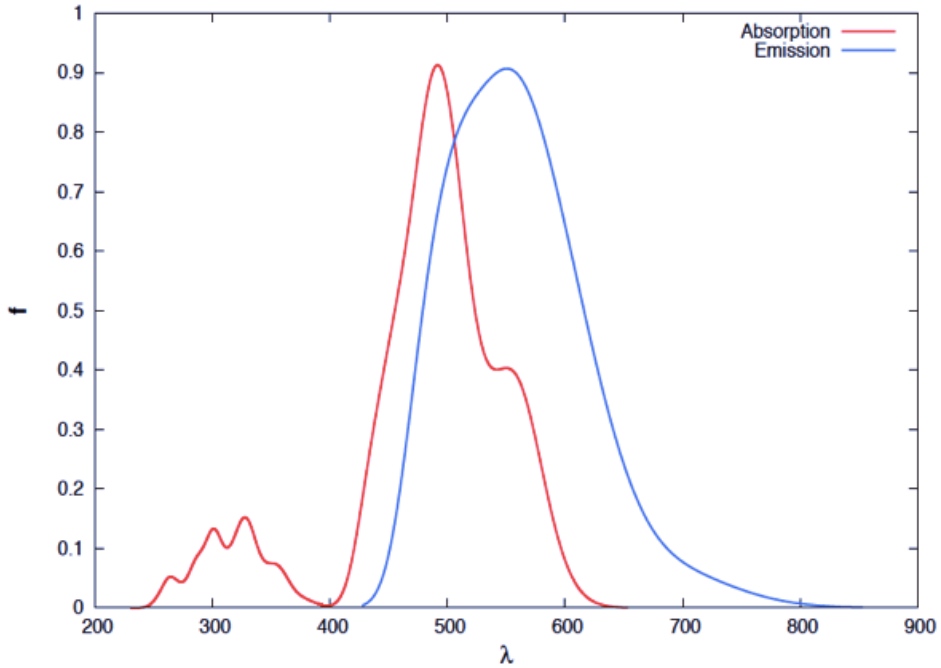

Figure 5.12: Absorption (red) and fluorescence (blue) spectra of DTP2.

and presented in Figure 5.11 and Figure 5.12. Comparing to the absorption spectra of a single conformational approach, involving the presence of vibrational effects, almost the same band shape was obtained as well as the fluorescence. In the presence of vibrational environment, the λ maxima (absorption and fluorescence) has revealed red-shifted values regarding static analysis for a range of 40-50 nm which is reasonable. Thus, the methodology confirms the photophysical characteristics can be reproduced by each strategy. On the other hand, the inclusion of the vibrational environment on the lowest energy conformation matches the experimental findings in a more realistic way. The reason behind this should be the high amplitude out-of-plane normal modes, low frequencies are reproduced with this method which breaks the conjugation patterns of excited and ground states.

5.3.4. Intersystem Crossing Pathways

As with the excitation of the molecules to the probable states S_1 and S_2 with OPA and TPA, for the further analysis of relaxation pathways of the dyes; the potential energy surfaces and the relation between the states of interest are investigated (Figure 5.13). At first, the energy landscape between S_1 and T_1 minimum is searched for the probable singlet-triplet crossing and there is a small chance for a direct crossing to T_1 state. Despite having an energy gap around 0.5 eV and the moderate SOC value (around 0.2 cm^{-1}), there may be a possibility for intersystem crossing, but with a slow channel. S_1 is also energetically close to T_2, but the energy of the singlet state is lower.

Furthermore, indirect paths for the ISC system is investigated with S_2 state which is energetically degenerate with T_3 state for both dyes leading the path to be unfavorable and that is also correlated with the low spin-orbit coupling values. When the electronically excited states are close enough in energy, even in the presence of low spin-orbit interaction, intersystem crossing may occur. On the other hand, $S_2 \rightarrow T_3 \rightarrow T_2 \rightarrow T_1$ cascade is another channel for relaxation back to the ground state with a fast-internal conversion among the triplet states. Beyond that, the energy difference between S_2 and S_1 is around 1.3- 1.5 eV and one may extrapolate that ISC mechanism may also start with an internal conversion. The relaxation pathway may start from

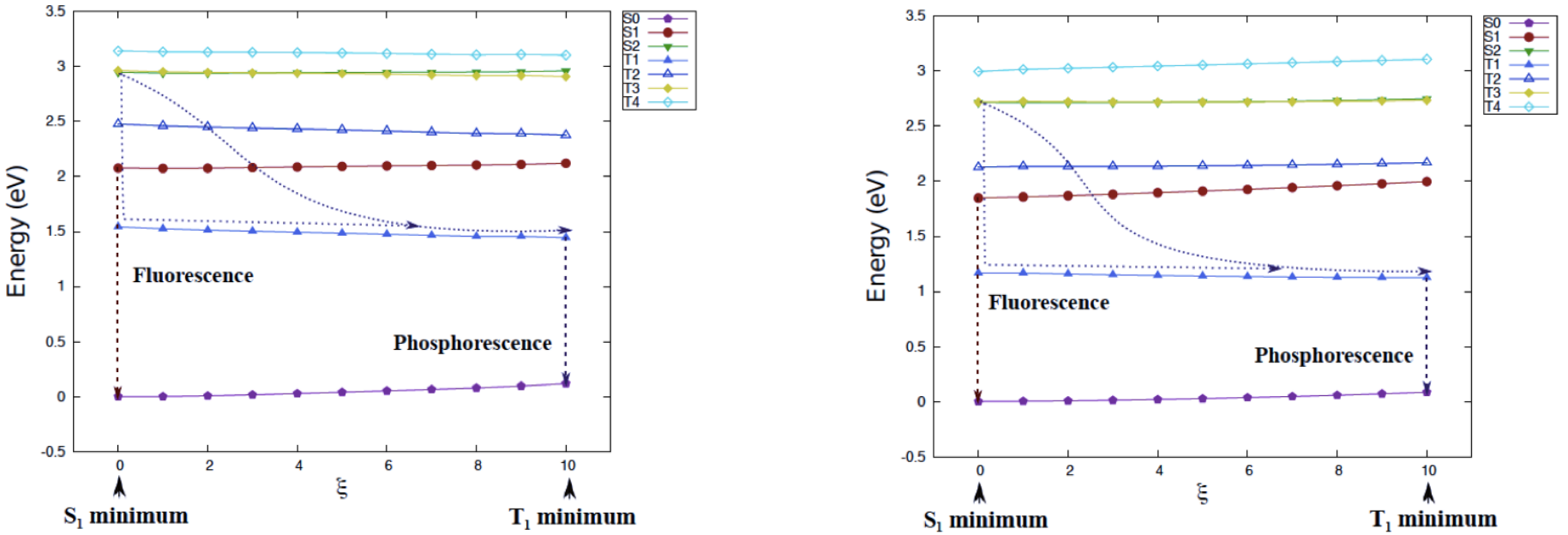

Figure 5.13: Simplified pathway (along an interpolation coordinate) between S_1 minima and T_1 minima, DTP1 (left) and DTP2 (right) (B3LYP/6-31G(d) with IEF-PCM in water).

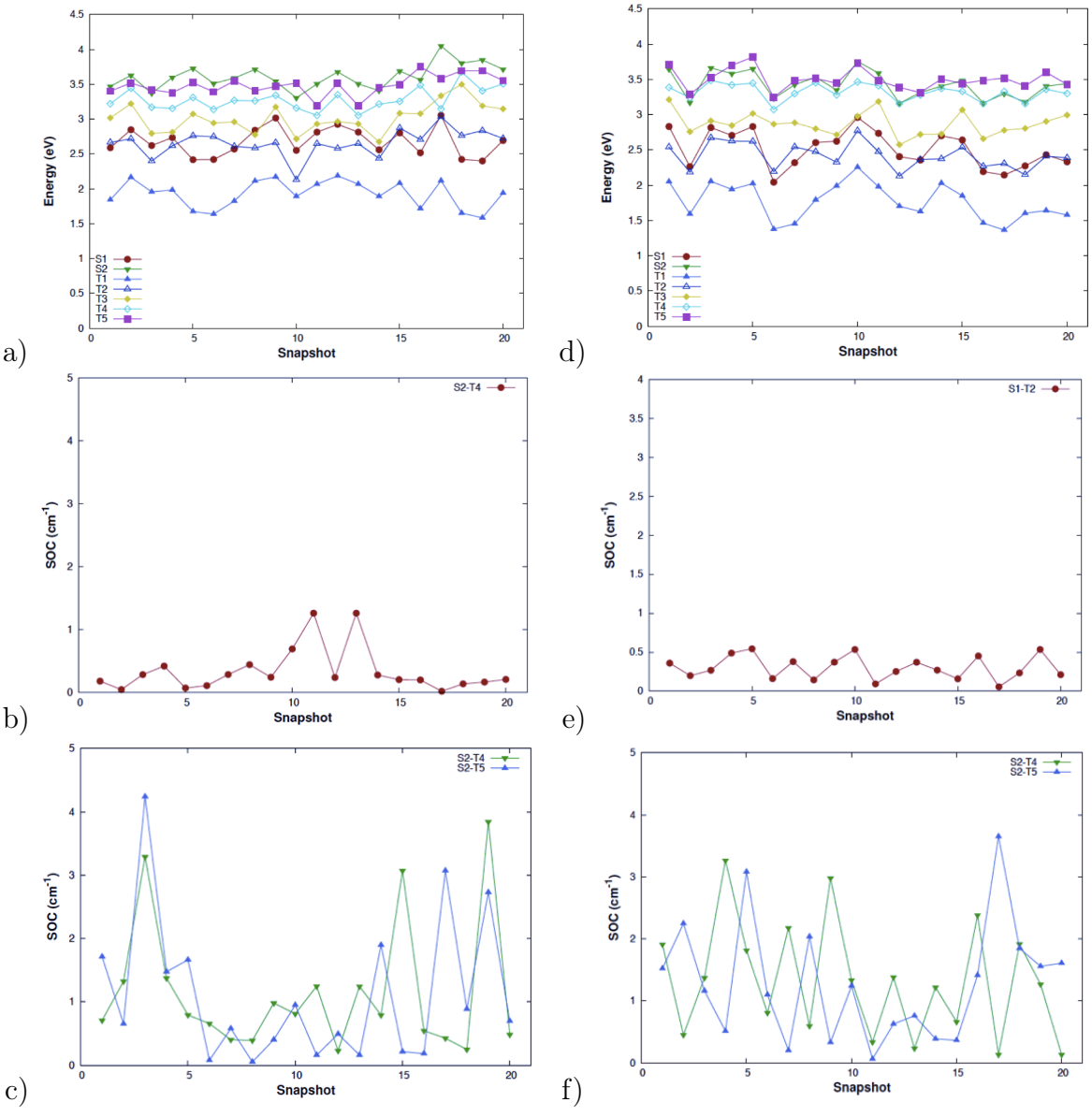

Figure 5.14: DTP1 (left) and DTP2 (right) energies of the lowest two excited singlet and five triplet states via Wigner distribution around S_0

both through direct $S_1 \rightarrow T_1$ or indirect $S_2 \rightarrow T_3 \rightarrow T_2 \rightarrow T_1$ triplet manifold population. Both dyes show a similar pattern in relative energies of states of interest and pathways that leads to similar conclusions.

When the compounds reached the triplet manifold, in T_1 region, the relaxation to the ground state will be followed by phosphorescence. Since it is an unfavorable process (because of the spin forbidden feature), in principle, the slow time scale may favor the generation of singlet oxygen. As considering the band gap of $^3O_2 \rightarrow {}^1O_2$ is 0.97 eV by infrared emission, a probable energy transfer could be forecasted from excited T_1 state to molecular oxygen for DTP1 and DTP2.

5.3.5. Conclusion

In the second part of the study, the non-linear absorption feature of the organic dyes and the photophysical behavior were assessed. Especially, two-photon absorption properties of the dyes were extensively studied with high state-of-art modeling methodologies. Two organic chromophores presented remarkably high cross-section values comparing to commercialized TPA absorbers for both excited states, $S_0 \rightarrow S_1$ (around 1000 GM for DTP2) and $S_0 \rightarrow S_2$ (almost 8000 GM for DTP2).

The probable pathways leading to ISC and the triplet manifold population were examined with two strategies: (i) creating a pathway (interpolation coordinate) among the relevant states on the potential energy surfaces in order to provide the energy difference and the critical point; (ii) the spin-orbit coupling is applied with the aim of defining a quantitative measurement for ISC mechanism. The results pointed a possible intersystem crossing, probably slow and the organic dyes could be ideal candidates for photodynamic therapy applications.

6. FUTURE REMARKS

Two recently synthesized poly-thiophene dyes (DTP1 and DTP2) were assessed through their photophysical and photochemistry properties in terms of state-of-art computational methodologies. The excited state nature of two potentially promised photosensitizers was extensively studied in two hot topics; dye sensitized solar cells and singlet oxygen generation.

The study of linear and non-linear approach with the combination of conformational effects and in the presence of the vibrational environment were included in the research of optical features. The electronic density re-organization revealed that the dyes were not exactly compatible in using DSSC due to moderate charge separation. On the other hand, the spectacularly high two photon absorption values in the red and infrared region of the spectrum (for $S_0 \rightarrow S_1$ and $S_0 \rightarrow S_2$) further triggered the study towards biological applications in means of photodynamic therapy. Relatively higher spatial resolution than conventional methods is the desired outcome of TPA which increase the feasibility of reaching deeper regions of the tumors. The high cross section values construct the photosensitizers as potential candidates for 2PE-PDT drugs. Considering the ideal properties and for this reason, the study is extended to singlet and triplet state characteristics, investigating and understanding of singlet oxygen generation. A multiconformational static approach and a singleconformation dynamic approach were represented methodologically. The peculiar feature of the photosensitizers act as noncentrosymmetric (A-π-D) for $S_0 \rightarrow S_1$ and centrosymmetric (A-π-D-π-A) for $S_0 \rightarrow S_2$ excitations lead to the possibility of intersystem crossing and triplet manifold population even in a slow pace. Hence, the high probability of producing singlet oxygen is shown that the dyes particularly suited for PDT applications. Medical studies are also required for the dark toxicity and bioavailability aspects; however, this is clearly beyond the scope of the current work.

The presented theoretical studies propose a quite complete picture of the photochemistry and photophysics of the chromophores. In the future, the study will be

extended to photosensitization properties of the molecules towards biological membranes.

REFERENCES

1. Sun, S.-S. and L. R. Dalton, *Introduction to Organic Electronic and Optoelectronic Materials and Devices*, CRC Press, Boca Raton, 2016.

2. O'Regan, M., B.and Gra̋tzel, "A Low-Cost,High-Efficiency Solar Cell Based on Dye-Sensitized Colloidal TiO_2 Films.", *Nature*, p. 737−740, 1991.

3. Hagfeldt, A., G. Boschloo, L. Sun, L.Kloo and H. Pettersson, "Dye-Sensitized Solar Cells.", *Chem. Rev.*, p. 6595−6663, 2010.

4. Tian, H., Boschloo, G. Hagfeldt and E. A., *Molecular Devices for Solar Energy Conversion and Storage*, Springer: Berlin, 2018.

5. Frischmann, P. D., K. Mahata and F. Würthner, "Powering the future of molecular artificial photosynthesis with light-harvesting metallosupramolecular dye assemblies", *Chemical Society Reviews*, Vol. 42, No. 4, pp. 1847–1870, 2013.

6. Astumian, R. D., S. Mukherjee and A. Warshel, "The Physics and Physical Chemistry of Molecular Machines", *ChemPhysChem*, pp. 1719–1741, 2016.

7. Colasson, B., A. Credi and G. Ragazzon, "Light-driven molecular machines based on ruthenium(II) polypyridine complexes: Strategies and recent advances", *Coordination Chemistry Reviews*, Vol. 325, pp. 125–134, 2016.

8. Browne, W. R. and B. L. Feringa, "Making molecular machines work", *Nature nanotechnology*, Vol. 1, No. 1, pp. 25–35, 2006.

9. Nyman, E. S. and P. H. Hynninen, "Research advances in the use of tetrapyrrolic photosensitizers for photodynamic therapy", *Journal of Photochemistry and Photobiology B: Biology*, Vol. 73, No. 1-2, pp. 1–28, 2004.

10. Ethirajan, M., Y. Chen, P. Joshi and R. K. Pandey, "The role of porphyrin chemistry in tumor imaging and photodynamic therapy", *Chemical Society Reviews*, Vol. 40, No. 1, pp. 340–362, 2011.

11. Z.Huang and H.Xu and A.D.Meyers and A.L.Musani and L.Wang, R.Tagg and A.B.Barqawi and Y.K.Chen, "Photodynamic Therapy for Treatment of Solid Tumor", *Technol. Cancer Res. Treat.*, Vol. 7, No. 4, p. 309, 2008.

12. Li, Z. and K. B. Grant, "DNA photo-cleaving agents in the far-red to near-infrared range - A review", *RSC Advances*, Vol. 6, No. 29, pp. 24617–24634, 2016.

13. Allison, R. R. and K. Moghissi, "Oncologic photodynamic therapy: Clinical strategies that modulate mechanisms of action", *Photodiagnosis and Photodynamic Therapy*, Vol. 10, No. 4, pp. 331–341, 2013.

14. Pawlicki, M., H. A. Collins, R. G. Denning and H. L. Anderson, "Two-photon absorption and the design of two-photon dyes", *Angewandte Chemie - International Edition*, Vol. 48, No. 18, pp. 3244–3266, 2009.

15. Lachaud, F., C. Jeandon, A. Monari, X. Assfeld, M. Beley, R. Ruppert and P. C. Gros, "New Dyads Using (Metallo)porphyrins as Ancillary Ligands in Polypyridine Ruthenium Complexes. Synthesis and Electronic Properties.", *Dalton Trans.*, p. 12865−12871., 2012.

16. Pastore, M., T. Duchanois, L. Liu, A. Monari, X. Assfeld, S. Haacke and P. C. Gros, "Interfacial Charge Separation and Photovoltaic Efficiency in Fe(II)-Carbene Sensitized Solar Cells.", *Phys. Chem. Chem. Phys.*, p. 28069−28081., 2016.

17. Zhou, H., F. Zhou, S. Tang, P. Wu, Y. Chen, Y. Tu, J. Wu and Y. Tian, "Two-photon absorption dyes with thiophene as π electron bridge: Synthesis, photophysical properties and optical data storage", *Dyes and Pigments*, Vol. 92, No. 1, pp. 633–641, 2012.

18. Zheng, Y. C., M. L. Zheng, K. Li, S. Chen, Z. S. Zhao, X. S. Wang and X. M. Duan, "Novel carbazole-based two-photon photosensitizer for efficient DNA photocleavage in anaerobic condition using near-infrared light", *RSC Advances*, Vol. 5, No. 1, pp. 770–774, 2015.

19. Dantola, M. L., L. O. Reid, C. Castaño, C. Lorente, E. Oliveros and A. H. Thomas, "Photosensitization of Peptides and Proteins by Pterin Derivatives.", *Pteridines*, Vol. 28, 2017.

20. Epe, B., "DNA Damage Spectra Induced by Photosensitization.", *Photochem. Photobiol. Sci.*, p. 98−106, 2012.

21. Cuquerella, M. C., V. Lhiaubet-Vallet, J. Cadet and M. A. Miranda, "Benzophenone photosensitized DNA damage", *Accounts of Chemical Research*, Vol. 45, No. 9, pp. 1558–1570, 2012.

22. Sharmoukh, W., A. Attanzio, E. Busatto, T. Etienne, S. Carli, A. Monari, X. Assfeld, M. Beley, S. Caramori and P. C. Gros, "2,5-Dithienylpyrrole (DTP) as a donor component in DTP–π–A organic sensitizers: photophysical and photovoltaic properties", *RSC Advances*, Vol. 5, No. 6, pp. 4041–4050, 2015.

23. Parr, R. G. and T. Weitao, *Density Functional Theory of Atoms and Molecules*, Oxford University Press, 1989.

24. Becke, A. D., "A new mixing of Hartree-Fock and local density-functional theories", *The Journal of Chemical Physics*, Vol. 98, No. 2, pp. 1372–1377, 1993.

25. Becke, A. D., "Density Functional Exchange Energy Approximation with Correct Asymptotic Behavior", *Physical Review A*, , No. 6, p. 3098–3100, 1988.

26. Walker, B., A. B. Tamayo, X.-D. Dang, P. Zalar, J. H. Seo, A. Garcia, M. Tantiwiwat and T.-Q. Nguyen, "Nanoscale Phase Separation and High Photovoltaic Efficiency in Solution-Processed, Small-Molecule Bulk Heterojunction Solar Cells",

Advanced Functional Materials, , No. 19, p. 3063–3069, 2009.

27. Lee, C., Y. Weitao and G. R. Parr, "Development of the Colle-Salvetti Correlation Energy Formula into a Functional of the Electron Density", *Physical Review B*, , No. 2, p. 785–789, 1988.

28. Becke, A. D., "Density-functional thermochemistry. III. The role of exact exchange", *The Journal of Chemical Physics*, Vol. 98, No. 7, pp. 5648–5652, 1993.

29. Pauling, L., "The Nature of the Chemical Bond. IV. The Energy of Single Bonds and the Relavitve Electronegativity of Atoms", *Journal of the American Chemical Society*, , No. 9, p. 3570–3582, 1932.

30. Tapia, B. J., *Solvent Effects and Chemical Reactivity*, Kluwer Academic Publishers, 1984.

31. Cramer, J. C. and D. G. Truhlar, *Implicit Solvation Models: Equilibria, Structure, Spectra, and Dynamics*, 8, Chemical Reviews, 1999.

32. Tomasi, J., B. Mennucci and R. Cammi, *Quantum Mechanical Continuum Solvation Models*, 8, Chemical Reviews, 2005.

33. Wigner, E., "On the quantum correction for thermodynamic equilibrium", *Physical Review*, Vol. 40, No. 5, pp. 749–759, 1932.

34. Perdew, J. P., K. Burke and M. Ernzerhof, "Generalized Gradient Approximation Made Simple", *Physical Review Letters*, pp. 3865–3868, 1996.

35. Becke, A., "B3LYP", *The Journal of Chemical Physics*, pp. 5648–5652, 1993.

36. Yanai, T., D. P. Tew and N. C. Handy, "A new hybrid exchange-correlation functional using the Coulomb-attenuating method (CAM-B3LYP)", *Chemical Physics Letters*, pp. 51–57, 2004.

37. Zhao, Y. and D. G. Truhlar, "M062X and M06", *Theoretical Chemistry Accounts*, pp. 215–241, 2008.

38. Bostan, A., A. V. Gheorge and V. Dulgheru, *Resilient Energy Systems[U+202F]: Renewables: Wind, Solar, Hydro*, Springer Dordrecht Heidelber, New York London, 2013.

39. Kamat, P. V., "Meeting the Clean Energy Demand: Nanostructure Architectures for Solar Energy Conversion", *The Journal of Physical Chemistry C*, pp. 2834–2860, 2007.

40. Chapin, D. M., C. S. Fuller and G. L. Pearson, "A New Silicon p-n Junction Photocell for Converting Solar Radiation into Electrical Power", *J. Appl. Phys.*, 1954.

41. Goetzberger, A. and C. Hebling, "Photovoltaic materials, past, present, future", *Solar Energy Materials and Solar Cells*, Vol. 62, No. 1, pp. 1–19, 2000.

42. Saga, T., "Advances in crystalline silicon solar cell technology for industrial mass production", *NPG Asia Materials*, Vol. 2, No. 3, pp. 96–102, 2010.

43. Frisch, M. J., G. W. Trucks, H. B. Schlegel, G. E. Scuseria, M. A. Robb, J. R. Cheeseman and G. S. *et al.*, *Gaussian 09 Revision E.01*, Gaussian Inc., Wallingford CT, 2009.

44. Etienne, T., X. Assfeld and A. Monari, "Toward a quantitative assessment of electronic transitions, charge-transfer character", *Journal of Chemical Theory and Computation*, Vol. 10, No. 9, pp. 3896–3905, 2014.

45. Sengul, O., E. B. Boydas, M. Pastore, W. Sharmouk, P. C. Gros, S. Catak and A. Monari, "Probing optical properties of thiophene derivatives for two-photon absorption", *Theoretical Chemistry Accounts*, Vol. 136, No. 6, 2017.

46. Patrice, T., *Photodynamic Therapy*, The Royal Society of Chemistry, 2003.

47. 0.Raab, "Ueber die Wirkung Fluorescierenden Stoffe auf Infusorien.", *Z. Biol.*, Vol. 39, pp. 524–546, 1900.

48. von Tappeiner, H., "Ueber die Wirkung fluorescierenden Stoffe auf Infusiorien nach Versuchen von 0.Raab.", *Munch Med. Wochenschr.*, Vol. 47, p. 5., 1900.

49. Scherer, H. and A. D., "Chemical-physiological", *Chem. Pharm*, 1841.

50. Lipson, R. and E. Baldes, "The photodynamic properties of a particular haematoporphyrin derivative.", *Arch. Dermatol.*, Vol. 82, pp. 508–516, 1960.

51. S. Schwartz, H. V., K. Absolon, "Some relationship of porphyrins, X-rays and tumors.", *Univ. Minn. Med. Bull.*, Vol. 27, pp. 1–37, 1955.

52. Dougherty, T., "A brief history of clinical photodynamic therapy development at Roswell Park Cancer Institute", *J. Clin. Laser Med. Surg.*, Vol. 14, pp. 219–221, 1996.

53. Collins, H. A., M. Khurana, E. H. Moriyama, A. Mariampillai, E. Dahlstedt, M. Balaz, M. K. Kuimova, M. Drobizhev, V. X. Yang, D. Phillips, A. Rebane, B. C. Wilson and H. L. Anderson, "Blood-vessel closure using photosensitizers engineered for two-photon excitation", *Nature Photonics*, Vol. 2, No. 7, pp. 420–424, 2008.

54. Zou, Q., H. Zhao, Y. Zhao, Y. Fang, D. Chen, J. Ren, X. Wang, Y. Wang, Y. Gu and F. Wu, "Effective Two-Photon Excited Photodynamic Therapy of Xenograft Tumors Sensitized by Water-Soluble Bis(arylidene)cycloalkanone Photosensitizers", *Journal of Medicinal Chemistry*, Vol. 58, No. 20, pp. 7949–7958, 2015.

55. Dreuw, A., J. L. Weisman and M. Head-Gordon, "Long-range charge-transfer excited states in time-dependent density functional theory require non-local ex-

change", *Journal of Chemical Physics*, Vol. 119, No. 6, pp. 2943–2946, 2003.

56. Elliott, P., S. Goldson, C. Canahui and N. T. Maitra, "Perspectives on double-excitations in TDDFT", *Chemical Physics*, Vol. 391, No. 1, pp. 110–119, 2011.

57. Grüning, M., A. Marini and X. Gonze, "Exciton-plasmon states in nanoscale materials: Breakdown of the tamm-dancoff approximation", *Nano Letters*, Vol. 9, No. 8, pp. 2820–2824, 2009.

58. Bai, Z., J. Demmel, J. Dongarra, A. Ruhe and H. van der Vorst, *Templates for the solution of algebraic eigenvalue problems: a practical guide*, SIAM, 2000.

59. McWeeny, R., *Methods of molecular quantum mechanics*, Academic press, 1992.

60. Sengul, O., M. Marazzi, A. Monari and S. Catak, "Photophysical Properties of Novel Two-Photon Absorbing Dyes: Assessing Their Possible Use for Singlet Oxygen Generation", *Journal of Physical Chemistry C*, 2018.

APPENDIX A: ARTICLES

A.1. Probing Optical Properties of Thiophene Derivatives for Two-Photon Absorption

A full-text version of the article regarding part I is given in this section.

Theor Chem Acc (2017) 136:67
DOI 10.1007/s00214-017-2094-y

REGULAR ARTICLE

Probing optical properties of thiophene derivatives for two-photon absorption

Ozlem Sengul[1] · Esma Birsen Boydas[1] · Mariachiara Pastore[2,3] · Walid Sharmouk[4] · Philippe C. Gros[5,6] · Saron Catak[1] · Antonio Monari[2,3]

Received: 25 January 2017 / Accepted: 18 April 2017 / Published online: 12 May 2017

Abstract We report a state-of-the-art characterization of the linear and nonlinear optical properties of two recent synthesized organic dyes based on the 2,5-dithienylpyrrole motifs. In particular after a careful conformational search was performed, the absorption spectra have been obtained at time-dependent density functional theory level taking into account vibrational and dynamical effects via a Wigner exploration of the potential energy surface. Furthermore, the excited state topology and electronic density reorganization have been characterized using natural transition orbitals and the charge transfer character quantified through recent developed descriptors, also allowing for the rationalization of the poor interfacial electron injection properties exhibited by the dyes when grafted on TiO_2 surfaces. Finally, two-photon absorption spectra have been calculated, extremely high cross sections have been obtained in the infrared region paving the way to the possible exploitation of the previous dyes for the development of photoactive smart materials or photodynamic therapy.

Keywords Two-photon absorption (TPA) · 2,5-Dithienylpyrrole (DTP) · Time-dependent density functional (TD-DFT) · Vibrational resolved spectra

1 Introduction

The impressive advancement in the control of light-induced function at the molecular level has triggered a spectacular development of light-active molecular materials covering a broad range of applications. As a non-exhaustive example, one can cite molecular photocatalysis [1–3], or smart materials based on light-triggered optical switch leading to molecular machines [4–6]. The latter development has most notably been awarded the Nobel Prize in Chemistry in 2016 [7]. Optically active compounds and dyes have also found successful applications in the field of solar energy conversion as light harvesting components in the dye-sensitized

Published as part of the special collection of articles derived from the 10th Congress on Electronic Structure: Principles and Applications (ESPA-2016).

Ozlem Sengul and Esma Birsen Boydas have contributed equally and have to be regarded as joint first authors.

Electronic supplementary material The online version of this article (doi:10.1007/s00214-017-2094-y) contains supplementary material, which is available to authorized users.

✉ Saron Catak
saron.catak@boun.edu.tr

✉ Antonio Monari
antonio.monari@univ-lorraine.fr

[1] Department of Chemistry, Bogazici University, Bebek, Istanbul 34342, Turkey

[2] Théorie-Modélisation-Simulation, SRSMC, Université de Lorraine – Nancy, Boulevard Des Aiguillettes, Vandoeuvre-lès-Nancy, Nancy, France

[3] Théorie-Modélisation-Simulation, SRSMC, CNRS, Boulevard Des Aiguillettes, Vandoeuvre-Lès-Nancy, Nancy, France

[4] Department of Inorganic Chemistry, National Research Centre, Dokki, Giza 12622, Egypt

[5] Hecrin SRSMC, Université de Lorraine – Nancy, Boulevard des Aiguillettes, Vandoeuvre-Lès-Nancy, Nancy, France

[6] Hecrin SRSMC, CNRS, Boulevard des Aiguillettes, Vandoeuvre-Lès-Nancy, Nancy, France

Figure A.1: Article 1.

solar cells (DSSCs) [8], developed in 1991 by Grätzel and O'Regan [9] and recently arrived to full commercialization.

Furthermore, dyes absorbing in the visible or infrared are also exploited for therapeutic purposes such as for instance the photodynamic therapy [10–13] used in antiviral [14], antimicrobial [15] and anticancer [16, 17] treatments. This strategy notably allows a significant reduction in the drug side effects by its specific spatial activation achieved through irradiation.

In order to increase the efficiency and the applicability of light-active materials and compounds, one should seek high intensity absorption at long wavelengths. Indeed, red or infrared light is much more penetrating than the shorter wavelengths, especially in biological tissues. In order to allow the treatment of lesions located deeper than the epidermis layer absorption in the so-called therapeutic window (600–800 nm) [18] is needed. In addition with red light photons, being less energetic, the possibility of collateral photodamages is strongly reduced.

Different strategies have been developed to allow for efficient red light absorption such as extended π-conjugation or the combination of π-bridged donor acceptor molecules (D-π-A). A promising alternative consists in the exploitation of nonlinear optical properties and particular two-photon absorption (TPA) phenomena [19–21]. If we consider irradiation by a monochromatic laser source, the energy needed by the photon to resonate with the chromophore and induce electronic transition will be half the excitation energy, as a consequence absorption wavelength will be doubled. Furthermore since TPA is a nonlinear phenomenon, the absorption probability will depend on the square of the light source intensity, in contrast to the linear dependence of one-photon absorption. Hence, absorption, and light activation, will be restricted only to the focal region of the laser source allowing for an optimal spatial resolution definitively desired in medical, or high technology, applications.

Different empirical or theoretical rules have been developed in the last years to rationalize the relationship between chromophores structure and TPA intensity (cross section). For instance, centrosymmetric molecules such as donor-π-acceptor-π-donor (D-π-A-π-D) [22] give generally high cross section for the $S_0 \rightarrow S_2$ transition. Polythiophenes structures have also been recognized as efficient TPA absorber [23] as confirmed both experimentally [24] and computationally [25].

In the past, we reported the synthesis and the characterization of two poly-thiophene-based dyes 2,5-dithienylpyrrole: DTP1 and DTP2 (Scheme 1; Fig. 1) [26]. The two D-π-A chromophore were designed to provide reasonable light-induced charge transfer to be exploited as DSSC sensitizers. The all-organic devices were assembled by TiO_2 sensitization and their performance measured, despite of good absorption properties and surface coverage, the produced photocurrent was relatively low, suggesting non-optimal interfacial electron separation and injection [26].

Taken into account the good optical properties of the DTP dyes, we perform an extensive state-of-the-art modeling investigation of their linear and nonlinear optical spectroscopy. This includes the sampling of their conformational space taking into account the dynamic and vibrational effects on the optical properties. As recently shown in a number of diverse applications [27–30], dynamic effects can be crucial especially in the case of large-scale low-frequency vibration, such as out-of-plane bending of conjugated rings. Moreover, such effects can be efficiently included by semiclassical molecular dynamics or hessian-based (Wigner) sampling of the ground state potential energy surface [25, 31]. The topological analysis of the excited states density reorganization, also performed via the use of newly developed charge transfer descriptors [32–34], allows for rationalizing the rather poor interfacial charge separation. In addition to the one-photon absorption, we also report the calculated TPA spectra, which show remarkably high cross sections in the infrared region, thus making our two dyes good candidates for nonlinear optical applications.

2 Computational methodology

A conformational analysis was performed on both dyes in order to obtain the most stable geometries. Hybrid B3LYP [35] and meta-hybrid GGA M06-2X [36] functionals were used for ground state optimizations. Both ground and excited states were calculated using the Gaussian09 [37]

Scheme 1 Chemical formula of the DTP1 and DTP2 molecules

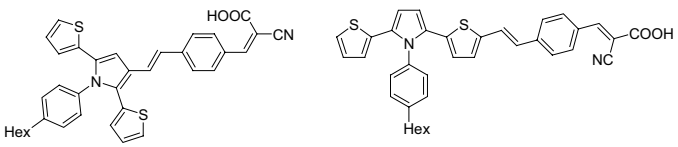

DTP1 DTP2

Figure A.1. Article 1. (cont.)

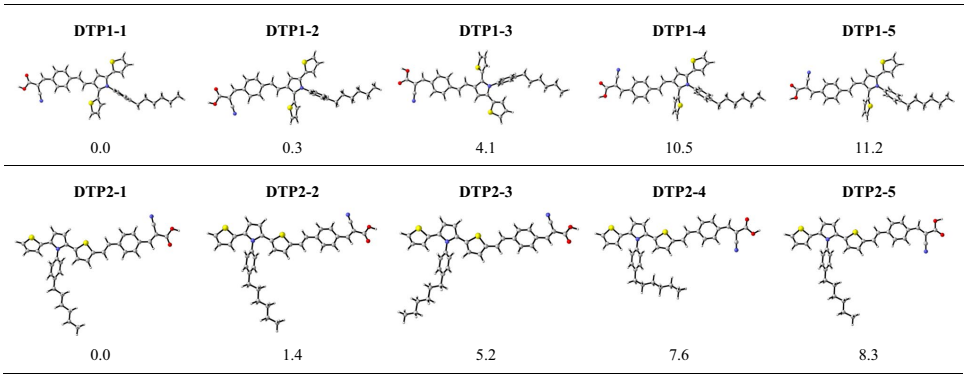

Fig. 1 Optimized structures (B3LYP/6-31G(d) with IEF-PCM in DCM) and relative Gibbs free energies (kJ/mol) for selected conformations of DTP1 and DTP2

software package. Long-range corrected hybrid functionals were used for vertical excitations, since they include the long-range exact Hartree–Fock [38] (HF) exchange which compensates for known limitations of DFT in the description of charge transfer states [39]. CAM-B3LYP [40] and ωB97XD [41] functionals and 6-31+G(d,p) basis set were used to model the excited states of the dyes. Solvent effects were taken into account using polarizable continuum method (IEF-PCM) [42, 43] in dichloromethane (DCM) both for conformation analysis and in the calculation of excitation energies.

To quantitatively characterize the charge transfer nature of the electronic excited states, the Φ_s index [32–34] is calculated for the target dyes. It mainly describes the overlap between the electron density in ground state and the rearranged electron density in excited state. When the value of Φs index is close to 1, a local transition can be postulated because of the high overlap between ground and excited state densities. On the other hand values close to 0, stem from a small overlap indicates a charge transfer character for the corresponding electronic transition. Φs and natural transition orbitals (NTO) [44] have been calculated with the Nancy_EX code [34].

To gain more insight into optical properties, dynamic and vibrational effects were included. A total of 20, 40 and 60 initial conditions were randomly sampled from the Wigner distribution [45] which is obtained as a quantum mechanical harmonic oscillator of the ground vibrational state, as implemented in the Newton-X [46] program. From all the chosen, Wigner conformation vertical transition energies were obtained using ωB97XD level of theory and 6-31+G(d,p) basis set. The initial conditions were generated using vibrational frequencies and normal mode vectors of the ground state optimized geometries (B3LYP/6-31G(d) level of theory) for absorption. To obtain a better representation of the spectrum, vertical transitions have been convoluted with Gaussian functions of fixed width at half length (FWHL) of 0.2 eV.

Two-photon absorption [47] (TPA) cross sections are calculated using the linear response formalism as implemented in DALTON2016 [48] program package. CAM-B3LYP/6-31G* level of theory is used. Cross section values are tabulated in Göppert-Mayer units (10^{-50} cm^4 photon^{-1}) in order to settle a direct comparison with the experiments. In addition, as for one-photon absorption dynamic effects on TPA have been estimated by Wigner distribution using 20 initial conditions.

3 Results and discussion

Structural and optical properties of two organic dyes, DTP1 and DTP2, were investigated to gain insight into their charge induction capabilities for use in dye-sensitized solar cells as well as their potential for use in nonlinear optical processes such as two-photon absorption (TPA), which is known to be enhanced by the presence of thiophene groups.

3.1 Conformational analysis of the ground state

To accurately assess the optical properties for both organic dyes, their conformational spaces were thoroughly scanned. A selection of the lowest energy conformers—within a free energy range of ~10 kJ/mol—was chosen for further analysis. Both functionals point to the same set of the lowest energy conformers, albeit some

Figure A.1. Article 1. (cont.)

minor differences in their relative free energies are found. B3LYP-optimized structures and relative free energies for the selected conformers of DTP1 and DTP2 are depicted in Fig. 1. The complete set of conformers and their relative energies (B3LYP and M06-2X) are given in Table S1 (in supporting info).

Conformers of DTP1 mainly show structural differences with respect to the positions of their cyano and carboxylate functionalities. While the isoenergetic **DTP1-1** and **DTP1-2** have these two groups facing opposite directions, the other three have them facing the same side, possibly leading to electronic repulsion and increasing their relative energies. For the isoenergetic conformations, the main structural differences stem from the positions of the relative orientation of the thiophene rings, which results in a 0.3 kJ/mol difference between the two conformations.

With the exception of **DTP2-5** presenting a trans-orientation, all the others conformers of DTP2 have the same conformation with respect to the cyano and carboxylate groups aforementioned. The energy difference between **DTP2-1**, **DTP2-2** and **DTP2-3** is mainly originated from the positions of the thiophene rings and the alignment of hexyl. The effect of hexane, for the **DTP2-2** and **DTP2-3** conformers, result in a 3.8 kJ/mol differences. This effect also can be seen for conformers **DTP2-4** and **DTP2-5**. Compared to DTP1, the position of hexyl group has a remarkable effect on the energy of DTP2. Indeed, the effect of the hexyl chain may be seen as a competition between enthropic factors and dispersion-driven attraction with the latter aspect favoring more compact structures; the analysis of the free energy differences provided in Fig. 1 unambiguously points toward the prevalence of enthropic disorder that is also enhanced by the fact that the disordered structures allows for a better solvent accessibility and hence a larger solvation stabilization.

3.2 Static level of theory assessment: functional performance

Absorption spectra were calculated for all optimized conformations of DTP1 and DTP2 depicted in Fig. 1. Table 1 collects the ωB97X-D and CAM-B3LYP values of λ_{max} in both nm and eV.

For both dyes, CAM-B3LYP λ_{max} values are red-shifted compared to ωB97X-D. Both functionals account for the non-Coulomb part of exchange functionals, however, ωB97X-D functional also includes an empirical atom–atom dispersion correction [41] which may partially account for the different trends in the static results. Also, when only a small charge separation is present, CAM-B3LYP may experience important deviations in reproducing excitation energies [49, 50]. The differences in the vertical transition energies are in the order of 10^{-2} eV, which further reinforces the use of ωB97XD as a functional quite suitable for reproducing absorption properties of these molecules.

The outcome of the static results are promising as the experimental values [26] was reproduced for almost each conformer. When the structures of the two organic dyes are compared, the extended conjugation in DTP2 is seen to cause the extension of the absorption toward the low-energy region of the spectrum, both experimentally and theoretically.

3.3 Excited state topologies and NTO's

Vertical transitions from each ground state conformer to their respective first excited (S_1) and second excited states (S_2) have been taken into account to model the charge transfer character. The Φ_s index, which describes the overlap between the electron density removed from the ground state (detachment density) and rearranged in the excited state (attachment density), was calculated to obtain a

Table 1 Benchmark calculations and experimental results [26] for absorption of DTP1 and DTP2 conformers

	λ_{ab} for DTP1				λ_{ab} for DTP2		
	ωB97X-D[a]	CAM-B3LYP[a]	Expt.		ωB97X-D[a]	CAM-B3LYP[a]	Expt.
DTP1-1	414 (2.99) 306 (4.05)	431 (2.87) 311 (3.98)	415 (2.98) 334 (3.71)	**DTP2-1**	458 (2.70) 291 (4.26)	479 (2.58) 316 (3.92)	457 (2.71) 364 (3.40)
DTP1-2	414 (2.99) 306 (4.05)	431 (2.87) 311 (3.98)		**DTP2-2**	458 (2.70) 292 (4.24)		
DTP1-3	415 (2.98) 305 (4.07)	431 (2.87) 310 (3.99)		**DTP2-3**	458 (2.70) 290 (4.27)	479 (2.58) 318 (3.89)	
DTP1-4	405 (3.06) 287 (4.32)	418 (2.96) 290 (4.27)		**DTP2-4**	457 (2.71) 291 (4.26)	478 (2.59) 316 (3.92)	
DTP1-5	405 (3.06) 287 (4.32)	419 (2.95) 290 (4.27)		**DTP2-5**	455 (2.72) 290 (4.27)	477 (2.60) 315 (3.93)	

λ_{max} values are given in nm (eV in parentheses)

[a] All vertical excitations were calculated on B3LYP/6-31G(d)-optimized geometries using 6-31+G(d,p) basis set and IEFPCM in DCM

Figure A.1. Article 1. (cont.)

quantitative measure for the ease of charge transfer upon photon absorption and gives an indirect assessment of the potential for charge injection in DSSC's. Φ_s values for DTP1 and DTP2, illustrated in Fig. 2, are close to 1, indicating a high level of overlap between the two aforementioned densities; hence, a local charge transfer, which deems them ineffective for use in solar cells. This also explains the low level of efficiency previously observed experimentally [26]. Furthermore, occupied and virtual NTOs, describing vertical transitions for $S_0 \rightarrow S_1$ and $S_0 \rightarrow S_2$, are depicted in Fig. 2. Consistent with the high Φ_s values obtained for both dyes, visual inspection of oNTO and vNTO's for each transition show an almost localized charge transfer.

3.4 Dynamic and vibrational effects on optical properties

As mentioned earlier, due to the extended conjugation in the chromophore systems under study herein, the dynamic and vibrational effects are expected to be significant. Hence, the ground state conformational space is explored using a Wigner distribution obtained from vibrational frequencies that were calculated for each conformer. To include dynamic effects, the initial conditions of 20, 40 and 60 structures were generated by sampling from a Wigner distribution as implemented in the Newton-X program. The spectra obtained from this distribution were compared with static calculations and experimental results.

As reported in Table 2, for both dye molecules, deviations from the corresponding experimental values can be noticed and all molecules have shown their λ_{max} in visible and near-UV region for absorption. Almost all of the chosen conformations are red-shifted when dynamic effects are present. Having 40 initial conditions results in some improvement when compared to 20 initials.

Conformation **2** shows blue shift in its $\lambda_{ab\text{-}20}$ and $\lambda_{ab\text{-}60}$ values for **DTP1**, even though 40 different coordinates and momenta produces a very strong red shift. This indicates that there is no direct correlation between the number of the initial conditions present in the Wigner procedure and the vertical excitation energy.

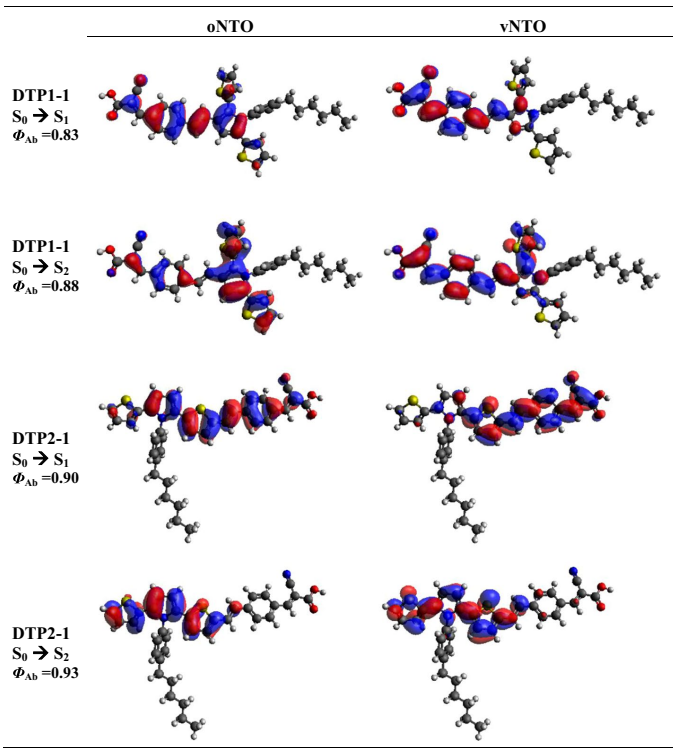

Fig. 2 Occupied and virtual NTO's for the lowest energy conformers of DTP1 and DTP2

Figure A.1. Article 1. (cont.)

Table 2 Wigner distribution results for absorption of DTP1 and DTP2 conformers, ωB97X-D/6-31+G(d,p)[a] calculated band maxima λ^{b}_{max} and experimental results

	$\lambda_{ab\text{-}20}$	$\lambda_{ab\text{-}40}$	$\lambda_{ab\text{-}60}$	λ^{c}_{ab}	$\lambda_{ab\text{-}Expt}$
DTP1-1	431 (2.87)	432 (2.87)	423 (2.93)	414 (2.99)	415 (2.98)
DTP1-2	406 (3.05)	448 (2.76)	408 (3.03)	414 (2.99)	
DTP1-3	443 (2.79)	445 (2.78)	425 (2.91)	415 (2.98)	
DTP1-4	385 (3.22)	420 (2.95)	421 (2.94)	405 (3.06)	
DTP1-5	392 (3.16)	423 (2.93)	427 (2.90)	405 (3.06)	
DTP2-1	446 (2.77)	483 (2.56)	476 (2.60)	458 (2.70)	457 (2.71)
DTP2-2	452 (2.74)	456 (2.71)	466 (2.66)	458 (2.70)	
DTP2-3	449 (2.76)	459 (2.70)	463 (2.67)	458 (2.70)	
DTP2-4	467 (2.65)	470 (2.63)	501 (2.47)	457 (2.71)	
DTP2-5	466 (2.66)	462 (2.68)	462 (2.68)	455 (2.72)	

[a] All vertical excitations were calculated on B3LYP/6-31G(d)-optimized geometries with IEFPCM in DCM

[b] λ_{max} values are given in nm (eV in parentheses)

[c] Static results from Table 1

When it comes to **DTP2**, one can immediately see that again most of the values are red-shifted. The lowest energy conformation **DTP2-1** gave absorption values within the 0.2 eV limit. For conformations **2, 3** and **4**, increasing number of the initial conditions extended the absorption toward the lower energy region, but a very large deviation is seen for conformation **4** in its $\lambda_{ab\text{-}60}$ value. When compared to the static TD-DFT calculations, a significant improvement cannot be observed in terms of λ_{max} values in the Wigner distribution results.

The final dynamic resolved spectra are obtained by convoluting the vertical excitations calculated for each snapshot. Figure 3 depicts the absorption spectra for the lowest energy conformers of DTP1 and DTP2 and nicely illustrate the convergence of the spectra. Absorption spectra for all conformers of DTP1 and DTP2 are given in SI.

To better reproduce the experimentally resolved band shape, 60 vertical transitions obtained from Wigner distribution for each conformer have been Boltzmann-weighted and subsequently convoluted with Gaussian functions.

Figure 4 shows Boltzmann-weighted Wigner distribution calculations for absorption spectra of DTP1 and DTP2, while the obtained absorption maxima are reported in Table 3. The value of the λ maxima compares quite well with the experimental ones [26] with differences of only 0.04 and 0.07 eV for DTP1 and DTP2, respectively. Also the general band shape, and in particular the evident shoulder in the case of DTP1, is nicely recovered evidencing the need of considering both conformational sampling and a proper treatment of vibrational effects.

3.5 Two-photon absorption

TPA is the result of simultaneous absorption of two photons of identical frequencies, since the total energy absorbed is doubled, the photons will populate electronic excited states having higher energy than in the case of one-photon absorption. Hence, TPA spectra will appear at much longer wavelengths, lower energy regions than conventional one-photon absorption.

Two-photon absorption cross sections are shown in Table 4 and Fig. 5 obtained from a Wigner distribution of the most stable conformer of the two molecules, respectively. Static TPA calculation for all the conformers are reported in supplementary information, notice that the difference in absorption maximum wavelengths

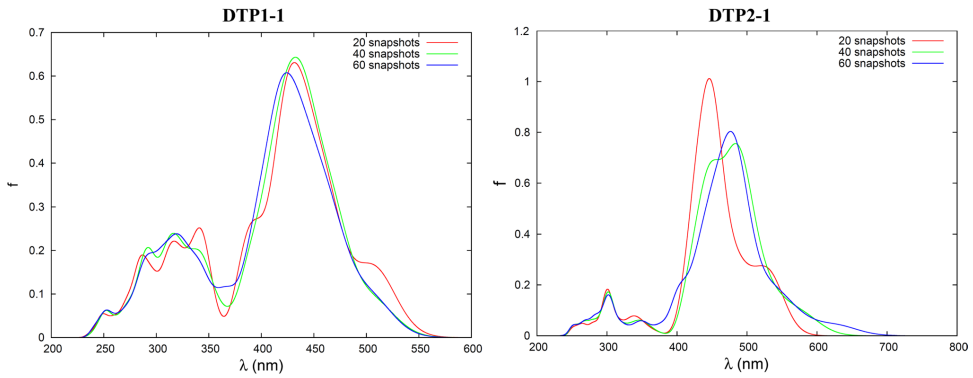

Fig. 3 Wigner distribution calculations for absorption spectra of the lowest energy conformations of DTP1 and DTP2

Figure A.1. Article 1. (cont.)

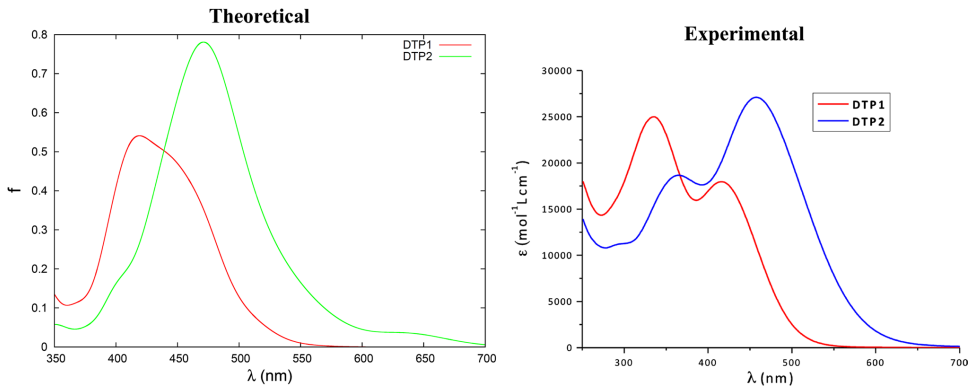

Fig. 4 Boltzmann-weighted Wigner distribution calculations for absorption spectra of DTP1 and DTP2 (*left panel*) and the corresponding experimental spectra (*right panel*)

Table 3 Absorption maxima from Boltzmann-weighted for DTP1 and DTP2

DTP1		DTP2	
λ_{ab} (nm)	Expt.	λ_{ab} (nm)	Expt.
418 (2.96)	415 (2.98)	470 (2.63)	457 (2.71)

Table 4 Calculated two-photon absorption cross sections and wavelengths via snapshots from Wigner distribution of DTP1 and DTP2 conformers

	DTP1			DTP2	
	λ_{Max} (nm)	Φ (GM)		λ_{Max} (nm)	Φ (GM)
DTP1-1	820	442.0	DTP2-1	870	742
	566	1243.6		624	6977.7

between the conformers never exceed 5 nm. As expected, both DTP1 and DTP2 absorb in the red to near infrared region, making them ideal candidates for optical applications requiring long wavelength excitations, in particular both DTP1 and DTP2 covers efficiently the therapeutic window allowing penetration in deep human tissues. As shown in Fig. 5, the $S_0 \rightarrow S_1$ absorption happens around 850 nm and gives rise to a broad symmetric band. Cross sections are of the order of 450 Göppert-Mayer (GM) for DTP1 while the larger conjugation of the polythiophene motifs in DTP2 increases the cross section up to 740 GM. The $S_0 \rightarrow S_2$ transition is also characterized by high TPA with maximum absorption at 566 nm for DTP1 and 624 nm for DTP2. Cross sections are extremely high exceeding 1000 GM for DTP1 and reaching the impressive value of 7000 GM for DTP2. The band relative to the second excited state is also more asymmetric and presents a wide tail extending to the red and infrared part of the spectrum. This is particularly significative for DTP1 since even if its $S_0 \rightarrow S_2$ absorption maximum falls outside the therapeutic windows cross section of the order of 400 GM can still be reached between 600 and 700 nm.

4 Conclusion

We report a state-of-the-art computational modeling study of the linear and nonlinear optical properties of two polythiophene organic dyes, DTP1 and DTP2. By performing a combination of conformational search and potential energy sampling through Wigner distribution, we have calculated the one-photon absorption spectra taking into account vibrational and conformational flexibility. Furthermore, we have analyzed the nature of the lowest lying excited states with a particular emphasis of their charge transfer nature. The photoinduced charge separation is quite modest as confirmed by the almost unitary value of the overlap between ground and excited state density matrices (Φ_s). This aspect can explain the previously observed moderate performance as DSSC sensitizers exhibited by the two dyes. On the contrary, remarkably high TPA cross section has been observed for DTP1 and especially DTP2, with absorption wavelengths in the red and infrared region of the spectrum both for $S_0 \rightarrow S_1$ and $S_0 \rightarrow S_2$ transitions. Hence, both dyes have to be regarded as extremely promising candidates for TPA sensitization in material science or biological and medical application.

Figure A.1. Article 1. (cont.)

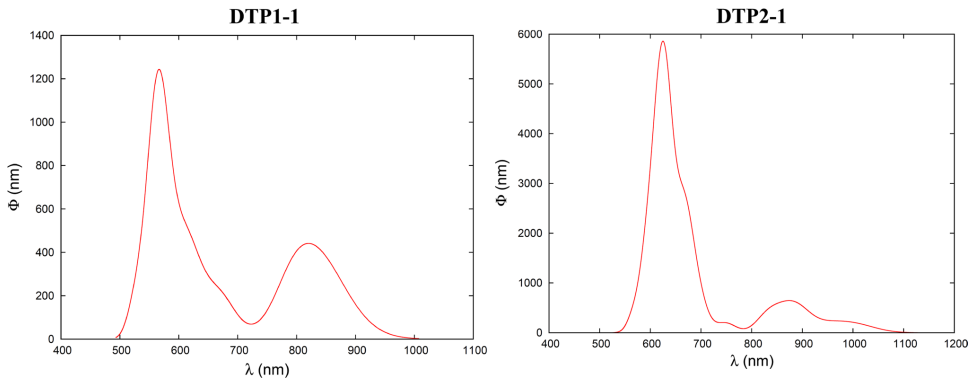

Fig. 5 Calculated TPA spectra using Wigner distribution for DTP1 and DTP2 chromophores

In the future, we plan to extend the study of the photophysical properties of both dyes in particular concerning the exploration of their singlet and triplet manifold both from a static point of view and via non-adiabatic state hopping dynamics to describe the time evolution of the different excited states.

Acknowledgements Support from the University of Lorraine and French CNRS is gratefully acknowledged. AM thanks Campus France for support under the bilateral "Bosphorus" 35649PL PHC program covering students mobility. SC acknowledges TUBITAK-PIA (Project No: 115Z863) for financial support.

References

1. Schultz DM, Yoon TP (2014) Solar synthesis: prospects in visible light photocatalysis. Science 343:1239176-1–1239176-8
2. Berardi S, Drouet S, Francàs L et al (2014) Molecular artificial photosynthesis. Chem Soc Rev 43:7501–7519
3. Frischmann PD, Mahata K, Würthner F et al (2013) Powering the future of molecular artificial photosynthesis with light-harvesting metallosupramolecular dye assemblies. Chem Soc Rev 42:1847–1870
4. Colasson B, Credi A, Ragazzon G (2016) Light-driven molecular machines based on ruthenium (II) polypyridine complexes: strategies and recent advances. Coord Chem Rev 325:125–134
5. Browne WR, Feringa BL (2006) Making molecular machines work. Nat Nanotechnol 1:25–35
6. Astumian RD, Mukherjee S, Warshel A (2016) The physics and physical chemistry of molecular machines. Chemphyschem 17:1719–1741
7. Le Bailly B (2016) Nobel prize in chemistry: welcome to the machine. Nat Nanotechnol 11:923
8. Hagfeldt A, Boschloo G, Sun L et al (2010) Dye-sensitized solar cells. Chem Rev 110:6595–6663
9. O'Regan B, Grätzel M (1991) A low-cost, high-efficiency solar cell based on dye-sensitized colloidal TiO_2 films. Nature 353:737–740
10. Bonnett R (1995) Photosensitizers of the porphyrin and phthalocyanine series for photodynamic therapy. Chem Soc Rev 24:19–33
11. Pandey RK (2000) Recent advances in photodynamic therapy. J Porphyr Phthalocyanines 4:368–373
12. Yuan Q, Wu Y, Wang J et al (2013) Targeted bioimaging and photodynamic therapy nanoplatform using an aptamer-guided G-quadruplex DNA carrier and near-infrared light. Angew Chem Int Ed 52:13965–13969
13. Babilas P, Landthaler M, Szeimies R-M (2006) Photodynamic therapy in dermatology. Eur J Dermatol 16:340–348
14. Winkler K, Simon C, Finke M et al (2016) Photodynamic inactivation of multidrug-resistant *Staphylococcus aureus* by chlorin e6 and red light ($\lambda = 670$ nm). J Photochem Photobiol B Biol 162:340–347
15. Koshi E, Mohan A, Rajesh S, Philip K (2011) Antimicrobial photodynamic therapy: an overview. J Indian Soc Periodontol 15:323
16. Allison RR, Moghissi K (2013) Oncologic photodynamic therapy: clinical strategies that modulate mechanisms of action. Photodiagnosis Photodyn Ther 10:331–341
17. Allison RR, Sibata CH (2010) Oncologic photodynamic therapy photosensitizers: a clinical review. Photodiagnosis Photodyn Ther 7:61–75
18. Tsai C-L, Chen J-C, Wang W-J (2001) Near-infrared absorption property of biological soft tissue constituents. J Med Biol Eng 21:7–14
19. Zhou H, Zhou F, Tang S et al (2012) Two-photon absorption dyes with thiophene as π electron bridge: synthesis, photophysical properties and optical data storage. Dye Pigment 92:633–641
20. Zou Q, Zhao H, Zhao Y et al (2015) Effective two-photon excited photodynamic therapy of xenograft tumors sensitized by water-soluble bis(arylidene) cycloalkanone photosensitizers. J Med Chem 58:7949–7958
21. Zheng Y-C, Zheng M-L, Li K et al (2015) Novel carbazole-based two-photon photosensitizer for efficient DNA photocleavage in anaerobic condition using near-infrared light. RSC Adv 5:770–774
22. Abbotto A, Beverina L, Bozio R et al (2002) Novel heterocycle-based two-photon absorbing dyes. Org Lett 4(9):1495–1498

Figure A.1. Article 1. (cont.)

Probing Thiophene-Derivatives for Two-Photon Absorption

Authors: Ozlem, et al.

[1] Bogazici University, Faculty of Arts and Sciences, Department of Chemistry, 34342 Bebek Istanbul, Turkey

[2] Théorie-Modélisation-Simulation, Université de Lorraine − Nancy, SRSMC Boulevard des Aiguillettes, Vandoeuvre-lès-Nancy, Nancy, France

[3] Théorie-Modélisation-Simulation, CNRS, SRSMC Boulevard des Aiguillettes, Vandoeuvre-lès-Nancy, Nancy, France

Electronic Supplementary Information (ESI)

Table of Contents

Figure A.1. Article 1. (cont.)

Conformational Analysis

Table S1. Relative energies (kj/mol) of different conformations of DTP1*

DTP1		B3LYP/6-31G(d)	M06-2X/6-31+G(d,p)
DTP1-1	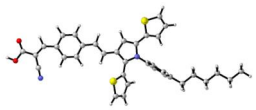	0	0
DTP1-2	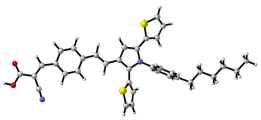	0.26	5.71
DTP1-3	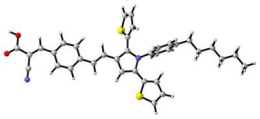	4.05	12.41
DTP1-4	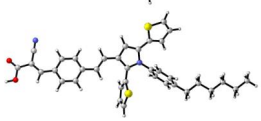	10.78	7.20
DTP1-5	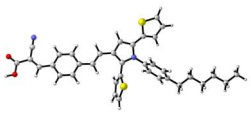	11.47	7.17
DTP1-6	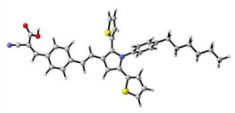	26.64	19.05
DTP1-7	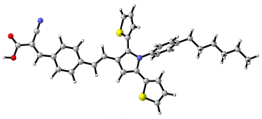	3.42	2.08
DTP1-8	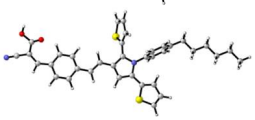	26.16	17.80
DTP1-9	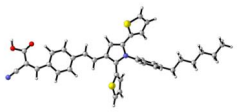	21.54	31.57
DTP1-10	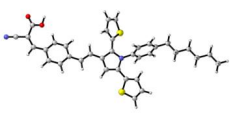	28.27	27.34

Figure A.1. Article 1. (cont.)

DTP1-11	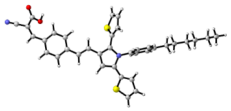	34.79	38.82
DTP1-12	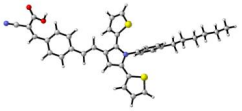	31.81	35.91
DTP1-13	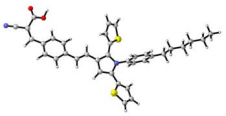	33.22	36.55
DTP1-14	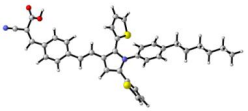	31.06	26.60

***All calculations are done by using DCM.**

3

Figure A.1. Article 1. (cont.)

Table S2. Relative energies (kj/mol) of different conformations of DTP2*

DTP2		B3LYP/6-31G(d)	M06-2X/6-31+G(d,p)
DTP2-1	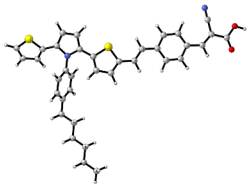	0.0	4.7
DTP2-2	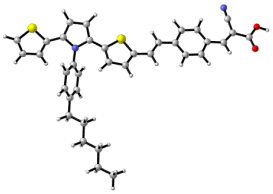	1.4	0.0
DTP2-3	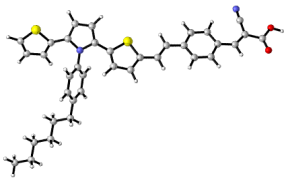	5.2	6.2
DTP2-4	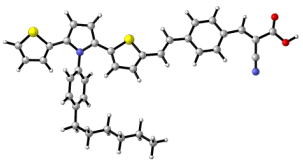	7.6	5.1
DTP2-5	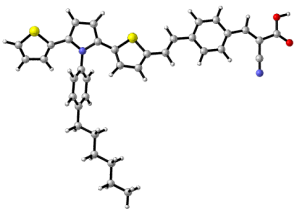	8.3	3.1
DTP2-6	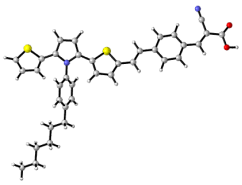	9.8	7.7

4

Figure A.1. Article 1. (cont.)

DTP2-7	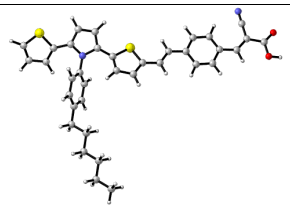	6.5	8.7
DTP2-8	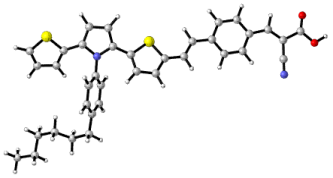	11.3	13.1
DTP2-9	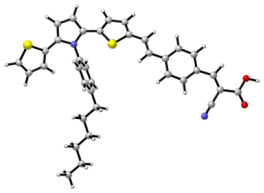	12.9	12.2
DTP2-10	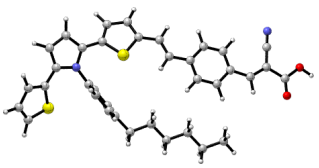	8.0	0.4
DTP2-11	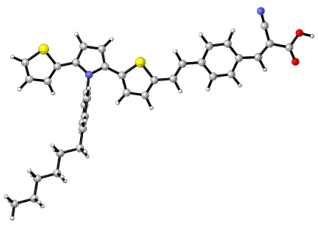	7.3	11.7
DTP2-12	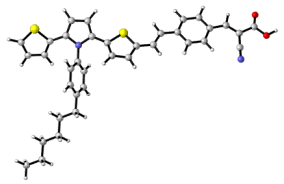	4.2	5.6

***All calculations are done by using DCM.**

5

Figure A.1. Article 1. (cont.)

Table S13. Benchmark Calculations and Experimental Results for Absorption of DTP1 with different conformations by using ωB97X-D / 6-31+G(d,p) level of theory [a-b]

DTP1	B3LYP/6-31G(d)	M06-2X/6-31+G(d,p)	Experimental
DTP-3	415 (2.98)	395(3.13)	415(2.98)
	305 (4.07)	297(4.17)	334(3.71)
DTP-1	414 (2.99)	395(3.13)	
	306 (4.05)	296(4.18)	
DTP-2	414 (2.99)	395(3.13)	
	306 (4.05)	294(3.14)	
DTP-5	405(3.06)	389(3.18)	
	287(4.32)	290(4.27)	
DTP-4	405(3.06)	389(3.18)	
	287(4.32)	290(4.27)	

[a] λ_{max} values are given in nm and, in parentheses, in eV

[b] All calculations are done by using DCM

Table S14 . Benchmark Calculations and Experimental Results for Absorption of DTP2 with different conformations by using ωB97X-D / 6-31+G(d,p) level of theory [a-b]

DTP2	B3LYP/6-31G(d)	M06-2X/6-31+G(d,p)	Experimental
DTP2-1	457 (2.71)	430 (2.88)	457 (2.71)
	291 (4.26)	285 (4.35)	364 (3.40)
DTP2-3	458 (2.70)	427 (2.90)	
	290 (4.27)	284 (4.37)	
DTP2-2	458 (2.70)	428 (2.90)	
	292 (4.24)	283 (4.38)	
DTP2-4	457 (2.71)	429 (2.89)	
	291 (4.26)	285 (4.35)	
DTP2-5	455 (2.72)	427 (2.90)	
	290 (4.27)	284 (4.37)	

[a] λ_{max} values are given in nm and, in parentheses, in eV

[b] All calculations are done by using DCM.

Figure A.1. Article 1. (cont.)

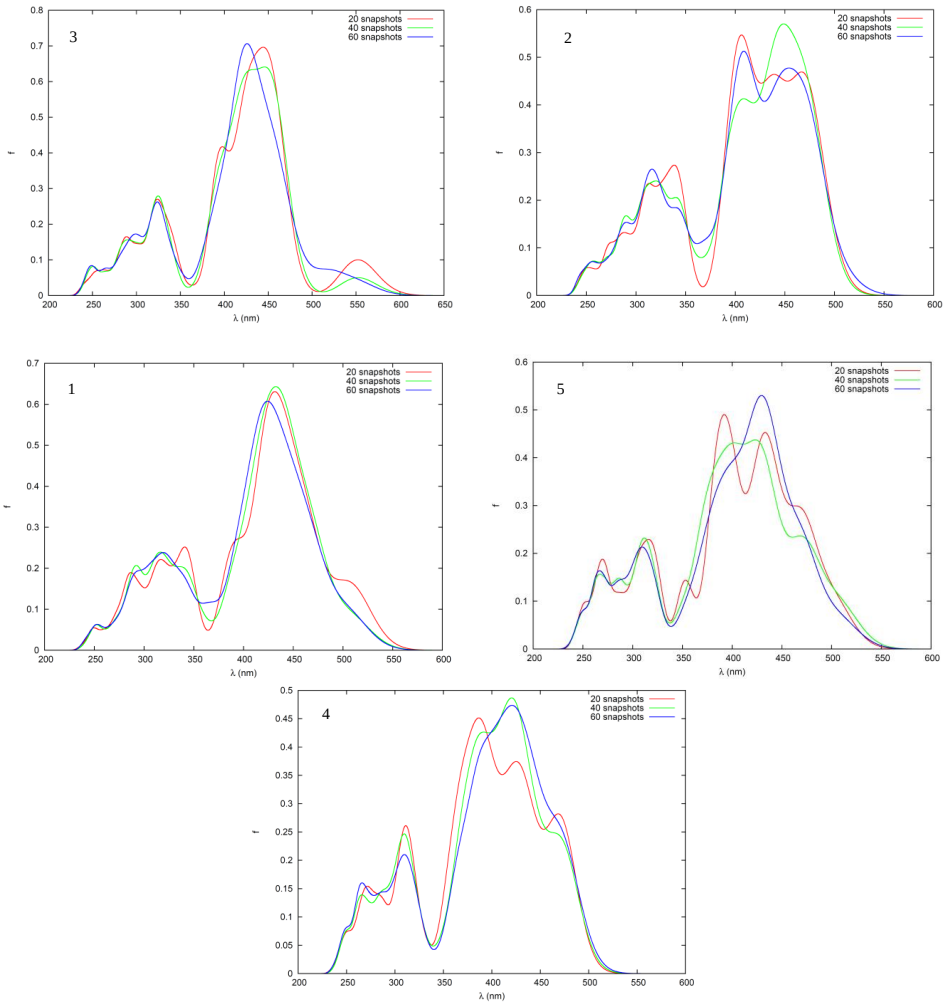

Fig S1. Results of the Wigner distribution calculations for absorption spectra of DTP1 by using different conformations. All the vertical transitions have been convoluted with Gaussian functions of fixed width at half length of 0.2 eV

Figure A.1. Article 1. (cont.)

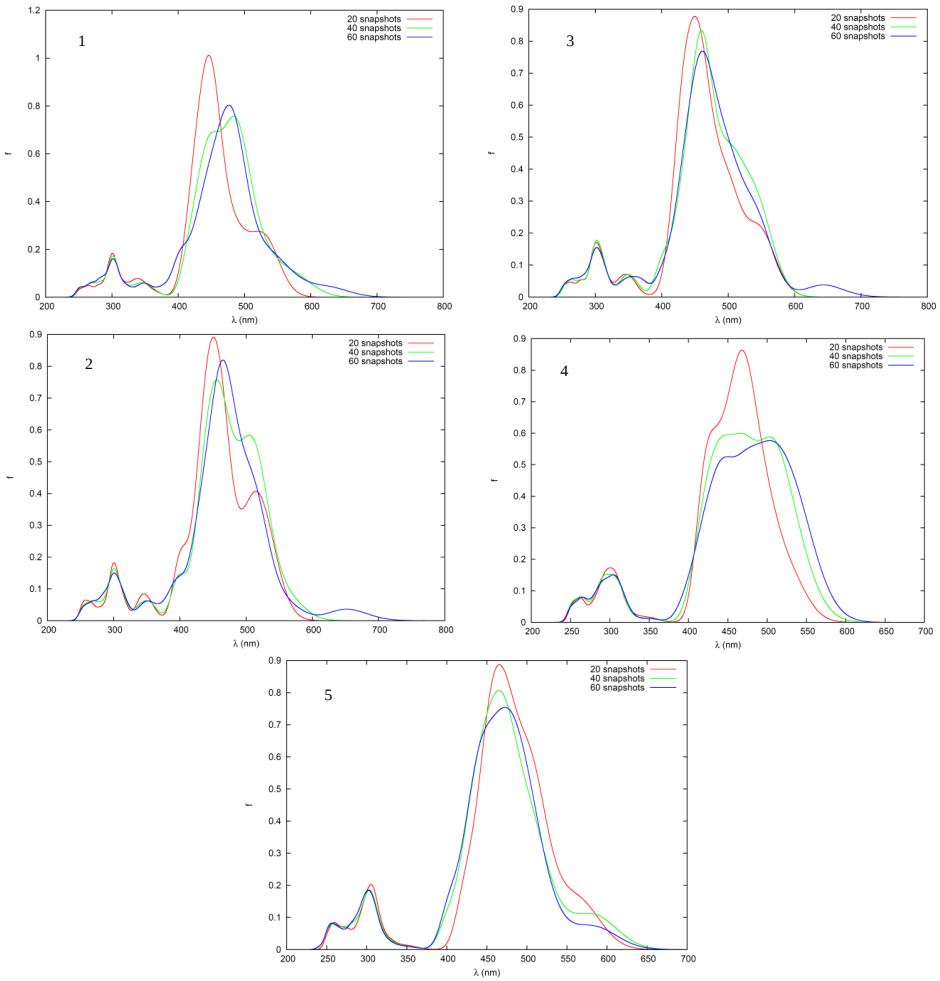

Fig S2. Results of the Wigner distribution calculations for absorption spectra of DTP2 by using different conformations. All the vertical transitions have been convoluted with Gaussian functions of fixed width at half length of 0.2 eV

Figure A.1. Article 1. (cont.)

A.2. Photophysical Properties of Novel Two-Photon Absorbing Dyes: Assessing Their Possible Use for Singlet Oxygen Generation

A full-text version of the article regarding part II is given in this section.

THE JOURNAL OF PHYSICAL CHEMISTRY C

Article

Cite This: J. Phys. Chem. C 2018, 122, 16315−16324

pubs.acs.org/JPCC

Photophysical Properties of Novel Two-Photon Absorbing Dyes: Assessing Their Possible Use for Singlet Oxygen Generation

Ozlem Sengul,[†] Marco Marazzi,[‡,§] Antonio Monari,[§] and Saron Catak[*,†]

[†]Department of Chemistry, Bogazici University, Bebek, 34342 Istanbul, Turkey

[‡]Departamento de Química, Centro de Investigación en Síntesis Química (CISQ), Universidad de La Rioja, Madre de Dios, 53, 26006 Logroño, Spain

[§]Université de Lorraine and CNRS, LPCT UMR 7019, F-54000 Nancy, France

Supporting Information

ABSTRACT: Herein, we assess the nonlinear absorption properties and the photophysical profile and behavior of two recently synthesized polythiophene-based dyes. In particular, using high level state-of-the-art molecular modeling methodologies, we clearly underline the remarkable two-photon absorption (TPA) cross-section. Furthermore, the possible pathways leading to the intersystem crossing and triplet manifold population are investigated by considering the energy difference between the relevant triplet and singlet states on the potential energy surfaces as the key critical points. The spin−orbit coupling is also assessed, and the results globally point to a possible, albeit probably slow, intersystem crossing that could allow the use of the two dyes as singlet oxygen photosensitizers, for instance in photodynamic therapy, owing to their high TPA cross-sections.

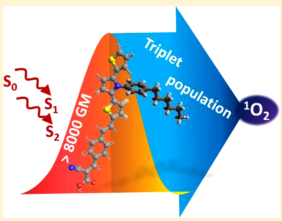

INTRODUCTION

The development and production of optically active materials[1] and dyes has experienced an impressive surge in recent years. Scientific efforts have been driven by the possibility to develop systems with applications as varied as clean energy production,[2−5] molecular machines,[6−8] as well as biological and medical devices for imaging[9,10] or therapy.[11−15] In particular, it appears evident that the precise modification of the chemical structure of the optically active units may lead to an impressive and unprecedented control of their functions. In this context, the role played by molecular modeling and simulation cannot be underestimated.[16] Indeed, the possibility to clearly assess and rationalize all the complex mechanisms—involving nonadiabatic transitions[17,18] between different electronic states, driving the photochemical and photophysical properties—at an electronic level allows us to propose a clear rational design of novel and more efficient materials and systems.[19−22]

In this context, one of the most sought properties of optically active materials is an absorption spectrum, sufficiently low in energy, that allows activation with red or infrared light sources. Indeed, such a characteristic property would allow achieving a much deeper penetration of the activating source and hence, should be considered most beneficial. One option to obtain a global red-shift of the absorption spectrum is to increase the conjugation pattern of the chromophore. However, this strategy could, in certain cases, lead to a strong modification of other photophysical and photochemical properties.

Alternatively, as emerging in recent years, one can resolve towards nonlinear optical properties and in particular two-photon absorption (TPA).[23,24] Indeed, in TPA, first theoretically formalized by Göppert-Meyer in the 1930s, the chromophore simultaneously absorbs two photons to be promoted to a certain excited state. Hence, if one supposes a monochromatic light source, the energy of the photons needed to provide the vertical electronic excitation will be divided by two compared to one-photon absorption (OPA) phenomena, and consequently, the absorption wavelength will be doubled. However, one has to take into account that TPA selection rules will be different from the ones ruling OPA, hence, specific design strategies should be used to obtain efficient TPA chromophores. More specifically, following the common theoretical framework of the intermediate state, one recognizes that the centrosymmetric molecules, as well as the charge-transfer electronic states, usually increase TPA cross-section over OPA absorption. On the other hand, a secondary advantage of TPA over OPA is due to the former being a nonlinear process and requiring the simultaneous absorption of two photons, therefore, its probability is proportional to the square of the light source intensity. Consequently, TPA efficiency diminishes much faster than the corresponding OPA and, hence, will occur only in the focal region of the laser, allowing a much better spatial resolution and control of the

Received: May 21, 2018
Revised: June 24, 2018
Published: July 3, 2018

DOI: 10.1021/acs.jpcc.8b04824
J. Phys. Chem. C 2018, 122, 16315−16324

Figure A.2: Article 2.

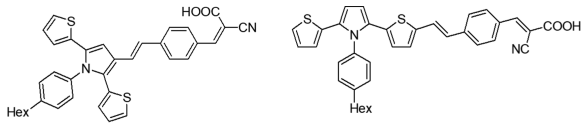

DTP1 DTP2

Figure 1. Chemical formula of DTP1 and DTP2.

optically active material. In fact, the combination of a red-shifted absorption and the extremely high spatial resolution make TPA particularly attractive for medical applications, both for therapeutic purposes, or for imaging;[25,26] lately the development of drugs allowing to simultaneously perform diagnosis and treatment (theranostics)[9] have also emerged based on TPA chromophores.

In the past few decades, the exploitation of light for therapeutic objectives has attracted renowned interest, pushed by the possibility of an efficient and selective treatment limiting the unwanted side effects of more conventional approaches.[15,27] In this domain, in particular, the photosensitization of biological macromolecular structures, such as nucleic acids,[26,28,29] membranes,[30,31] and proteins,[32] is performed to induce the death of undesired cellular lines, such as cancer cells or bacteria. Light-assisted therapy exploits the photophysical or photochemical processes triggered by the initial photoexcitation of a specific drug interacting with a specific cellular compartment. In particular, it usually requires the population of the drug's triplet manifold, followed by either direct photosensitization via electron or energy transfer to the biological structures, or the energy transfer to molecular oxygen to produce the highly reactive singlet oxygen ($^1O_2$) that will subsequently induce oxidative lesions leading to cellular death.[29,33] Even though, the former represents the most common processes in light-assisted therapy, other mechanisms involving different photochemical channels, such as photo-induced hydrogen abstraction[34] or photoionization[25,26] are possible and have been reported. The activation of $^1O_2$, however, is by far the most commonly exploited phenomenon and gives rise to the so-called photodynamic therapy (PDT)[35] approach that has found successful applications in antibacterial,[27] antiviral,[36,37] and anticancer applications.[15,38] Obviously, selectivity in light-induced therapy and PDT is assured by the fact that the drug should be nontoxic in the dark and, hence, a general systemic effect should be avoided by the selective application of the light stimulus. An efficient PDT agent should possess a certain number of properties, such as an absorption in the therapeutic window (650−1350 nm) to allow penetration in the deep body tissues and, hence, the treatment of nonsuperficial lesions. In addition, it should also be characterized by an efficient intersystem crossing (ISC), without the presence of competitive deactivation channels, hence, leading to the population of the triplet state manifold necessary to achieve oxygen activation. Obviously, the general bioavailability profile and the interaction with the biological systems should also be taken into account.

From the previous consideration, it is clear that TPA-based drugs for PDT are particularly attractive to obtain a significant red-shifted absorption profile, however, the design of TPA active compounds should not alter the photophysical properties leading to efficient intersystem crossing.

In the present contribution, we present the detailed photophysical analysis of two recently synthesized chromophores, based on the 2,5-dithienylpyrrole motif (DTP1 and DTP2),[39,40] that could show relevant TPA absorption and could lead to efficient singlet oxygen activation. The two chromophores have been synthesized for applications in solar cell energy production and are constituted by a polythiophene core. Their donor−π−acceptor (D−π−A) global structure (Figure 1) also allows the presence of charge-transfer electronic excited states.

In addition to simulating the OPA and TPA spectra, taking into account vibrational and dynamical effects, we also evaluate the intersystem crossing efficiency. We show that although DTP1 and DTP2 show an efficient TPA cross-section in the infrared portion of the spectrum, their intersystem crossing efficiency should be comparable to one of the commonly used PDT photosensitizers, such as porphycenes.

METHODS AND COMPUTATIONAL DETAILS

To properly assess all the relevant photophysical properties, and appropriately take into account the conformational flexibility, conformational analysis has been applied to characterize all the critical points. In particular, to model the photophysical features of the two polythiophene-based dyes, we considered the relative positions of the different singlet and triplet excited states and we optimized the geometries of the S_0, S_1, and T_1 states. Density functional theory (DFT) was used to optimize the ground state of each spin multiplicity, whereas the Tamm−Dancoff approximation (TDA) was employed for the excited state calculations. This choice is due to the fact that the TDA method provides a more balanced description of both triplet and singlet excited states, and compared to time-dependent DFT (TD-DFT) it is free from triplet instability problems.[41] Geometry optimization was performed using the hybrid B3LYP[42] exchange correlation functional and the 6-31G(d) basis set, the energy and the nature of the excited states were also estimated at the CAM-B3LYP[43]/6-31+G(d,p) level of theory to take into account the error arising from the presence of charge-transfer states. Solvent, i.e., water, has been implicitly taken into account as a polarizable continuum (PCM) method in all calculations.[44,45]

To sample the potential energy surface in the vicinity of the critical points, and to include dynamic and vibrational effects, 20 snapshots have been obtained from Wigner distribution[46] calculated from the harmonic vibrational frequencies (Hessians) of the corresponding minimum, using the Newton-X code.[47] Notably, the snapshots have been used to calculate an ensemble of vertical transitions, necessary to obtain the absorption, fluorescence, and phosphorescence final spectra.[16,39,48−50] In particular, Gaussian functions of 0.2 eV full width at half maximum have been used to convolute the vertical transitions. The one-photon absorption (OPA)

DOI: 10.1021/acs.jpcc.8b04824
J. Phys. Chem. C 2018, 122, 16315−16324

Figure A.2. Article 2. (cont.)

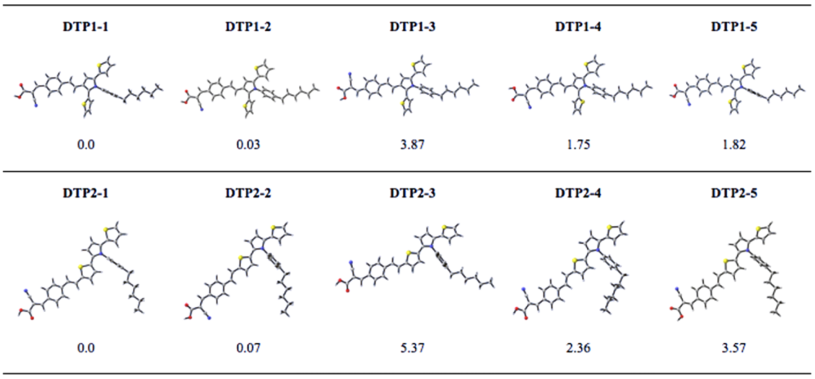

Figure 2. S_1 optimized structures in water and the corresponding relative Gibbs free energies (kJ/mol) for selected DTP1 and DTP2 conformations.

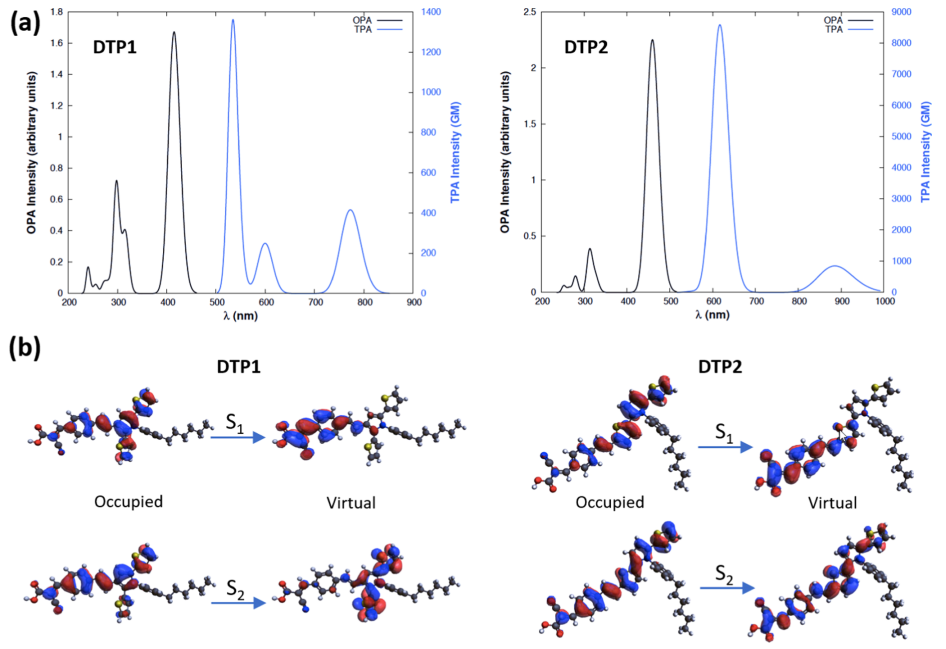

Figure 3. One- and two-photon absorption spectra (OPA in black and TPA in blue, respectively) of DTP1 and DTP2, simulated in water (a). Natural transition orbitals showing $S_0 \rightarrow S_1$ and $S_0 \rightarrow S_2$ transitions for both dyes (b).

spectrum has been modeled by convolution of the vertical transitions from the ground state (S_0) to the singlet excited state manifold. The fluorescence spectra, i.e., radiative emission from the S_1 state, are computed as convolution of vertical transitions from the S_1 minimum geometry to S_0. To take into account solvent geometrical reorganization in the fluorescence equilibrium spectrum, state-specific PCM[51] is used. Phosphorescence, originated between the states of different spin multiplicity (i.e., emission from T_1 to S_0), is analyzed as an alternative photophysical phenomenon. All quantum chemistry calculations were carried out with the Gaussian 09 (revision E.01) software package,[52] phosphorescence intensities (oscillator strengths) were calculated using the Dalton2016 code.[53,54] The excited state nature was characterized in terms

DOI: 10.1021/acs.jpcc.8b04824
J. Phys. Chem. C 2018, 122, 16315−16324

Figure A.2. Article 2. (cont.)

of natural transition orbitals (NTOs)[55,56] to analyze the electronic density reorganization, NTOs were obtained using the Nancy_EX code.[56,57]

Two-photon absorption (TPA) cross-sections are computed at the TD-DFT level (CAM-B3LYP/6-31G(d)) using a linear response methodology as implemented by Rizzo and co-workers[58] by using the DALTON2016 code[53,54] and the cross-section values are represented in Göppert-Mayer (GM) units (10^{-50} cm^4/photon).

Finally, to properly quantify the intersystem crossing mechanism, the relative positions of triplet and singlet states along a generalized coordinate connecting S_1 and T_1 minima are calculated at the B3LYP/6-31G(d) level. In addition, spin−orbit couplings (SOCs) have been calculated at the relevant critical points, on the snapshots obtained from the Wigner distribution, and along the interpolation coordinate. SOC calculations have been performed with the Amsterdam density functional[59,60] code at the CAM-B3LYP/DZP level of theory. Please note that the choice of using different code packages for different calculations is due to the fact that some of the rather specific properties (such as SOC at the TD-DFT level or TPA cross-sections) are optimized, or even only available in some particular codes. Furthermore, while computational results are obviously noncode dependent, the effect of changing the basis set from Gaussian to Slater functions has only a very limited effect on the excitation energies.

RESULTS AND DISCUSSION

Conformational Analysis of the Ground State (S_0) and Lowest Optically Bright State (S_1). The ground state conformational analysis of both DTP1 and DTP2 compounds were previously performed by some of the authors at the B3LYP/6-31G(d) level of theory, including dichloromethane as the solvent via PCM.[39] A representative selection of the lowest energy conformers (free energy range within ca. 10 kJ/mol, resulting in 5 DTP1 and 5 DTP2 structures) was analyzed. The chosen S_0 optimized structures can differ in the relative positions of their cyano and carboxylate groups, possibly leading to some electronic repulsion, as well as in the orientation of their thiophene rings and hexyl groups. Indeed, the alignment of the hexyl group is found as the factor marking the main differences between DTP1 and DTP2 conformers, since the former has almost a constant alignment, whereas the latter assumes various positions, pointing finally toward the relevance of entropic disorder, allowing solvent accessibility, and hence, favoring solvent stabilization.

In this study, to properly assess the photophysical properties of the molecules, the complete set of S_0 conformers was further optimized on the optically bright lowest singlet excited state (S_1) at the B3LYP/6-31G(d) level, finding only a slight difference in their relative free energies (max. 5.37 kJ/mol, see Figure 2). However, since once again the main difference observed is related to the alkyl chain orientation and, hence, will have no effect on the optical photophysical properties, only the lowest DTP1 and DTP2 S_0 and S_1 (DTP1-1 and DTP2-1) energy conformers were considered for the following analysis including the vibrational effects (through the Wigner distribution). For comparison purposes, the optical properties obtained as vertical transitions from the different S_0 and S_1 optimized conformations were also taken into account.

One- and Two-Photon Absorption Spectra. Linear (OPA) and nonlinear (TPA) absorption spectra for both DTP1 and DTP2 are shown in Figure 3a. As for OPA, the absorption to the lowest excited singlet state ($S_0 \rightarrow S_1$) corresponds to the peak with the highest intensity for both compounds (maxima at 415 and 460 nm for DTP1 and DTP2, respectively). These values are in remarkable agreement with the experimentally reported values in dichloromethane (415 and 457 nm for DTP1 and DTP2, respectively).[39,61] Even though our simulated spectra are performed in water, solvent effects are known to be only moderate for both dyes,[39,61] validating our approach. At higher energies, OPA to higher lying singlet excited states do appear (around 300 nm, assigned mostly to $S_0 \rightarrow S_2$), suggesting that the S_1 state could be in principle selectively irradiated, a desired feature to activate a certain photophysical pathway on an exclusive base. Indeed, as reported in the Supporting Information, almost no effect on the ground state equilibrium geometry is found when changing the solvent. Furthermore, the comparison of the OPA absorption spectrum in water and dichloromethane shows that the main optical properties are conserved despite a slight red-shift of about 25 nm induced by the more polar water solvent.

Concerning TPA, as expected, the energy window reaches the red and near infrared regions of the spectrum. TPA cross-sections are remarkably high, especially for the $S_0 \rightarrow S_2$ transition (between 500 and 700 nm): more than 1300 and 8000 GM for DTP1 and DTP2, respectively. Hence, especially DTP2 offers a TPA intensity among the highest found in the literature for neutral compounds.[24] Notably high are also the $S_0 \rightarrow S_1$ TPA cross-sections observed in the 700−1000 nm spectral window: more than 400 and almost 1000 GM for DTP1 and DTP2, respectively. The high TPA cross-section values calculated for both compounds can be easily related to the presence of conjugated thiophene rings, as already found in boron containing arenes previously studied by some of the authors.[62] Notably, in this case, TPA cross-sections of the order of 1000 GM were found for $S_0 \rightarrow S_2$ transitions, when three thiophene rings were linearly linked. Similarly, in this case, three five-membered rings are indeed linearly linked, hence enhancing the effect when a thiophene ring is covalently linked to the π-bridge, i.e., for DTP2.

Regarding the molecular orbital descriptions, NTOs are shown in Figure 3b for both DTP1 and DTP2. First, we should note that the *p*-(hexyl)phenyl group is not involved in the description of the electronic transitions. This is due to the fact that the phenyl group is almost orthogonal to the rest of the chromophore, thus not participating to the π-conjugated backbone.

Hence, the NTOs are located in the rest of the molecule. Particularly, the different organic groups can act as a donor (D) or an acceptor (A) depending on the vertical excitation: the $S_0 \rightarrow S_1$ NTOs depict noncentrosymmetric dipolar chromophores A−π−D, with a clear charge transfer allowed from the thiophene ending toward the cyano group, across a π-bridge. Indeed, it is known that the excited charge-transfer states are required for relevant TPA cross-sections.[63] Nevertheless, two additional requirements need to be fulfilled to maximize TPA properties: (i) the chromophore should be centrosymmetric, thus favoring the presence of (ii) an intermediate state between the ground and the final excited state. This intermediate state should possibly lie as near in energy as possible to the nonstationary virtual state generated by the superposition of ground and final excited states, hence corresponding to half TPA energy (resonance conditions).[16] These supplementary conditions are actually satisfied by the

DOI: 10.1021/acs.jpcc.8b04824
J. Phys. Chem. C 2018, 122, 16315−16324

Figure A.2. Article 2. (cont.)

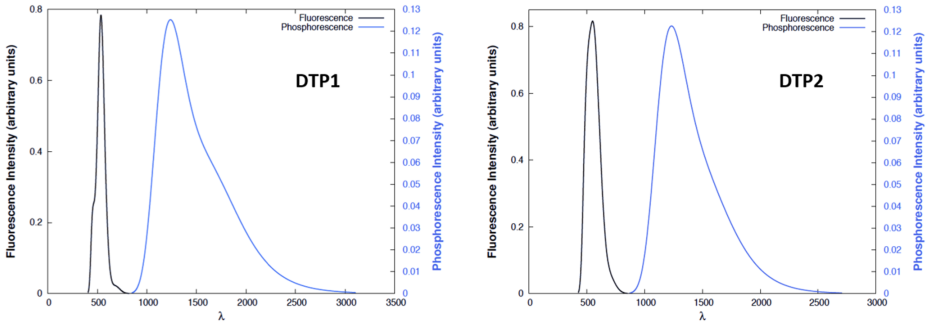

Figure 4. Fluorescence (black) and phosphorescence (blue) spectra of DTP1 (left) and DTP2 (right) simulated in water.

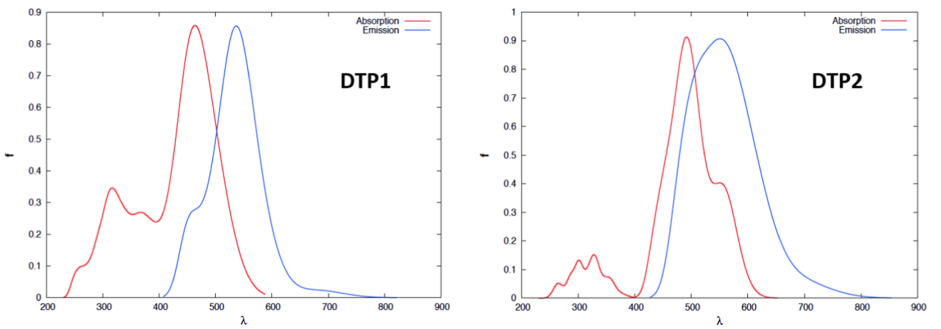

Figure 5. DTP1 (left) and DTP2 (right) absorption (red) and fluorescence (blue) spectra, calculated by convoluting over the complete set of conformations for both S_0 and S_1 minima.

same dyes when looking at the $S_0 \rightarrow S_2$ NTOs: first, the S_1 state can be considered as an intermediate state almost in resonance conditions with the virtual state. Moreover, the dyes behave as almost centrosymmetric A−π−D−π−A systems: in DTP1 both thiophene terminal rings act as acceptors, whereas the central π-conjugated backbone is the donor; on the other hand, in DTP2 the thiophenes and the cyano moieties act as acceptors, with the central phenyl ring being the donor. The higher $S_0 \rightarrow S_2$ TPA cross-section found for DTP2 could be indeed inferred to the higher centrosymmetry and more extended conjugation, compared to DTP1.

This can also explain the inversion in the peak intensity between OPA and TPA spectra: the $S_0 \rightarrow S_1$ ($S_0 \rightarrow S_2$) transition is much brighter than the $S_0 \rightarrow S_2$ ($S_0 \rightarrow S_1$) for OPA (TPA), almost conserving the intensity ratio.

Just after absorption to S_1 or S_2, two main photophysical pathways could follow: relaxation on the S_1 state (eventually following a rapid $S_2 \rightarrow S_1$ internal conversion) or intersystem crossing (ISC) to the triplet manifold. The latter option was evaluated by calculating the SOC among the excited singlet and triplet states found in the 4 eV energy window, for 20 geometries calculated by Wigner distribution around the Franck−Condon geometry (Figure S5). The ISC efficiency is mainly governed by two factors, (i) the singlet−triplet energy difference and (ii) the SOC: the lower the singlet−triplet energy difference and the higher the SOC, the higher the final ISC efficiency.

Looking at the energies (Figure S5a,d) for both compounds, the S_1 state is almost always closer to T_2, whereas S_2 lies in between T_4 and T_5. Hence, $S_1 \rightarrow T_2$ (Figure S5b,e) and $S_2 \rightarrow T_{4,5}$ (Figure S5c,f) SOCs were calculated in all cases, resulting in values lower than 5 cm^{-1}. We should therefore conclude that relaxation on the S_1 state is definitely preferred to ISC, at least in the vicinity of the Franck−Condon region.

Emission Spectra. Coherently, with the presence of two relaxation pathways, two emissive channels should in principle be considered as possible: fluorescence from the S_1 minimum or phosphorescence from the T_1 minimum. The calculated emission spectra are shown in Figure 4, depicting a similar behavior for both dyes. Note that geometry relaxation on both the excited singlet and triplet surface does not involve any important conformational change. As expected, fluorescence is more intense (almost a factor of 10) than phosphorescence, since the latter is formally spin forbidden. Looking at the shape, fluorescence appears much narrower than phosphorescence. As both spectra result from vertical transition of a Wigner distribution sampled around their respective minima (S_1 or T_1), this is an indirect evaluation of their potential energy surface: the T_1 minimum region is much smoother, giving rise to a flat region that corresponds to a wider

DOI: 10.1021/acs.jpcc.8b04824
J. Phys. Chem. C 2018, 122, 16315−16324

Figure A.2. Article 2. (cont.)

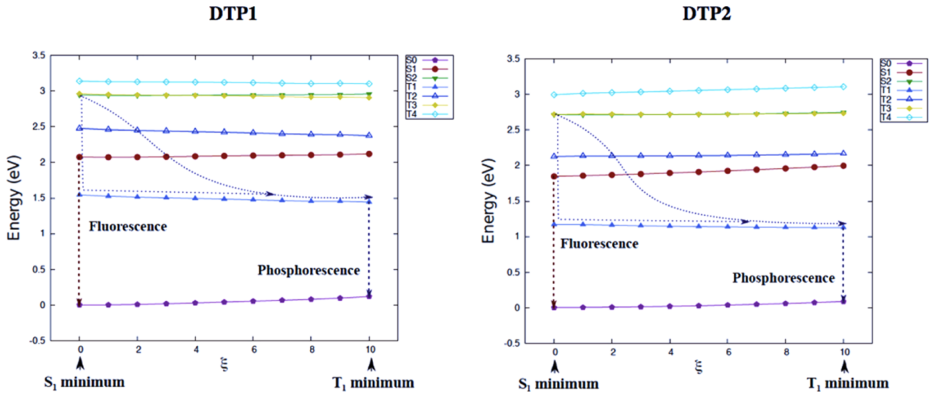

Figure 6. Simplified pathway (along an interpolation coordinate) between S_1 and T_1 minima structures for DTP1 (left) and DTP2 (right) at the B3LYP/6-31g(d) level of theory, including water as a solvent.

phosphorescence spectrum, ranging from 900 nm to almost 3000 nm. On the other hand, the S_1 minimum region is much steeper, resulting in a narrow fluorescence peak centered above 500 nm for both dyes (575 and 584 nm for DTP1 and DTP2, respectively). As a consequence, the Stokes shift observed for DTP1 (ca. 100 nm) is almost 50 nm larger than that for DTP2, due to DTP2 $S_0 \rightarrow S_1$ red-shifted absorption.

Looking at the SOC values around the S_1 minimum (Figure S6), we should conclude that the ISC efficiency is almost nonmodified compared to the Franck−Condon region. Indeed, the same triplet states are in principle energetically available (especially T_2 from S_1), but the SOC values are still rather low, even though nonnegligible for some structures. This scenario suggests that fluorescence should be observed in competition with singlet-to-triplet population, the latter being energetically feasible, but expected to occur on a slower time scale.

Conformational Effect on Absorption and Emission Properties. As previously explained, several almost isoenergetic conformers were found on both S_0 and S_1, mainly due to the structural flexibility offered by the dyes (see Figure 2). In Figure 5, we show the absorption (OPA) and emission (fluorescence) spectra calculated as a convolution of vertical transitions from five selected conformers, without taking into account vibrational effects (i.e., a multiconformational static approach). When compared to the spectra obtained with only the lowest energy conformer, but including vibrational effects by the Wigner distribution (i.e., a single-conformation dynamic approach; see Figures 3 and 5), the same structured band shape is observed for OPA, as well as the same energy window for fluorescence. Differences are observed in terms of energies corresponding to the maxima, being both (OPA and fluorescence) red-shifted by 40−50 nm. Hence, the Stokes' shifts are almost conserved confirming that, qualitatively, the photophysics and photoreactivity can be reasonably reproduced by both strategies. Nevertheless, when looking at the absorption experimental values (415 and 457 nm for DTP1 and DTP2, respectively, in dichloromethane[61]), we should conclude that the inclusion of vibrational effects on a single conformer results in a more realistic strategy than considering statically several energy minima conformers. The balance of two different factors could explain this result: at first, both S_0[39] and S_1 conformational analysis revealed that, despite structural flexibility, all conformers maintain nearly the same optical properties. Indeed, for the sake of clarity, a full conformational analysis, including the energies of the excited singlet and triplet states of all DTP1 and DTP2 conformers optimized on S_1, is shown in the Supporting Information (Figures S1 and S2). Hence, several shallow minima are found on both S_0 and S_1 potential energy surfaces, explaining especially the energy-wider absorption spectrum obtained by the multiconformational static approach, possibly better reproducing the experimental band shape. On the other hand, since quantitatively the minimum energy conformer alone represents the photophysics of the system quite well, the simulated absorption maximum values match the experiment better when including vibrational effects on this geometry. Indeed, some of the authors already found that the single-conformation dynamic approach applied by the Wigner distribution can reproduce almost quantitatively the optical properties of organic chromophores of different structural complexities,[64−67] including thiophene moieties.[62] The reason for this should be found in the low-frequency, high-amplitude out-of-plane normal modes reproduced by this strategy, that differentially break the conjugation patterns of the ground and excited states.

Intersystem Crossing Pathways. As explained in the previous sections, both DTP1 and DTP2 can be efficiently promoted to S_1 and S_2 by OPA and TPA, followed by the relaxation of the excited state. In particular, both S_1 and S_2 states relax into a minimum on their respective potential energy surface, corresponding to a highly similar structure (ξ = 0 in Figure 6), where they are expected to be trapped for a significant amount of time. To rationalize the channels leading to triplet population, a simplified pathway connecting the S_1 minimum and the T_1 minimum was generated by a linear interpolation coordinate ξ. Moreover, SOC values were calculated along the pathway (see Figure S3 in the Supporting Information), pointing toward the following ISC mechanisms: apart from fluorescence, from the S_1 minimum the only available ISC mechanism is a direct $S_1 \rightarrow T_1$ event. The energy

DOI: 10.1021/acs.jpcc.8b04824
J. Phys. Chem. C 2018, 122, 16315−16324

Figure A.2. Article 2. (cont.)

difference (0.5 eV) and the moderate SOC (below 0.2 cm^{-1}) suggest this as possible, but probably slow channel. Note that, although T_2 and S_1 lay quite close in energy, the singlet state's energy is lower. Hence, even if vibrationally allowed crossing of the two states could in principle be possible, this channel may be considered as energetically less probable. Nevertheless, additional ISC mechanisms could involve indirect pathways through S_2: this state almost constantly energetically degenerate with T_3, coupled to a nonzero SOC (ca. 0.2 cm^{-1}). Hence, a cascade $S_2 \rightarrow T_3 \rightarrow T_2 \rightarrow T_1$ mechanism can be suggested. In particular, from S_2, ISC should be preferred to $S_2 \rightarrow S_1$ internal conversion, the S_2–S_1 energy difference being ca. 1.3–1.5 eV along the interpolation coordinate. In any case, both direct $S_1 \rightarrow T_1$ and indirect $S_2 \rightarrow T_3 \rightarrow T_2 \rightarrow T_1$ mechanisms are coherent with the possible population of the triplet manifold. Both DTP1 and DTP2 compounds show similar energetics and pathways, leading to similar conclusions.

Once the compounds are in the T_1 minimum region, phosphorescence could follow, bringing the system back to the singlet ground state. Nevertheless, in the presence of molecular oxygen ($^3O_2$), an energy transfer process can be promoted, finally producing singlet oxygen ($^1O_2$).

Since phosphorescence is a kinetically unfavored process (due to its spin forbidden nature) its expected slow time scale should in principle favor $^1O_2$ generation. Indeed, since the $^3O_2 \rightarrow {}^1O_2$ band gap (from $^3\Sigma_g$ to $^1\Delta_g$) was measured to be ca. 1275 nm (0.97 eV) by infrared emission[68−72] we can finally conclude that a suitable energy transfer process can be forecasted from the triplet manifold of DTP1 and DTP2 to molecular oxygen (Figure 7).

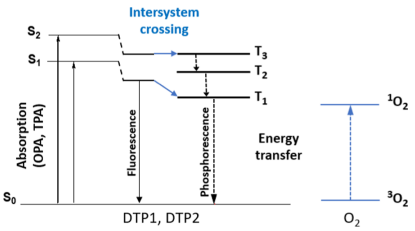

Figure 7. Energy scheme depicting the overall photoreactivity: for both compounds (DTP1 and DTP2), absorption is possible to S_1 and S_2 states, by both OPA and TPA, followed by intersystem crossing to the triplet manifold (in competition with fluorescence). Once the T_1 state is reached, two phenomena can be observed: phosphorescence or, in the presence of molecular oxygen, energy transfer to produce singlet oxygen.

CONCLUSIONS

We have studied the photophysics and photochemistry of two recently synthesized polythiophene-based dyes (DTP1 and DTP2), by means of high level state-of-the-art molecular modeling methodologies. More specifically, their ability as two-photon absorbers was highlighted by the calculation of remarkably high cross-sections for such neutral organic-based molecules, corresponding to the $S_0 \rightarrow S_2$ vertical excitation (over 8000 GM). It is noteworthy to mention that, compared to the known TPA absorbers used in materials science,[24] DTP1 and DTP2 show considerably high TPA cross-sections also for the $S_0 \rightarrow S_1$ excitation (around 1000 GM for DTP2). This desired and peculiar property is in apparent contrast with the usual TPA selection rules, by which a chromophore is usually considered as a centrosymmetric or noncentrosymmetric system. Indeed, the chromophore's symmetry will give raise to different selection rules. In the case of centrosymmetric chromophores high TPA cross-sections should be observed only when the intermediate states (e.g., S_1) act as a resonant state for the final absorption state (e.g., S_2). As a consequence, only higher excited states should have nonnegligible absorption. On the other hand, in noncentrosymmetric chromophores the $S_0 \rightarrow S_1$ TPA excitation can be relatively intense.[16]

In the case of DTP1 and DTP2, high cross-sections are observed for transitions to both excited states. This can be related to the fact that some organic moieties can act as a donor or acceptor group, depending on the specific electronic state (see Figure 3). Indeed, both chromophores act as noncentrosymmetric A–π–D molecules for $S_0 \rightarrow S_1$ excitation, and as centrosymmetric A–π–D–π–A for $S_0 \rightarrow S_2$ excitation. This peculiar feature notably increases their possible application as PDT agents, since they can be efficiently excited to the singlet manifold by red (S_2) and/or near infrared light (S_1). Most notably both S_1 and S_2 potential energy surfaces evolve toward a minimum, from which intersystem crossing is possible—even though not as an ultrafast event—hence, leading to triplet (T_1) population. From T_1, energy transfer to molecular oxygen would be easily allowed (as found by the calculation of the T_1 energetics), finally producing singlet oxygen, as envisaged for PDT. Hence, the use of DTP1 and DTP2 in PDT applications could be strongly suggested. However, such applications would also require studies concerning both the dye bioavailability and its toxicity in the dark, that obviously go beyond the scope of the present contribution.

Methodologically, we compared two different strategies to calculate absorption and emission properties: a multiconformational static approach (i.e., taking into account different conformers at their minimum energy structure) and a single-conformation dynamic approach (i.e., taking into account only the lowest energy conformer, but including vibrational effects by the Wigner distribution). The results point toward the importance of including dynamic effects to predict the absorption maximum wavelength, even though the inclusion of different conformers allows an improved description of the overall spectrum shape. In the future, we plan to design modifications to the proposed molecules, to maintain their exceptional TPA properties and, at the same time, increase the intersystem crossing efficiency.

ASSOCIATED CONTENT

Supporting Information

The Supporting Information is available free of charge on the ACS Publications website at DOI: 10.1021/acs.jpcc.8b04824.

Selected S_1 minimum geometries, including singlet and triplet energies of ground and excited states; spin–orbit coupling values between S_1 minimum and T_1 minimum, along a linear interpolation coordinate; comparison of the one-photon absorption spectra calculated by Wigner distribution in water and dichloromethane; comparison of the calculated one-absorption absorption maxima with available experimental values in dichloromethane; energies and spin–orbit couplings of the 20 structures

DOI: 10.1021/acs.jpcc.8b04824
J. Phys. Chem. C 2018, 122, 16315−16324

Figure A.2. Article 2. (cont.)

Supporting Information

Photophysical Properties of Novel Two-Photon Absorbing Dyes: Assessing their Possible Use for Singlet Oxygen Generation

Ozlem Sengul,[1] Marco Marazzi,[2,3] Antonio Monari,[3*] Saron Catak[1*]*

1) Department of Chemistry, Bogazici University, Bebek 34342 Istanbul, Turkey
2) Departamento de Química, Centro de Investigacíon en Sintesís Química (CISQ), Universidad de La Rioja, Madre de Dios, 53, 26006 Logroño, Spain
3) Université de Lorraine and CNRS, LPCT UMR 7019, F-54000 Nancy, France

Figure A.2. Article 2. (cont.)

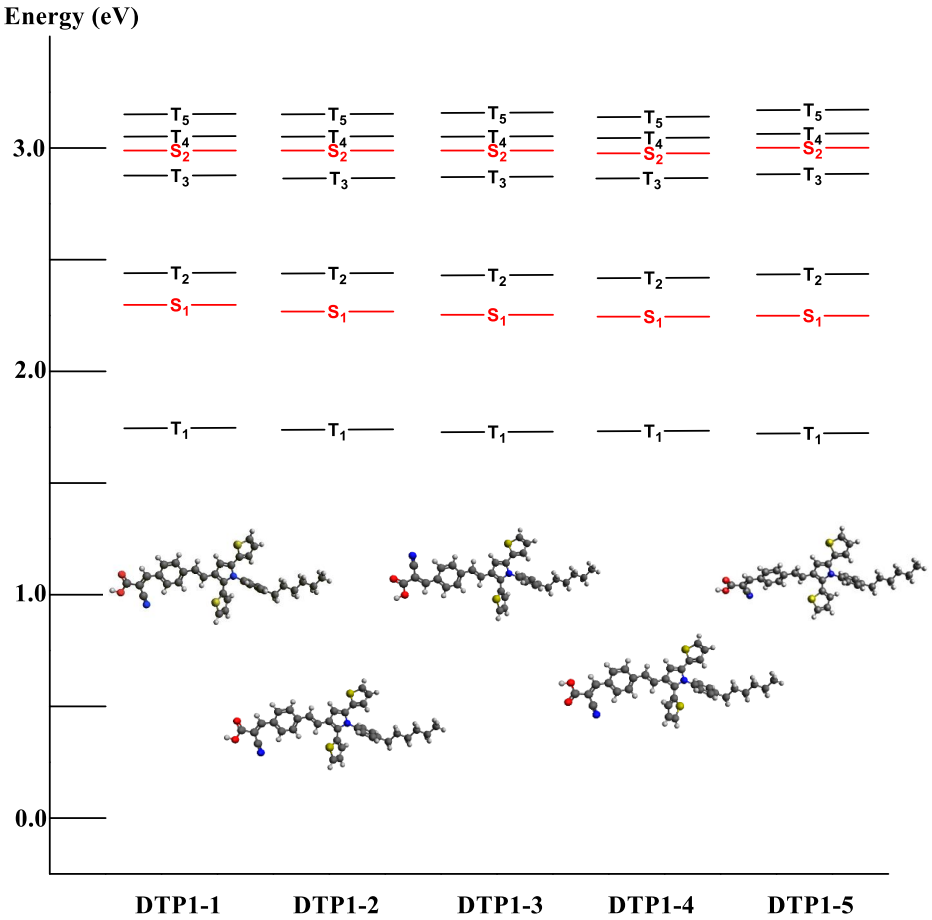

Figure S1. Comparison of the excited state energies of the selected conformers of DTP1 at B3LYP/6-31G(d) level of theory in water. The relevant S1 minima geometries are shown as well.

Figure A.2. Article 2. (cont.)

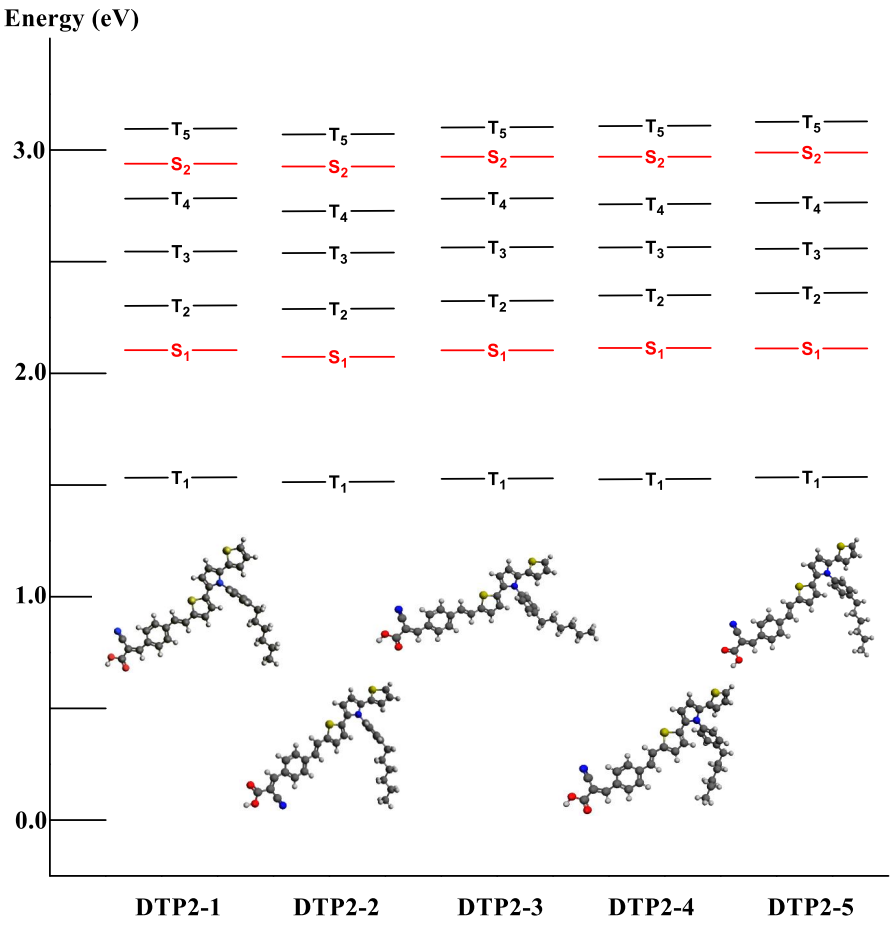

Figure S2. Comparison of the excited state energies of the selected conformers of DTP2 at B3LYP/6-31G(d) level of theory in water. The relevant S1 minima geometries are shown as well.

Figure A.2. Article 2. (cont.)

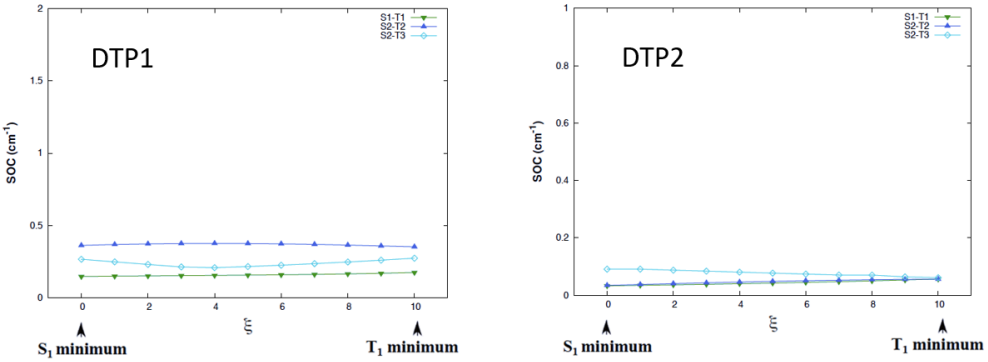

Figure S3. SOC values between the states of interest along an interpolation coordinate between S_1 and T_1 minima structures, for DTP1 (left) and DTP2 (right) at the B3LYP/DZP level of theory.

Figure A.2. Article 2. (cont.)

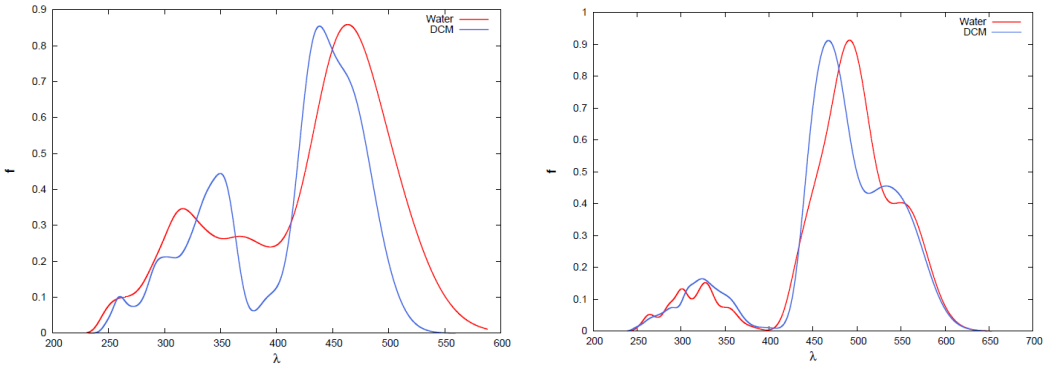

Figure S4. OPA absorption spectra calculated in water and DCM for DTP1 (left) and DTP2 (right), respectively.

Table S1. DTP1 and DTP2 absorption maxima obtained from the Wigner distribution calculations, compared to experimentally available values.

	λ_{max} for DTP1				λ_{max} for DTP2		
	DCM	Water	Exp.		DCM	Water	Exp.
DTP1-1	438 (2.83)	459(2.70)	415 (2.98)	**DTP2-1**	469 (2.64)	492(2.52)	457 (2.71)
	349 (3.55)	318(3.89)	334 (3.71)		323 (3.83)	329(3.76)	364 (3.40)

[a] All vertical excitations were calculated on B3LYP/6-31G(d) optimized geometries.
[b] λ_{max} values are given in nm (eV in parentheses)
[c] Experimental data are obtained with DCM as solvent.

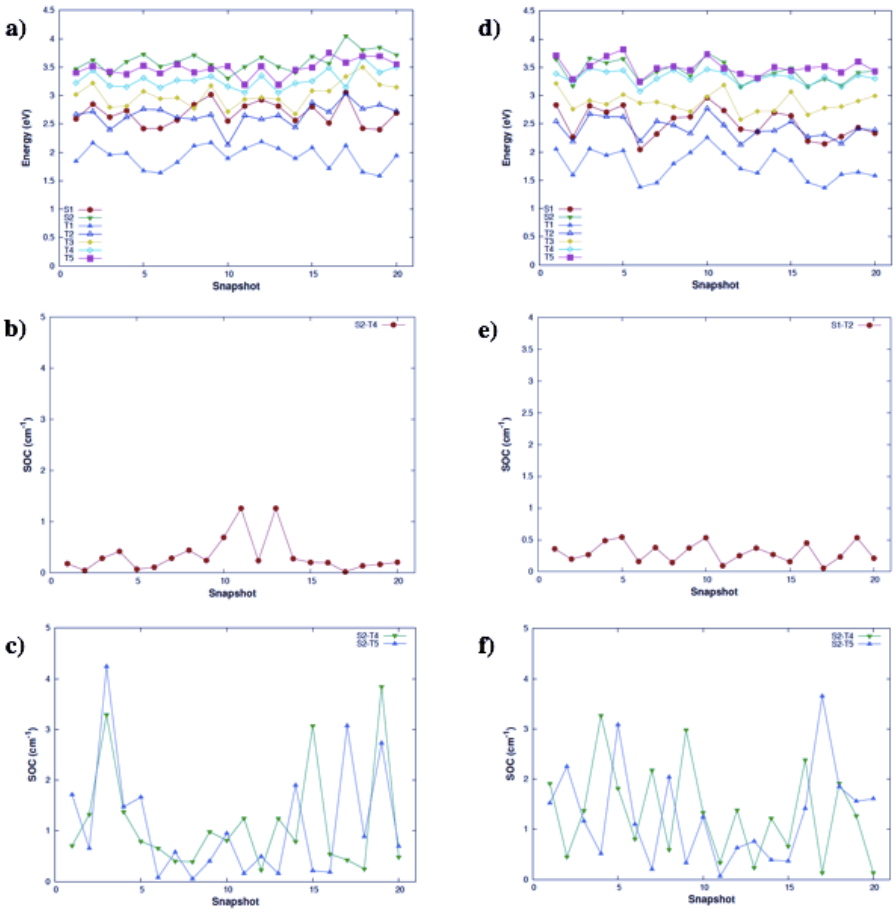

Figure S5. DTP1 (left) and DTP2 (right) energies of the lowest two excited-singlet and five triplet states, for each of the twenty structures sampled by the Wigner distribution around the ground state (S_0) minimum (a). The spin-orbit coupling (SOC) values are also shown for triplets close in energy to S_1 (b, e) and to S_2 (c, f).

Figure A.2. Article 2. (cont.)

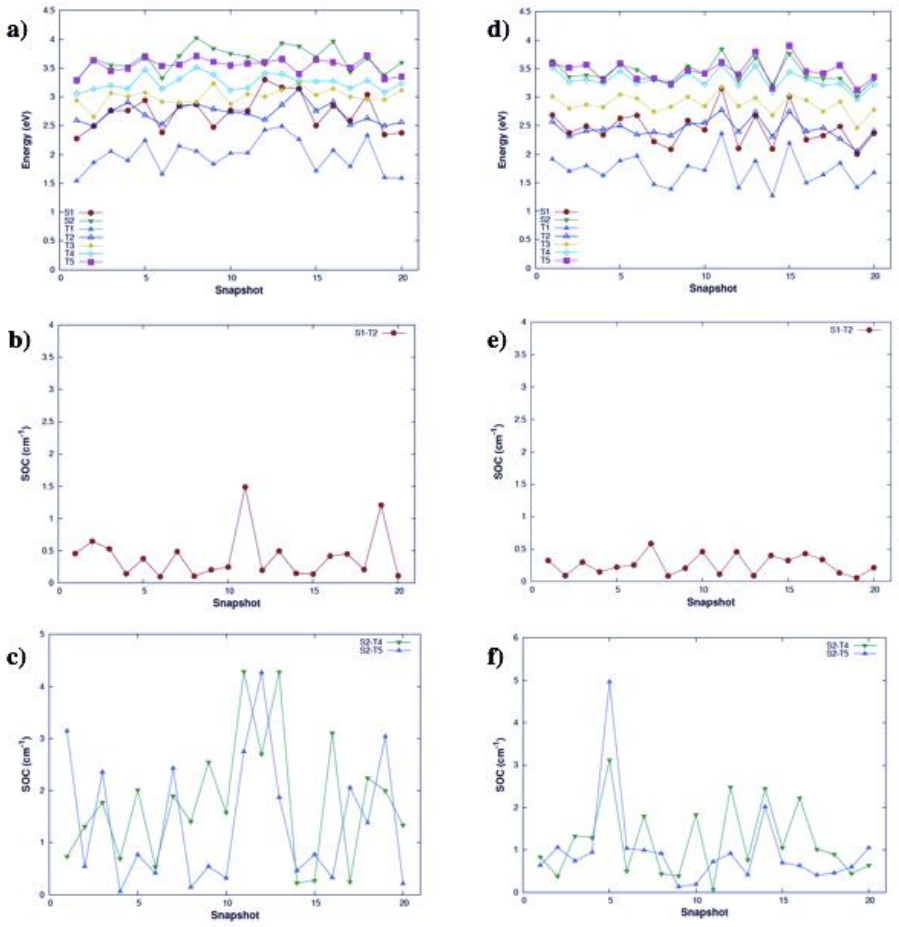

Figure S6. DTP1 (left) and DTP2 (right) energies of the lowest two excited-singlet and five triplet states, for each of the twenty structures sampled by the Wigner distribution around the excited state (S_1) minimum (a). The spin-orbit coupling (SOC) values are also shown for triplets close in energy to S_1 (b, e) and to S_2 (c, f).

Figure A.2. Article 2. (cont.)